DESIGN STUDY OF A MINIATURIZED MULTI-LAYERED METAMATERIAL-INSPIRED DYNAMICALLY TUNABLE ANTENNA

By

Joshua C. Myers

A THESIS

Submitted to
Michigan State University
in partial fulfillment of the requirements
for the degree of

Electrical Engineering – Master of Science

2014

ABSTRACT

DESIGN STUDY OF A MINIATURIZED MULTI-LAYERED
METAMATERIAL-INSPIRED DYNAMICALLY TUNABLE ANTENNA

By

Joshua C. Myers

A multi-layered metamaterial inspired minaturized antenna with pixel grid loading structures is introduced. The antenna consists of two conducting layers separated by a thin dielectric substrate. The first layer contains a folded monopole antenna surrounded by a metal pixel based loading structure, while the second layer is envisioned to consist of a photo conductive pixel grid utilized to tune the antenna. The state of each pixel is controlled by a binary genetic algorithm, which is implemented with a Matlab-HFSS interface. As a proof of concept, the pixel grid on the second layer is initially made of a metal conductor. HFSS simulations show that the second layer has a wide tuning ability with the appropriate state formed through optimization. A wide range of other conductivities are also shown to provide pixel combinations that meet the required antenna characteristics. The radiation efficiency of the antenna with the second layer is also examined and optimized, and the theoretical tuning range is investigated. Fabrication of multiple antenna configurations with the pixels made of metal conductors are explored. Thin PET films are first investigated to be used as simple loading elements that can be placed directly on the antenna. However, the airgap and misalignment between the layers caused by this method is shown to be too large. A novel multi-layer fabrication technique is then investigated which uses a SU-8 photoresist as the dielectric layer. This layer can be spun directly onto the antenna, eliminating the airgap. The alignment between the two layers using this method is also much better than the previous method. Multiple antenna configurations corresponding to a wide frequency range are constructed using this fabrication method. The measured reflection coefficients and radiation patterns are shown to be in good agreement with HFSS simulations, successfully demonstrating the ability to dramatically tune the antenna with a second pixel grid.

For my love Melissa, my beautiful Sunshine, and my comedian Shane.

ACKNOWLEDGMENTS

I would like to first thank my advisor Dr. Premjeet Chahal. Since first meeting him in ECE 405 as an undergraduate, I have learned more than I thought possible about electromagnetics. Although at times he may be a taskmaster, his creative and unique visions have inspired me with numerous research ideas that neither I nor anyone else could have envisioned. Without his research guidance and assistance I can truly say that I do not know what I would be doing with my life. In addition to all of this, I would like to thank him greatly for giving me the opportunity to complete my graduate degree and welcome me into the Electromagnetics Research Group at Michigan State University.

Second, I would like to thank Dr. Edward Rothwell for all of the meaningful and insightful conversations we have had not only about this research, but also about many other areas in electromagnetics and life. While his sarcasm is sometimes thick, I have had nothing but positive experiences working with him. Although he is not my advisor, he has treated me with the same respect and helpfulness that he typically reserves only for his students. I would also like to thank Dr. Nelson Sepulveda, not only for his excellent softball playing, but also his assistance in my research and for serving on my committee.

I would like to also acknowledge all of my excellent co-workers and friends in the EM group. In particular, I would like to thank Xianbo Yang not only for his friendship, but also for his knowledge and helpfulness in the cleanroom. Without him, I highly doubt this thesis would have been possible. In addition, I would like to sincerely thank Dr. Raoul Ouedraogo for the use of his GA optimization code that is the basis of the optimizer used in this work. Further, I would like to thank Benjamin Crowgey for his friendship and our frequent talks about sports that successfully distracted me from completing this thesis at an earlier date. I would also like to thank Junyan Tang for his help in soldering connectors, as well as his many tang-isms. Last but not least, I would like to thank my former co-worker Dr. Jose Hejase for not only his help with my research, but also his endearing friendship. Without

Jose I would never have came to work with Dr. Chahal. I don't think I could have ever found a better mentor and friend.

Most importantly, I would like to thank my wife Melissa Myers for all her support and love throughout this process. Without her I would have never known my beautiful daughter Sunshine and my amazing son Shane. For this I will be eternally grateful to her. Additionally, I would like to thank her parents and brothers for putting up with me all these years. I would also like to thank my parents Barbara and Darryl Myers. Without them I would obviously not be here. Their love and support has helped mold me into the person I am, and I am extremely lucky to be their son.

TABLE OF CONTENTS

LIST OF FIGURES

KEY TO SYMBOLS AND ABBREVIATIONS

- CPW: Coplanar Waveguide
- DNG: Double Negative Parameters
- DPS: Double Positive Parameters
- ENG: Epsilon Negative Parameters
- GA: Genetic Algorithm
- HFSS: High Frequency Structural Simulator
- MEMS: Micro-Electro-Mechanical Switches
- MNG: Mu Negative Parameters
- PET: Polyethylene terephthalate
- SRR: Split Ring Resonator
- SU-8: Novalac Epoxy Resin Photoresist

CHAPTER 1

Introduction and Background

1.1 Antenna Miniaturization

The need for small and compact antennas has increased rapidly over recent years. This increased interest has been primarily led by the desire to further shrink both military and consumer devices in size. Meanwhile, the need for antennas in nearly all modern devices has also increased exponentially as device connectivity has become crucial. While many of the other components in these devices can easily be reduced in size, antenna miniaturization presents a uniquely difficult problem. Since the operational band of an antenna is primarily determined by the size of the antenna with respect to a wavelength, reducing the size of antennas without losing the desired frequency of operation is somewhat counter-intuitive. In addition, the desire for small antennas to maintain an acceptable level of radiation efficiency, bandwidth, and preserve a reasonable radiation pattern while being much less than a wavelength in size further complicates the design process.

While the overall goal of antenna miniaturization is to reduce the geometric footprint of the antenna, the process used to accomplish this reduction can be through electrical or geometrical means. Perhaps the most intuitive means of antenna miniaturization is to simply reduce the overall size impact of the antenna through geometry modification. A

simple example of size reduction through geometry modification can be displayed for a simple monopole antenna. A monopole antenna is classically thought of as a single straight wire, which produces a omni-directional radiation pattern in the azimuth plane, and a bi-directional pattern in any of the elevation planes [1]. These characteristics can be expected of the monopole antenna when the length of the antenna is approximately equal to $\lambda/4$.

A monopole antenna can also be realized on a simple dielectric by creating a thin metal strip $\lambda/4$ in length on one side of the dielectric, and a ground plane on the other. As long as the overall length of the antenna is maintained, the shape of the monopole can be altered. A common method of changing the shape of the antenna to reduce its size is by simply folding the monopole back toward its excitation while maintaining the same overall length. The overall process of this miniaturization is shown in Figure 1.1.

More novel methods of antenna miniaturization through geometry modification are also commonly used. In [3]-[6], patch antennas are miniaturized using fractal structures. Size reductions are achieved by using complex fractal structures, such as minkowski and sierpinski fractals. Fractals are space filling contours, meaning electrically large features can be efficiently packed into small areas. A typical patch antenna is simply a rectangular radiating patch placed above a ground plane, usually with a dielectric used for separation [2]. The radiation achieved by the patch antenna is directly related to the current distribution of the surface of the patch. However, the rectangular patch can also be replaced by a more complex structure such as a fractal. These structures cause the current residing on the surface of the antenna to travel along a longer path than a traditional patch. If the structure is more compact than the patch, as in the case of a fractal, then less realization area is required for the antenna.

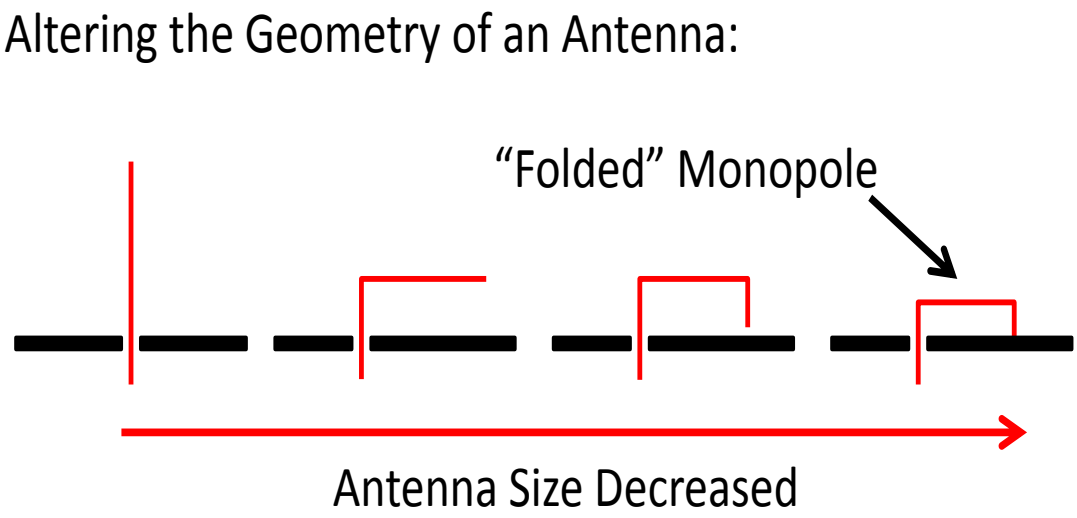

Figure 1.1 Geometrical miniaturization of a monopole antenna.

While modifying the antenna geometry can provide some antenna miniaturization, the miniaturization cannot be electrically controlled. In addition, only a modest amount of miniaturization can be achieved by modifying the geometry. Also, geometry modification does not alter the resonant frequency of the antenna, providing only a limited frequency tuning. Perhaps the simplest way of miniaturizing a patch antenna without modifying its geometry is by using a high permittivity dielectric. Since the resonant frequency of the patch is proportional to the relative permittivity of the dielectric by $1/\sqrt{\epsilon_r}$, increasing the permittivity will decrease the resonance frequency without altering the geometry [7]-[8]. Selecting a dielectric material with a large permittivity will dramatically decrease the resonance of the antenna compared with traditional patch antenna substrate materials.

Antennas can also be miniaturized through the use of capacitive and inductive shorting pins [11]-[14]. For a patch antenna, the miniaturization is achieved by altering the location of the dominant patch mode from the center to the edge through the use of shorting pins between the feed and edge of the patch. While a variety of size reductions are reported, a miniaturization of nearly 50 % can be achieved for a rectangular patch antenna. Much larger reductions have been investigated with more complex structures as shown in [15]-[16].

Another possible way to miniaturize an antenna is through the use of a variety of RLC loading structures. Placing a loading structure near the antenna will drive down the resonant frequency of the antenna, depending on the resonance of the loading structure. While the antenna geometry remains the same, the resonant frequency of the antenna is reduced. Thinking of the antenna size in terms of fractions of wavelength, if the antenna operating frequency is reduced, than the effective size of the antenna is also reduced. This creates a miniaturized antenna in terms of wavelength, even though the antenna dimensions are unchanged. This loading concept applied to a simple monopole antenna is shown in Figure 1.2.

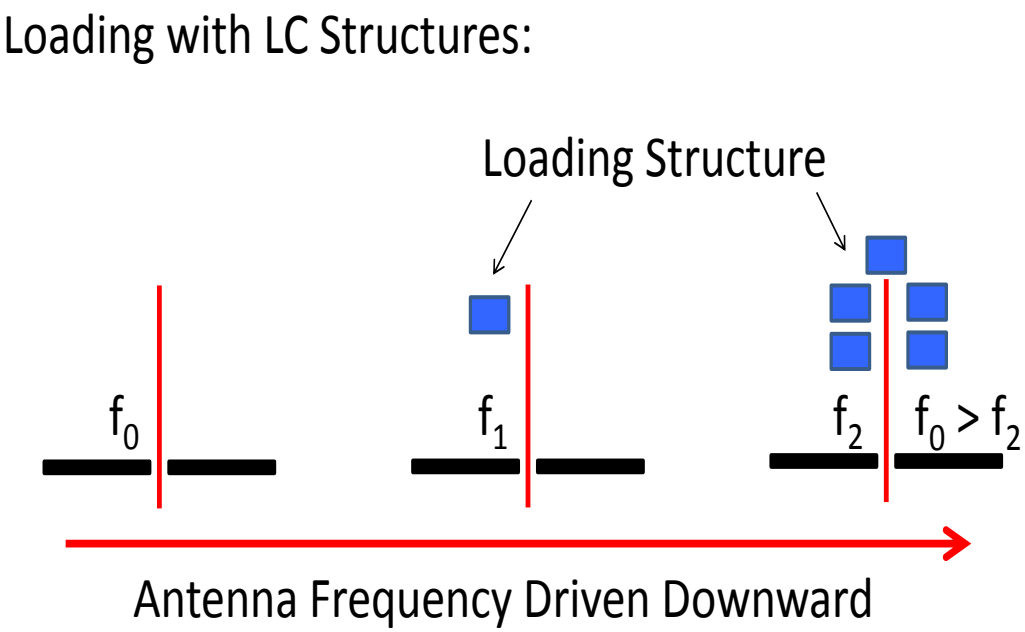

Figure 1.2 Miniaturization of a monopole antenna with LC loading.

Using loading structures for miniaturization increases the possible frequency tuning range of the antenna as the resonant frequency can be driven down based on the loading structure. Loading structures also offer a much greater amount of miniaturization compared with simply changing the antenna geometry. In addition, loading structures can easily become frequency tunable through the use of active devices and a variety of other methods. A simple example of a loading structure that reduces the resonance of an antenna is discussed in [17]. This work utilizes a series of loaded slits to miniaturize a slot antenna fed with a CPW line. This method is shown to allow for a 42% reduction in resonant frequency, while maintaining the radiation properties of the antenna. More complex cases of loading structures will be explored in section 1.3.1 of this thesis.

While this is only a small subset of techniques used to miniaturize antennas, it represents a relative overview of some of the simplest methods. However, in recent years a large amount of research has been applied to the use of metamaterials in antenna miniaturization.

1.2 Antenna Tuning and Reconfiguration

Unfortunately, loading antennas to achieve miniaturization only provides a fixed frequency change in resonance, based on the resonace of the loading material. Therefore, it is desirable to also make miniaturized antennas frequency tunable. One common way of frequency tuning antennas is through the use of varactor diodes. Varactor diodes are typically operated in a reverse-bias state. No current flows through the diode, but since the thickness of the depletion region in a diode is increased with applied voltage, the capacitance of the diode can be made to vary [20]. As the capacitance of a diode is dependent on the depletion region width, which is dependent on the square root of the applied voltage, a relation between the capacitance and applied voltage can be determined from the following relation.

$$C \propto \frac{1}{\sqrt{V_{applied}}} \tag{1.1}$$

While all diodes exhibit this behavior to a certain extent, varactor diodes are manufactured specifically to exploit this effect and increase the capacitance. Essentially, varactor diodes can be used as voltage controlled variable capacitors. These capacitors can often be used as loading elements on many types of antennas to tune the antenna in frequency [21]-[25]. These tuning elements also allow for a continuous tuning range as opposed to a discrete range created by tuning switches or pins. In [26] The operating frequency of a patch antenna is tuned using a varactor diode mounted onto one of the radiating edges, similar to the configuration shown in Figure 1.3. The patch is shown to be tunable from 4.9 to 5.4 GHz, with a supply voltage from 0 to 20V. In this case, the diodes provide an increase tuning range near the original resonant frequency of approximately 10%. Unfortunately, varactor diodes only provide a moderate increase in frequency tuning range.

Multiple types of switching methods have also been demonstrated for use in antenna frequency tuning systems. Simple switches can be placed between the patch antenna and its ground plane [27]. The resonance frequency of the antenna can be changed based on the location and switch position. Micro-Electro-Mechanical Switches (MEMS) devices have also been used in antenna tuning [28]-[29], where they are used as ultra-fast capacitive switches. In particular, [30] uses periodically placed MEMS on a co-planar waveguide feed to a patch antenna to tune the resonant frequency. Approximate 400 MHz of additional bandwidth is achieved in this work. However, to achieve adequate frequency tuning, usually a large number of switches or MEMS devices are necessary.

There are many additional frequency tuning methods besides just varactor diodes and switches. In [31] the reconfiguration of antenna operating frequency is achieved by pin diodes through switching states. Frequency tuning is achieved by changing

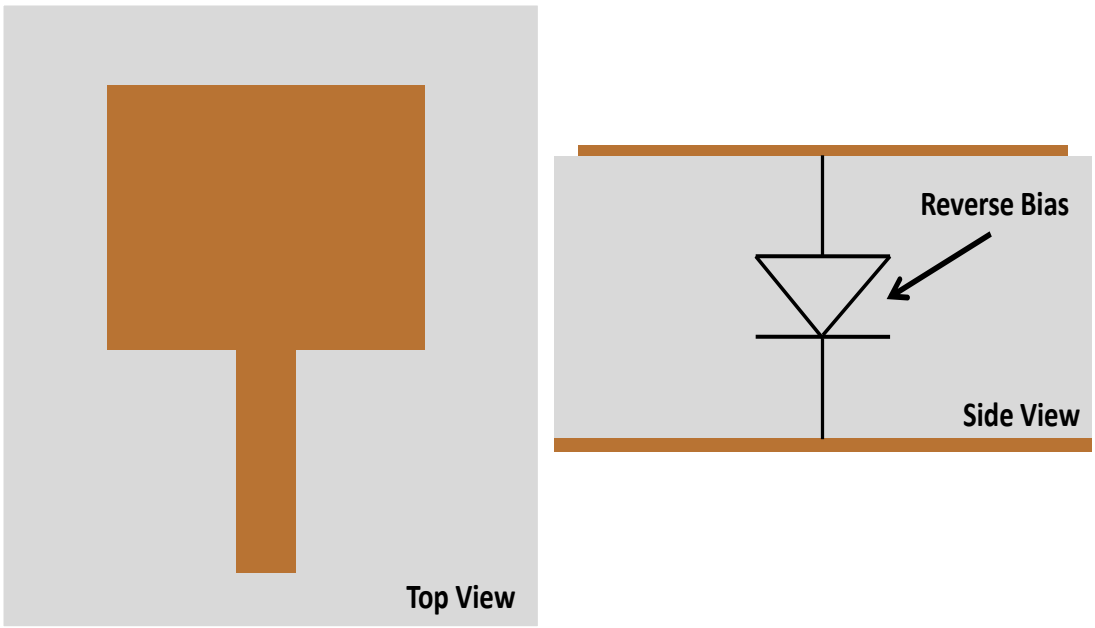

Figure 1.3 Simple configuration of a patch antenna loaded with a varactor diode.

the length of the coupled conductors. Mechanically means are also sometimes used to tune antennas in frequency [32]-[33]. As an example, in [34] a patch antenna with an air-glass substrate is tuned by mechanically changing the air-gap height between the antenna and ground plane. Frequency tuning of approximately 12% are reported, with a 400MHz resonance shift. A number of new methods have also been presented to both miniaturize and tune antenna systems. However, one method that is becoming increasingly important is in the use of metamaterials. An overview of these artificial materials, as well as selected applications concerning the miniaturization and tuning of antennas, is presented in the following section.

1.3 A Brief Overview of Metamaterials

The response of a system to an excitation can largely be determined by the properties of the materials involved. In the case of an electromagnetic response, the most important material properties are the permittivity (ϵ) and permeability (μ). The permittivity of a material describes the measure of the ability to support the formation of a electric field within itself, while the permeability of a material is a similar response, but for the support of magnetic fields.

Materials can then be classified depending on the values of (ϵ) and (μ). A material with both permittivity and permeability greater than zero ($\epsilon > 0, \mu > 0$) is generally referred to as a double-positive (DPS) medium. Most natural materials fall under this category, such as dielectrics. Materials with permittivity greater than zero, and permeability less than zero ($\epsilon > 0, \mu < 0$) are referred to as mu-negative (MNG) mediums [36]. Gyrotripic materials exhibit these properties naturally over certain frequency spectrums. Noble metals have been shown to exhibit negative permittivities in the IR and visible frequency spectrum. A material with permittivity below zero, and a permeability above zero ($\epsilon < 0, \mu > 0$) is referred to as a epsilon-negative material (ENG) [37]. Mediums with both negative permittivity and

permeability ($\epsilon < 0, \mu < 0$) are known as double-negative (DNG) materials [38]. The classifications of these mediums is shown in Figure 1.4.

Unlike the other mediums discussed above, DNG material properties have never been observed in nature. Mediums exhibiting these characteristics have been demonstrated with artificial constructs. Artificial materials have been constructed that also have DPS, ENG, and MNG properties. One of the first attempts to explore the concept of artificial materials dates back to the early nineteenth century, when Jagadish Bose conducted a series RF experiments on twisted structures, essentially artificial chiral elements [35]. Since then, artificially engineered materials have become the subject of research for many groups worldwide. However, materials with DNG parameters are of primary interest in this work. Artificially engineered materials that exhibit electromagnetic properties which are not naturally found (DNG paramaters) are commonly referred to as metamaterials.

In recent years, there has been a growing interest in metamaterials. In [39], the plane wave propagation in a material with DNG parameters is theoretically investigated. The direction of the poynting vector is found to be anti-parallel to the direction of propagation, as opposed to parallel for the case of plane wave propagation in conventional materials. The index of refraction has also been shown to be theoretically negative for DNG materials in several works, and also experimentally verified [40]-[42]. Metamaterial mediums have also been investigated through numerical means as well. In [43]-[45], finite-difference time-domain (FTDT) simulations are used to study the wave physics associated with DNG materials. Lossy Drude polarization and magnetization models are used in these simulations.

Metamaterials are also used for a variety of applications. two-dimensional metamaterials are readily used in many microstrip-based applications. In [46]-[47], two microstrip based

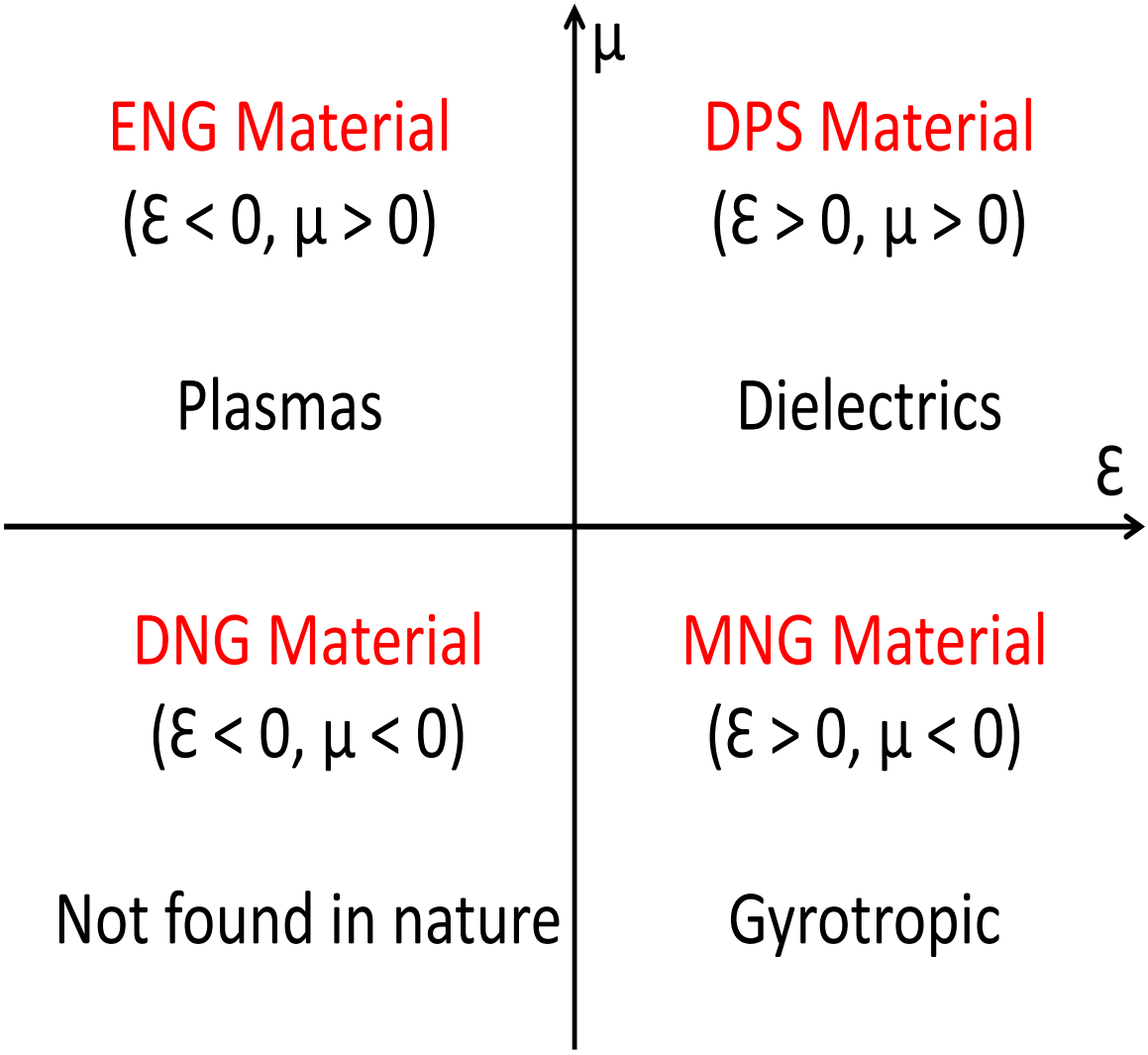

Figure 1.4 Summary of artificial material types.

coupler lines are presented. The first is a broadband backward-wave coupled-line directional coupler, while the second is a asymmetric phase coupler. Metamaterials also have a number of applications that are relevant in antenna design. In [48], a backward leaky-wave antenna is presented. The radiation is achieved by capacitive gaps which excite a TM radiating wave. Other antenna applications based on metamaterials include a dual-band ring antenna [49], complex artificial ground planes [50], and resonance cone antennas [51]-[52]. In addition, metamaterials have a wide range of uses in the miniaturization and tuning of antennas, which is further explored in the following sections.

1.3.1 Applications of Metamaterials to Antenna Miniaturization and Tuning

Metamaterials also have many applications in the miniaturization of antennas. This miniaturization can be achieved through a variety of techniques, though most of which involve some form of metamaterial loading. In [53] and [54], an electrically small dipole antenna is matched to free space by surrounding the antenna with a homogeneous shell having ENG properties. If the proper ENG parameters are selected for the shell, a match can be found between the shell and for any size dipole. This leaves an effectively miniaturized antenna. However, the large size of the required shell eliminates any advantage gained by miniaturizing the dipole. Figure 1.5

A similar concept is presented in [55], where a loop antenna is surrounded by a MNG layer. The MNG layer is created by an array of split-ring resonators (SRRs) surrounding the loop antenna. The resonance of the loop antenna is then reduced to that of the SRR elements. Since the resonance of a typical SRR is mcuh less than a wavelength, the antenna resonance is driven downward by at least $\lambda/10$. An even more compact design was is presented in [56], where the loop antenna is placed directly into a single SRR resonance. A microstrip patch antenna is also loaded with a DNG metamaterial so that the resonant frequency of the TM_{110} mode can be made as small as desired [57]. Outside of using SRRs directly as

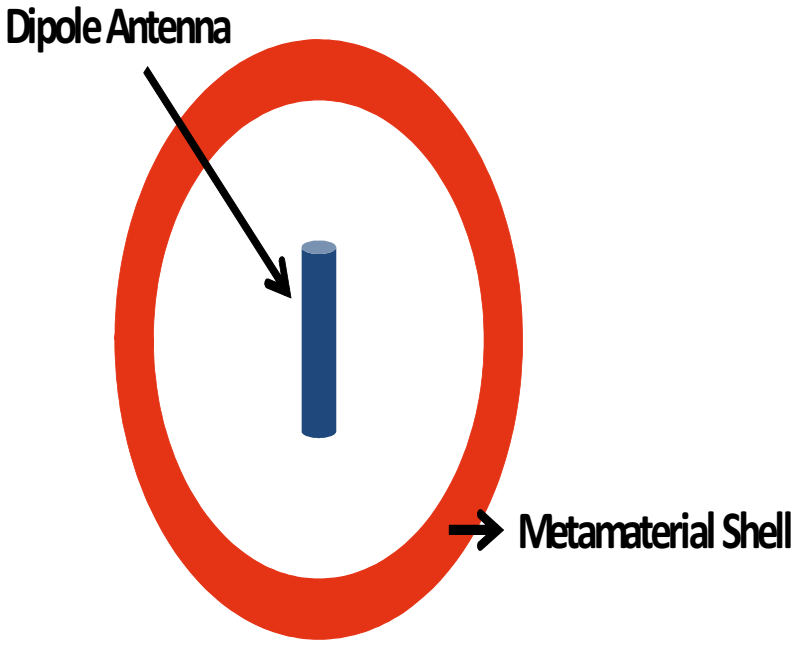

Figure 1.5 Dipole antenna surrounded by a metamaterial shell.

loading elements, metamaterials have been used in the place of ground planes to miniaturize antennas. A number of authors [58]-[60] have investigated etching SRRs on the ground plane of an antenna. The authors show that it is possible to lower the resonance of the radiating patch to the resonance frequency of the SRRs. Although easier to implement than the other techniques involving SRRs, only a size reduction of 31% is achieved in [58]. Additionally, altering the ground plane of the antenna can dramatically effect other aspects of the antenna, such as the radiation pattern and efficiency.

Metamaterials also have many potential applications in the tuning of antennas. Antennas that are miniaturized usually have relatively narrow bandwidth as discussed in the previous section. Due to these bandwidth limitations, it is commonly desirable to combine both antenna miniaturization and frequency tuning in the design of a metamaterial based antenna. A simple way of frequency tuning a miniaturized metamaterial antenna is presented in [61]. Varactor diodes are used to load an antenna miniaturized with SRRs. The varactor diodes are placed between the gaps in the SRR, changing the resonant frequency of the resonators. A tuning range of approximately 20% is reported. Similar results are also presented in [62]-[63], with more or less the same level of tuning.

Metamaterials themselves have also been used as antenna tuning elements. In [64], a metamaterial line antenna is tuned using two inductor poles. Changing the inductance allows for a shift of the antenna resonance without sacrificing the antenna performance. A number of other methods for antennas using metamaterials are presented in [65]-[67]. However, the loading effect of metamaterials for antenna tuning and miniaturization has inspired other techniques used for a similar purpose. In particular, the use of optimized LC structures in place of traditional metamaterials has been extensively investigated [68]-[71]. In these particular cases, a genetic algorithm (GA) optimization technique is used for both miniaturization and tuning of loop, patch, and monopole antennas. In the next section, the GA optimization technique is reviewed and explained in detail, and some select applications of GA optimization in electromagnetic systems are also presented.

1.4 Optimization Techniques in Electromagnetics

A number of problems in electromagnetics become difficult to solve with conventional analytic equations. Most of these problems can be solved using numerical means, however, a number of problems exist that require very complex structures with many possible variables. Optimization can be used to solve these types of problems, and is widely used in many area of electromagnetics such as antenna design and material characterization, along with others. There are three conventional categories of optimization and search methods used in the current literature. These three methods include calculus-based, exhaustive search, and random search methods [72]-[73]. All of these methods, as well as non-traditional optimization method based on natural selection, are subsequently introduced in this section.

1.4.1 Calculus-based Optimization Methods

Calculus-based methods are widely studied throughout a variety of research areas. These methods involve seeking local maxima and minima by solving the gradient of the desired objective function set equal to zero. Given a smooth objective function, finding a corresponding peak involves calculating derivatives in a local area and finding where they converge to zero. While this method is local in scope, for a function similar to the one shown in Figure 1.6 the peak location and value of the objective function can be easily found. However, this method is extremely dependent on the location of the initial guess for the search. Depending on the guess, there may be no way to tell if the maximum of the objective function is a local maxima, or a global maxima. This means that the solution the method converges to may not be the optimal, or even best, solution available. For example, if the domain of the function shown in Figure 1.6 is extended as shown in Figure 1.7. The current maxima is revealed to not be the global maxima in the area, meaning a better solution could be found with a different initial guess. In addition, these methods depend upon the existence of well defined derivatives which may not always be available.

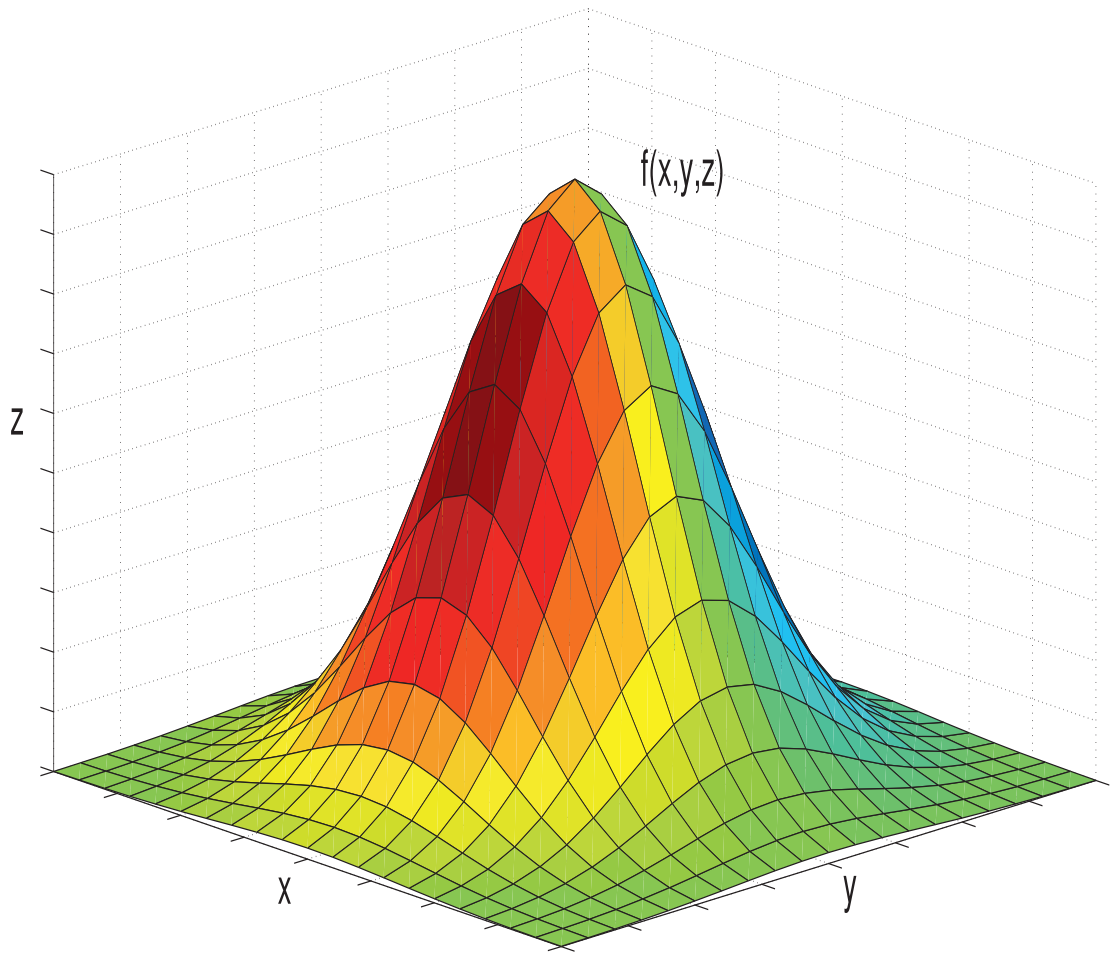

Figure 1.6 Local maximum of function f(x,y,z).

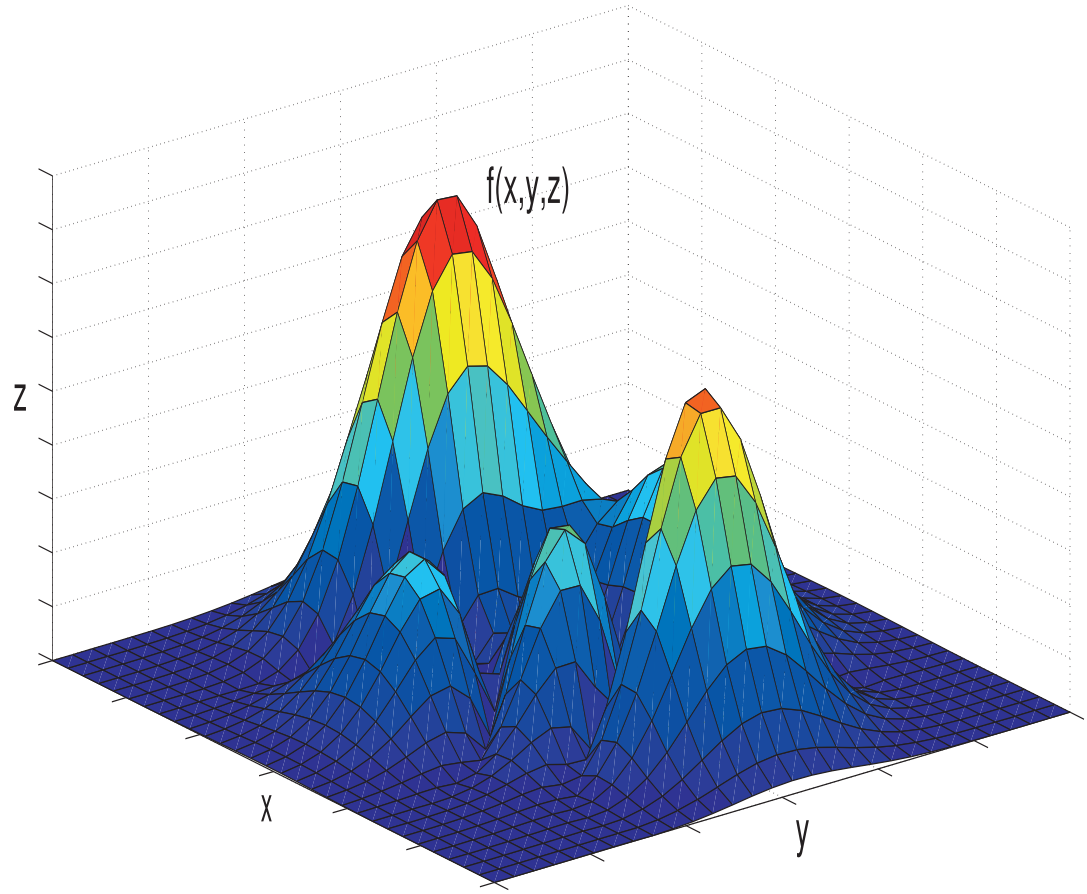

Figure 1.7 Extended domain of function f(x,y,z) showing multiple maximas.

1.4.2 Enumerative Optimization Schemes

The idea of an enumerative (also known as exhaustive) search is possibly the most straight forward method. Within a finite search space, the algorithm will evaluate the desired objective function at all possible points within the space. The simplicity of this search is very attractive, and for small solution spaces can be effective. However, for more complex problems, these methods lack the necessary efficiency. Searching a large sample space element by element simply takes far to long.

1.4.3 Random Search Algorithms

Random search algorithms have been shown to be effective for many problems. These search methods involve randomly selecting points along the desired solution space, as opposed to an exhaustive search searching every point. These techniques also have some of the short comings of the exhaustive searches. Once again, the efficiency of such a search can be far too low for very complex problems. However, for many desired solution spaces, a random search is able to find satisfactory results.

1.4.4 Genetic Algorithm Optimization

The genetic algorithm (GA) is an optimization and search technique based on the principles of natural selection. These algorithms are widely used in many different engineering applications in a wide range of fields. A GA allows a population composed of many individuals to "evolve" under specific rules in order to maximize a desired fitness, or cost, function associated with the current problem. GA optimization has many advantages over the optimization techniques described previously. For example, the GA can optimize with continuous or discrete values, although in this work only the discrete binary GA is used. In addition, this method does not require and derivative information. GAs can also simultaneously search a wide range of objective functions and deal with a large number of variables.

In addition, finding a local minimum or maximum as opposed to a global one is not an issue with a GA, meaning that extremely complex objective functions can be evaluated. Finally, GAs also work very well with numerically or experimentally generated data as opposed to analytic functions. These advantages provide an interesting optimization approach that can solve many problems the previous search and optimization methods cannot. A thorough explanation of the processes of the GA optimization technique is presented in the section, with each component explained separately. In addition, some current applications of GA optimization in electromagnetic problems are presented.

1.4.4.1 Fitness Functions and Chromosomes

A fitness function (sometimes called a cost function) represent the desired solution space that the GA will attempt to minimize (sometimes maximize). This function generates an output from a set of input variables. These input variables in the GA are referred to as a chromosome. The GA begins by defining a chromosome array to be optimized. If the length of the chromosome is N_{bits}, and each element of the chromosome are given by P_{Nbits}, then a chromosome can be written in the following way.

$$chromosome = [P_1, P_2, ..., P_{Nbits}] \tag{1.2}$$

1.4.4.2 Variable Selection

As the variables of the GA are represented as binary, the actual meaning of the variables must be translated into binary bits. To illustrate this concept, a sheet discretized into square pixels with equal sides of a length is shown in Figure 1.8. Each pixel can be in two possible states, on or off. In this case, a 1 can be thought of as an on state, and a 0 can be thought of as an off state. The grid has 10 rows and 10 columns, and the overall geometry is representative of a chromosome of 100 bit length. For example, the the chromosome representing the

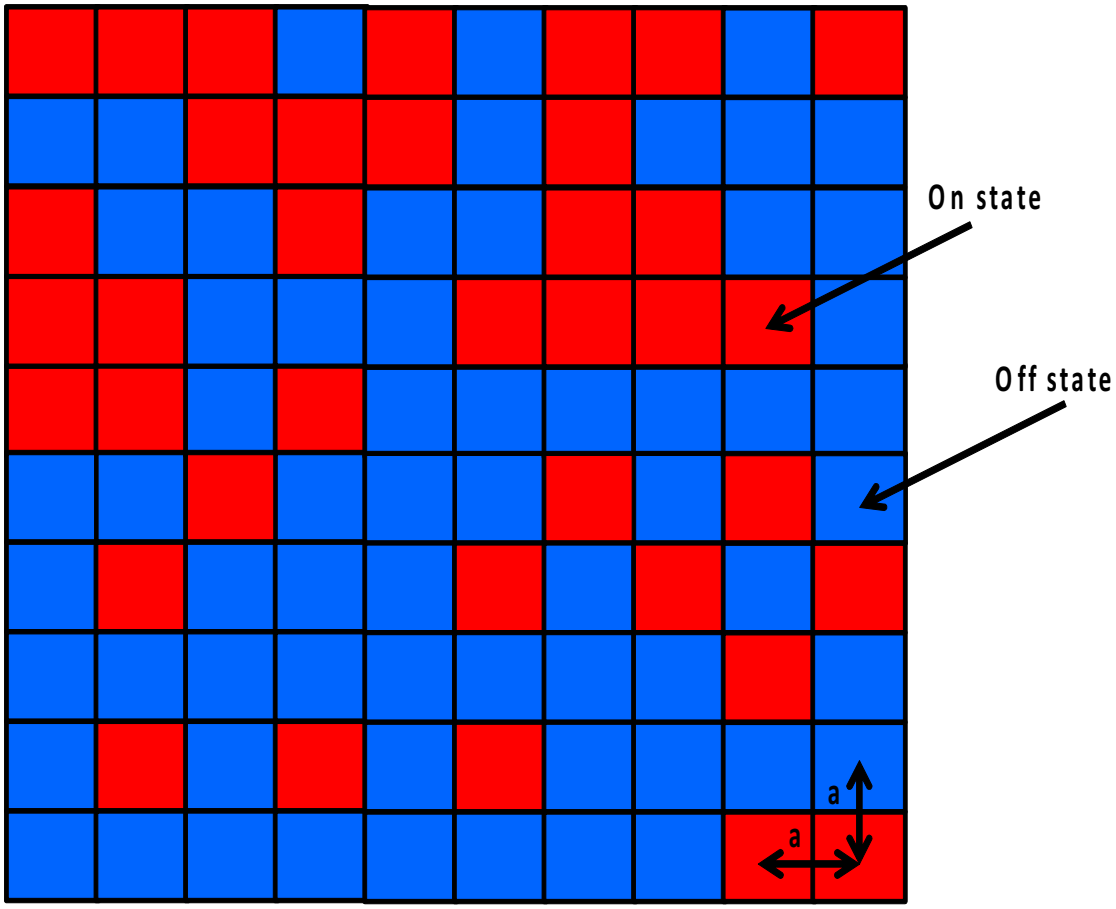

Figure 1.8 Sample discretized pixel grid.

geometry of the grid can be written as be represented as in equation 1.3.

$$chromosome = [1110101101....] \tag{1.3}$$

With this discretization, the binary bits are able to be represented in the geometry we wish to optimize.

1.4.4.3 Population

The collection of all the chromosomes within the GA is known as the population. The population has N_{pop} chromosomes and each chromosome has N_{bits} so the population will be an matrix of N_{pop} by N_{bits} in size. In order to begin the GA optimization process, an initial population must be generated. The initial population is found by performing a random search and filling the population with random ones and zeros. This initial population is then passed into the fitness function to be evaluated.

1.4.4.4 Selection

From the evaluation of the initial population, the best chromosomes are selected by the GA. This is done by first ranking the chromosomes from best to worse according to the desired fitness function. From here, only the best chromosomes are kept and the others are discarded. The number of chromosomes to be kept are selected based on the selection rate, X_{rate}, which represented the fraction of the N_{pop} chromosomes that are kept. The number of chromosomes that are kept are given by

$$N_{keep} = X_{rate} N_{pop} \tag{1.4}$$

Selection occurs at each iteration (known as a generation) of the algorithm. Deciding how

many chromosomes are kept depends on the application. However, keeping too few will limit the availability of genes in the offspring. Keeping too many chromosomes could bring in too many bad performers from the previous generation.

Two chromosomes are then selected from the remaining chromosomes N_{keep} to produce two new offspring until the discard chromosomes are replaced. While there are a number of techniques used for the selection of the new chromosomes, a tournament selection method is used throughout this thesis. Tournament selection involves randomly picking a small subset of chromosomes from the remaining pool, and the chromosome within this selection with the best fitness is chosen to become a parent. The tournament repeats until every parent needed to regenerate the population of chromosomes are found. This method works especially well for large populations because there is no extra sorting necessary.

1.4.4.5 Mating

Mating is the creation of offspring from the parents found in the selection process. The most common form of mating involves two parents which create two offspring. A crossover point between two parents is chosen randomly between the first and last bit of both parents chromosomes. The first parent will pass its binary code to the left of the crossover point to the first offspring. The second parent also passes its binary code to the second offspring from the left of the same crossover point. The binary code to the right of the crossover point of the first parent is then passed to the second offspring, while the binary bits to the right of the crossover point for the second parent are passed to the first offspring. This leaves us with two offspring with the genetic makeup of both parents, which are used to replace the two parents selected for N_{keep}. This process is summarized in Figure 1.9

1.4.4.6 Mutations

Random mutations are also used to alter the a percentage of the remaining population matrix. Mutation introduces another element to the optimization process by introducing traits into

the population that were not initially present in the selected parents and offspring. In the binary GA, mutation can be as simple as changing a single bit in a chromosome from a 1 to a 0, or vice versa. Mutation is important for the GA process as it introduces traits not found in the selected parents and offspring to fill the population. Without mutation, the GA may converge too quickly to an answer that does not include other possible combinations. The number of mutations are given by equation 1.5, where μ_{rate} is the desired number of mutations for the entire population.

$$mutations = \mu_{rate}(N_{pop} - 1)N_{bits} \tag{1.5}$$

1.4.4.7 Convergence and Future Generations

After the mutations takes place and the fitness functions associated with the offspring are calculated, the results are compared with a stopping criteria. If the stopping criteria is not met, the algorithm takes the current population and begins the selection process again in a new generation. If the criteria is met, the algorithm will stop and the results will be exported. The overall GA optimization process is shown in Figure 1.10.

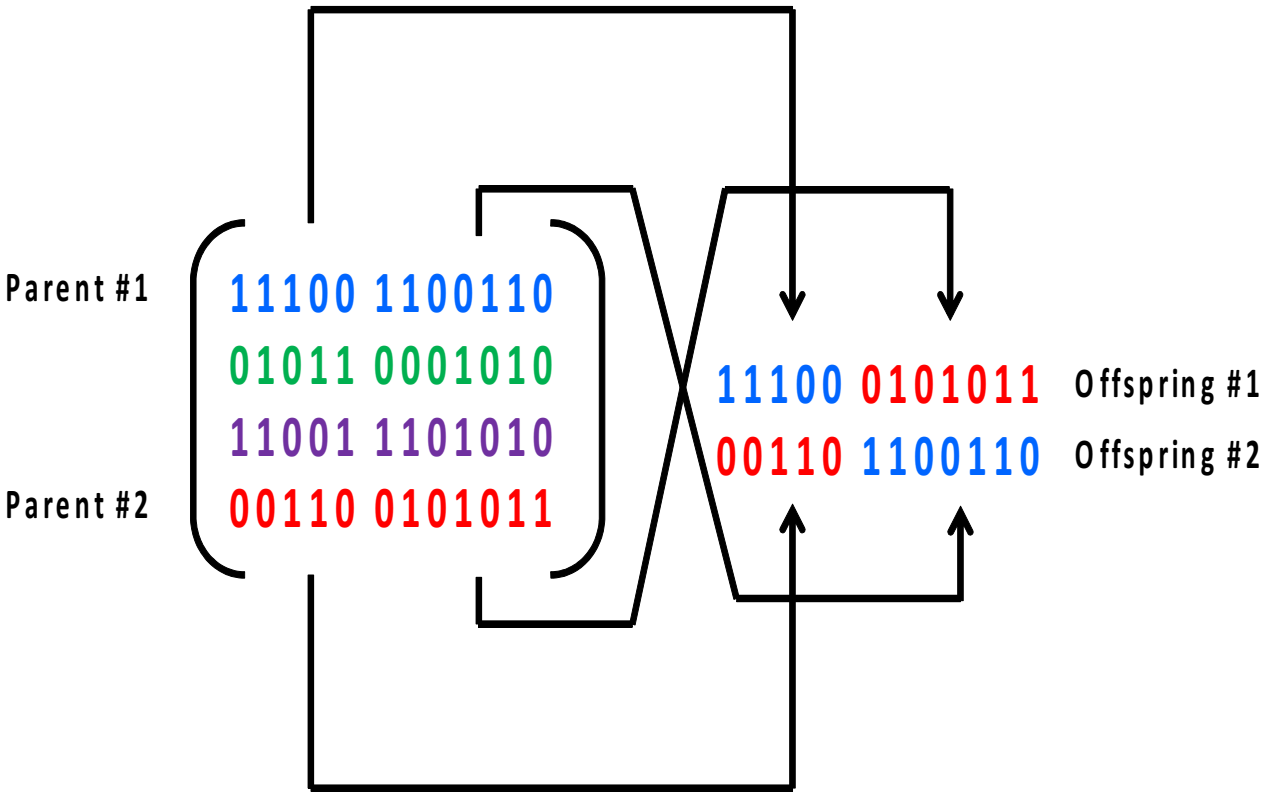

Figure 1.9 Mating process in the binary genetic algorithm.

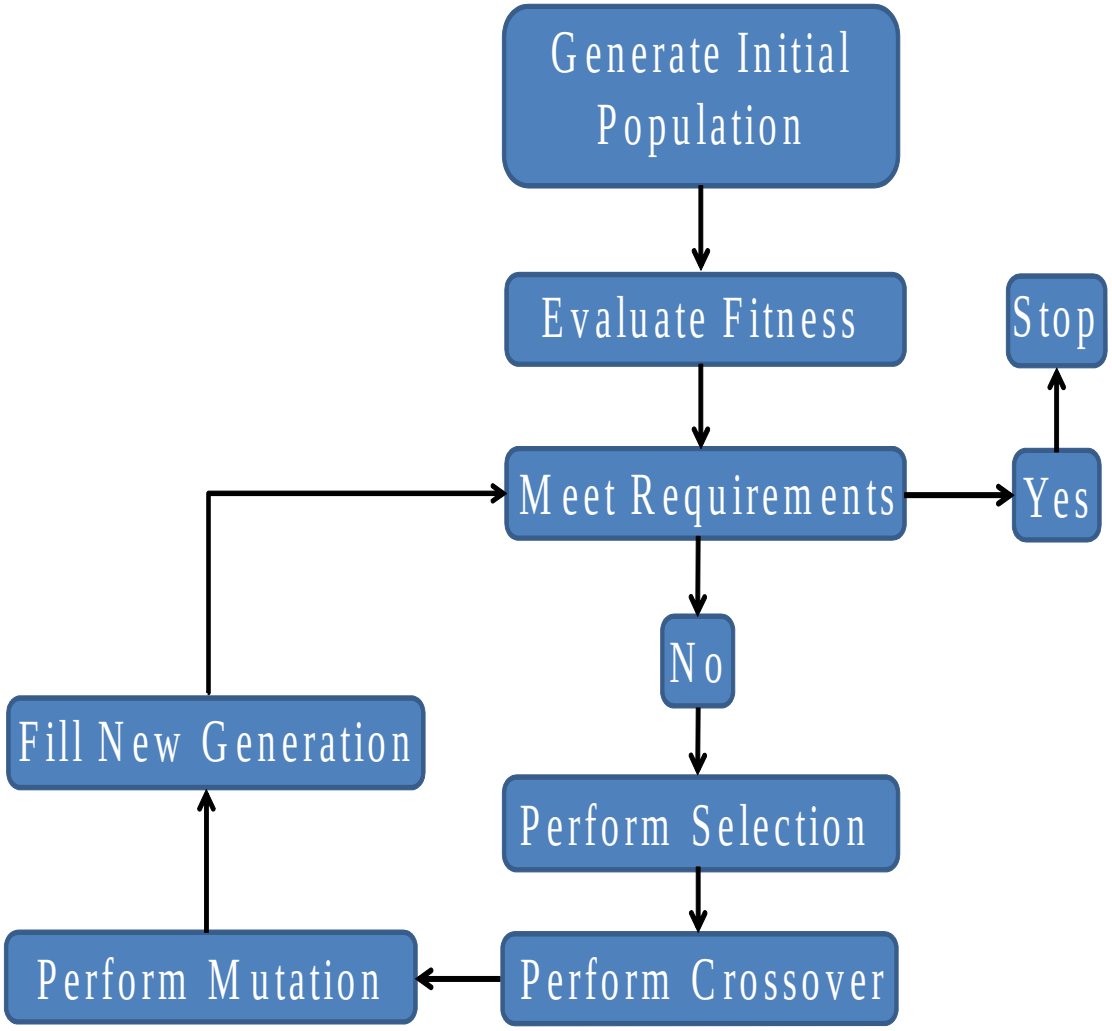

Figure 1.10 Summary of genetic algorithm optimization process.

1.4.5 Applications of Genetic Algorithms in Electromagnetics

Genetic algorithms are used as an optimization tool in a wide variety of Electromagnetics problems. In [75], genetic algorithms are used to synthesize light-weight, broadband microwave absorbers. The absorber is intended to be as light-weight as possible, while being thin and multi-layered, backed with a PEC conductor. Each layer of the antenna is optimized with a frequency dependent material, while the permittivity and permeability are varied. The reflectivity of the array is optimized while changing the materials in the array-stack, while keeping the stack as thin as possible. A wide range of frequency absorbers are designed, with reflection coefficients ranging from .2-8GHz.

These algorithms have also been used in the design of frequency selective surface (FSS) structures [76]. In this work, the FSS structures are desired to be used as waveguide filters. As the filter characteristics depend upon the shape and size of the individual elements, as well as the number of element layers, both are optimized with the GA. Very strong bandpass and bandstop filters are shown in this work, at frequencies as high as 25GHz.

GAs are also widely used in antenna array design. In [77], the sidelobe levels of an antenna array are decreased by thinning or removing the elements that makeup an array. This is done by representing the elements with a binary number, and turning them to either a 1 or 0 based on if the element is on or off. Extremely low sidelobe levels, as low as -22dB, are reported. Refrence [78] uses the genetic algorithm to optimize a linear antenna array to shape the mainbeam of the radiation pattern. In this case, the goal is to select a set of amplitude and phase coefficients for the antenna to achieve a narrow beam at a specific location.

Optimization has also been done extensively on single antenna elements. In [79], a patch antenna is optimized so that the bandwidth of the antenna is significantly wider than a traditional patch. The GA is coupled with a method of moments so that a binary string could represent the presence or absence of a subsection of metal in the patch. With this

method, the bandwidth of one patch was able to be increased by approximately 20%. The GA optimization method has also been recently used to miniaturize antennas.

In [69], a patch antenna is miniaturized by placing SRRs between the top layer of the antenna and the ground plane. The geometry of the SRRs are optimized with a GA, while the fitness function is designed to minimize the reflection coefficient of the antenna. A good impedance match and radiation characteristics are maintained with the optimization, and one state is shown to achieve a miniaturization of approximately 1/16th the size of the original patch. [68] presents a loop antenna that is miniaturized using a binary GA. The loop antenna is printed on a planar dielectric, with a pixelized sheet directly above it. Each pixel is controlled with the binary GA and the fitness function is chosen to miniaturize the reflection coefficient at a desired frequency.

Another miniaturization method is presented in [71]. In this work, a monopole antenna is surrounded by a metallic pixelized grid controlled by a binary GA. The pixel grid is used to miniaturize the antenna through control of the GA. The radiation characteristics of the monopole are well maintained throughout the miniaturization, and an overall miniaturization of $\lambda_0/26$ is achieved. All three of these methods are implemented using a HFSS-matlab interface, which will be discussed in detail in the following section.

1.5 HFSS-MATLAB Optimization Interface

In order to implement the GA optimization successfully with an electromagnetics problem, a numerical solution method must usually be implemented. While some simple problems can be solved through analytic equations, most require approximate solutions. There are many numerical solution techniques that can be used, however, perhaps the most popular method is in the use of commercial electromagnetics solvers. One such commercial solver is Ansys High Frequency Structural Simulator (HFSS), which is based on a finite element method. This solver has a CAD like interface which can be easily used and can implement a number

of solution methods in both the frequency and time domain.

Implementing a GA to solve a problem iteratively is unfortunately not available in HFSS. However, HFSS commands are able to be executed through simple macro scripts that can be imported and run in real time. These macros can be executed through MATLAB, and compiled into a script which can be imported to HFSS. This allows for the automated creation of geometry, boundary conditions, and excitations in HFSS. This allows the geometry to be altered after every iteration of a parameter, meaning a GA can be used to optimize structures with an interface between HFSS and matlab.

An overall flow of the optimization process is as follows. First, matlab is launched and the GA parameters are initialized. The geometry is then created for the first iteration of the GA. The script is then assembled and HFSS is launched. The script is passed to HFSS, and the geometry is drawn in real time. The structure is then simulated, and the relevant results are exported back to matlab for post processing. If these results meet the desired requirements, then the GA is stopped. However, if the results do not meet the requirements desired, the overall process is restarted with a new geometry and the next iteration of the GA is performed. The overall flowchart for this process is shown in Figure 1.11.

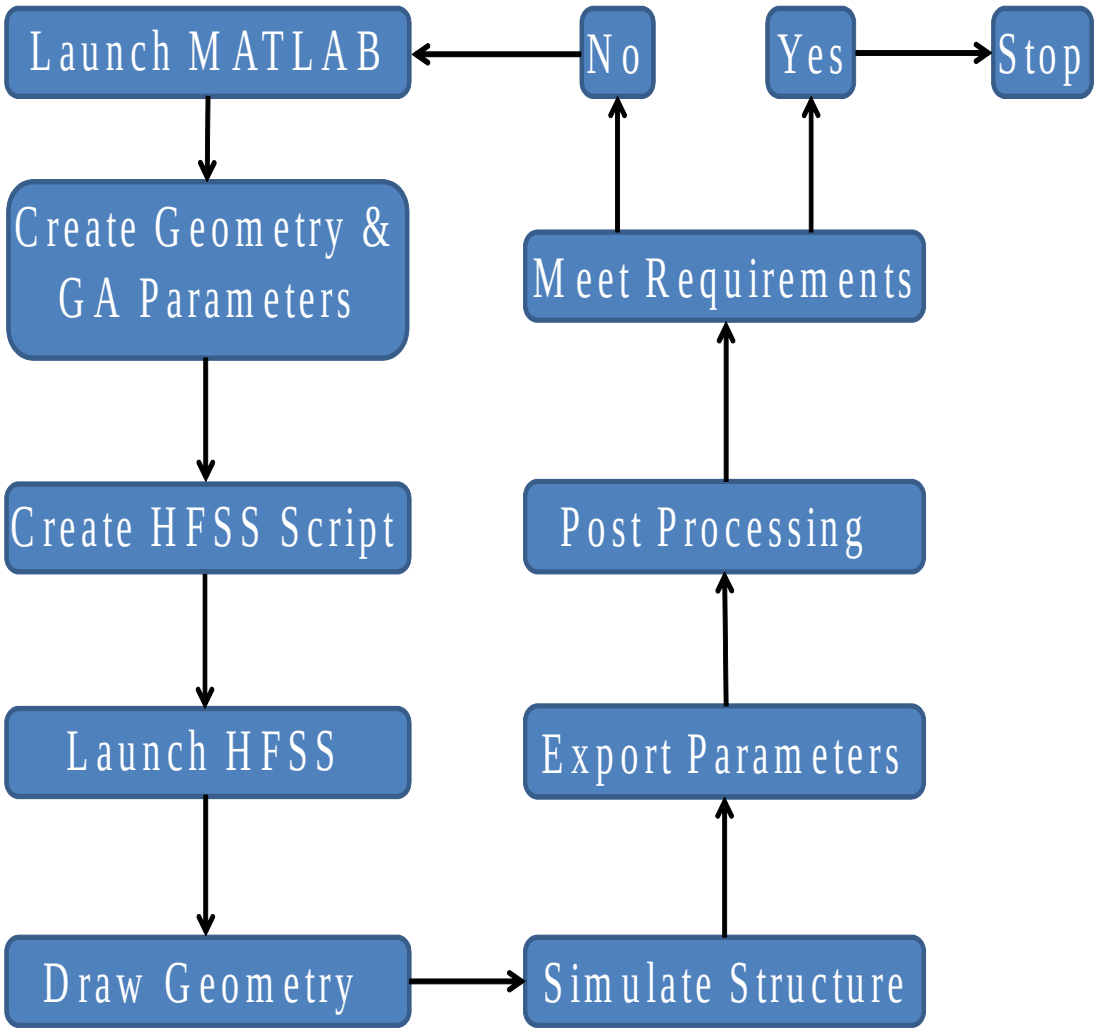

Figure 1.11 Genetic algorithm Matlab-HFSS interface flowchart

1.6 Research Overview

The work in this thesis introduces a new approach to the tuning of a miniaturized antenna. A distributed pixelized grid structure is placed on a thin substrate directly on top of the miniaturized antenna introduced in [71]. The pixel grid is envisioned to be composed of a photo conductive or phase change material layer, allowing each discrete pixel to be turned on or off through photo-illumination. This second grid layer is optimized via a binary GA in a similar manner to the bottom layer, where a 1 corresponds to a high conductivity (illuminated pixel) and a 0 corresponds to no pixel (no illumination). Once a suitable state for a desired frequency is found with the GA, each pixel corresponding to that state may be illuminated in real-time, tuning the antenna to the desired frequency. This overall process is shown in Figure 1.12.

Chapter 2 introduces the specifics regarding the original miniaturized antenna presented in [71]. A proof of concept of adding the second layer of the antenna is first presented. In this case, the reflection coefficients and radiation patterns of the antenna are studied as the layer and pixels are added to determine the level of effect on the monopole antenna characteristics. Next, the design of the second layer and numerous simulated results are presented. The radiation efficiency and reflection coefficients are optimized in unison using the HFSS-matlab GA interface. The theoretical tuning range of the second layer is also investigated. These simulations are first carried out using copper as the pixel material, however, a variety of conductivities are also tested showing a wide range of pixel materials are possible.

Chapter 3 describes the fabrication and measurement of the antennas with a copper tuning layer. Multiple states are fabricated that cover a wide range of frequencies to show the potential of the second layer as a tuning element. Thin Polyethylene terephthalate (PET) layers are first investigated to be used as a simple insert that can be placed on the antenna as a loading structure. The airgap and misalignment between the PET layer and

the antenna are investigated and prove to be to large of a obstacle to overcome. However, a multi-layer fabrication method is then presented which eliminates airgaps between the layers and minimizes misalignment. Measured reflection coefficients and radiation patterns are investigated of multiple states corresponding to a very wide frequency range. The final chapter discusses any concluding results and suggestions for future work.

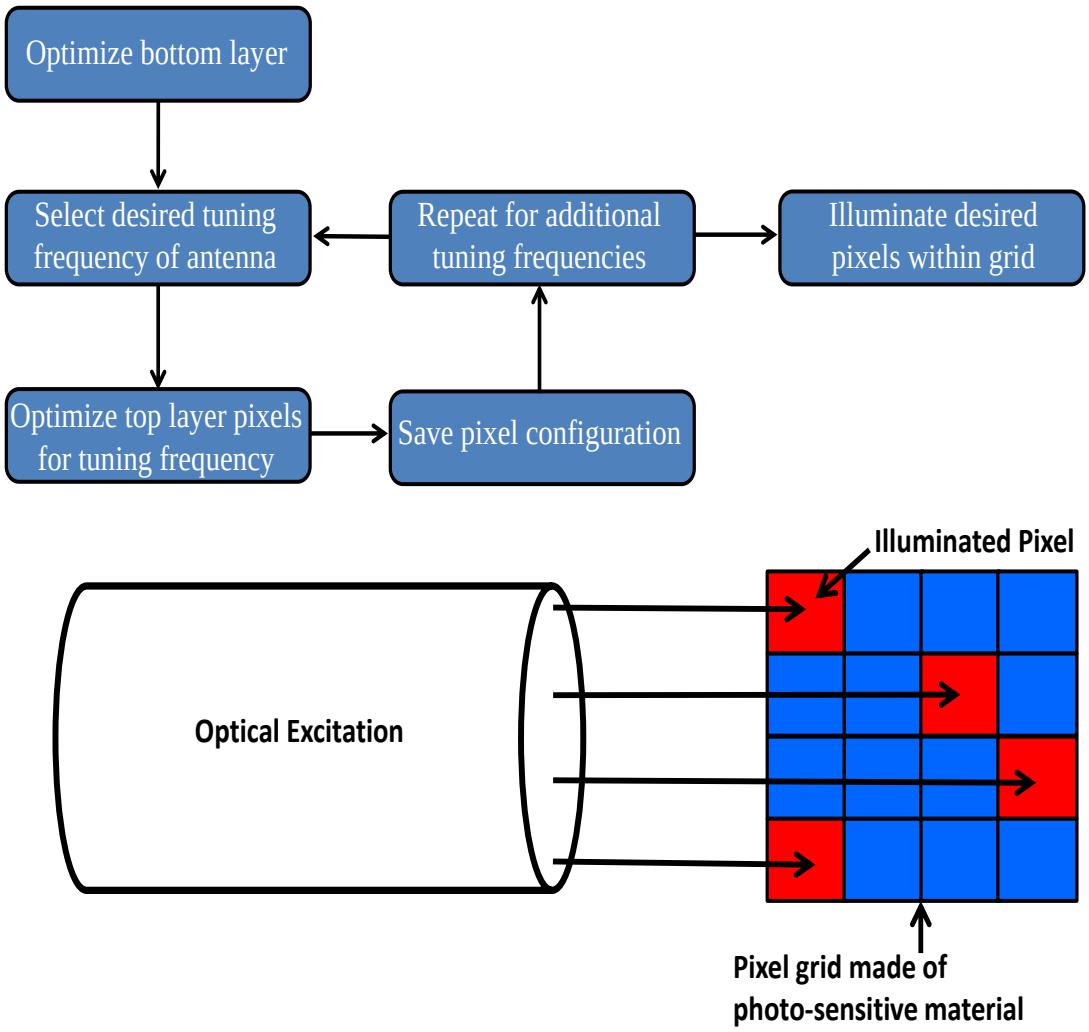

Figure 1.12 Optical excitation of second pixel grid.

CHAPTER 2

Design and Simulations

In this chapter, the miniaturized monopole antenna of [71]is briefly introduced. The bandwidth of this antenna is shown to be relatively small, leading to a need for a reliable frequency tuning technique. To tune the antenna in frequency, the pixelized grid is extended directly on top of the antenna. First, a brief proof of concept is presented, showing that the radiation and reflection characteristics of the antenna are largely unaltered by adding a second grid. The design of the second layer tuning grid is then introduced, and the GA used to optimize the structure is explained in detail. Next, the tuning layer is optimized over a wide range of frequencies, and a multitude of antenna configurations are able to be found with very good reflection coefficients over a wide frequency range. The pixel conductivities are also examined, showing that nearly any metal or conductive material can be used as the material for the pixel grid. Finally, the optimization is extended to not only minimize the reflection coefficient of the antenna, but also increase the radiation efficiency. This optimization is used to not only produce a more efficient antenna, but also demonstrate the theoretical tuning range of the second layer.

2.1 Miniaturization of a Monopole Antenna Using a Distributed Pixel Grid

The initial miniaturized antenna presented in [71] is briefly summarized in this section. A folded monopole antenna is fed by a co-planar waveguide (CPW) and surrounded by a metallic grid structure. The metallic grid structure is intended to be used as a parasitic loading element to alter the electrical characteristics of the patch. The monopole antenna and pixelized patch are placed on a .5mm thick Rogers RO4003 substrate, along with the co-planar ground plane. The Rogers RO4003 substrate has a dielectric constant of $\epsilon_r = 3.55$ and a loss tangent of $\delta = .0027$. The structure is shaped into a half-disk of radius 5.2mm to further miniaturize the overall size. the grid is discretized into 134 square pixels $500\mu m$ in size. The total number of possible combinations is then 2^{134} or $2.1778x10^{40}$ possible pixel states.

2.1.1 GA optimization

The large number of pixel configurations suggests the use of a binary optimizer capable of quickly finding pixel configurations that produce an acceptable performance. A brief summary of the GA optimization applied to the miniaturized antenna is presented here, but a more in depth explanation is presented in section 2.3.2 Each pixel is encoded with a binary 1 or 0, correspond to metal either being in place or absent. The geometry of this antenna is displayed in Figure 2.1, with one possible configuration shown in red. The state of each pixel is optimized with a binary GA, and the fitness function is given by equation 2.1.

$$fitness = 20log_{10}(|S_{11}|) \tag{2.1}$$

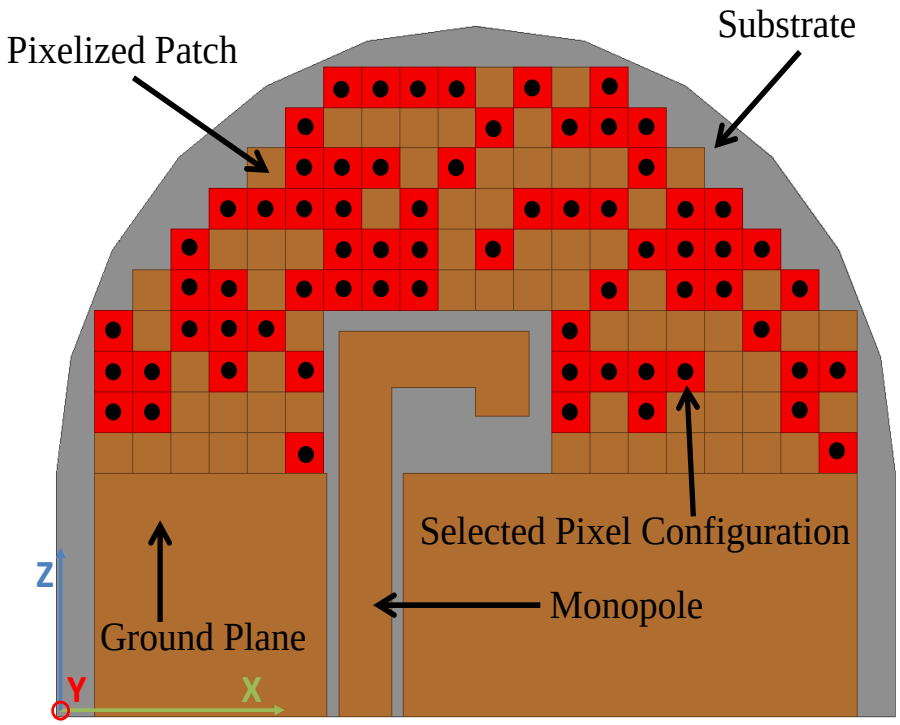

Figure 2.1 Geometry of miniaturized antenna. The selected pixel configuration is shown in red, corresponding to a resonance of 2.5 GHz.

The objective of the GA is to minimize this fitness function at a frequency of interest. The GA uses a tournament selection method with an initial population of 200 and a 10% selection rate. Each chromosome is then 134 bits long, with a population matrix with 134 by 200 entries. The mutation rate is also set at 20%, with a 2-point crossover with an evolving single bit mutation. The GA is allowed to run for a maximum of three generations or until the desired results are met. The GA is built in matalb, and interface with HFSS to allow for automation of the antenna geometry and solutions as described in section 1.5.

2.1.2 Demonstration of Antenna Miniaturization

A particular antenna configuration is selected which corresponds to a resonant frequency of 2.5 GHz. The pixels selected that compose this configuration are shown in red in Figure 2.1. To determine the amount of antenna miniaturization, the reflection coefficient before and after the added grid are studied. Both reflection coefficients are shown Figure 2.2. The resonance of the antenna without any of the pixels added is around 5GHz, with a magnitude of under -20dB. However, once the optimized pixels are added, the resonance shifts to approximately 2.5GHz. At this frequency the antenna is miniaturized by roughly 50%, and the overall size of the antenna is approximately $\lambda_0/24$, reduced from $\lambda_0/4$. The simulated radiation patterns are also investigated to determine if typical monopole antenna radiation characteristics are maintained. Figure 2.3 shows the radiation pattern in the azimuth (XY) and elevation (YZ) planes. Both patterns exhibit what we would expect from a monopole antenna, uni-directional in azimuth, and a bi-directional pattern in the elevation planes. From these results it can be seen that the antenna exhibits very high miniaturization in simulation, but the antenna must also be built and tested to determine its real world performance.

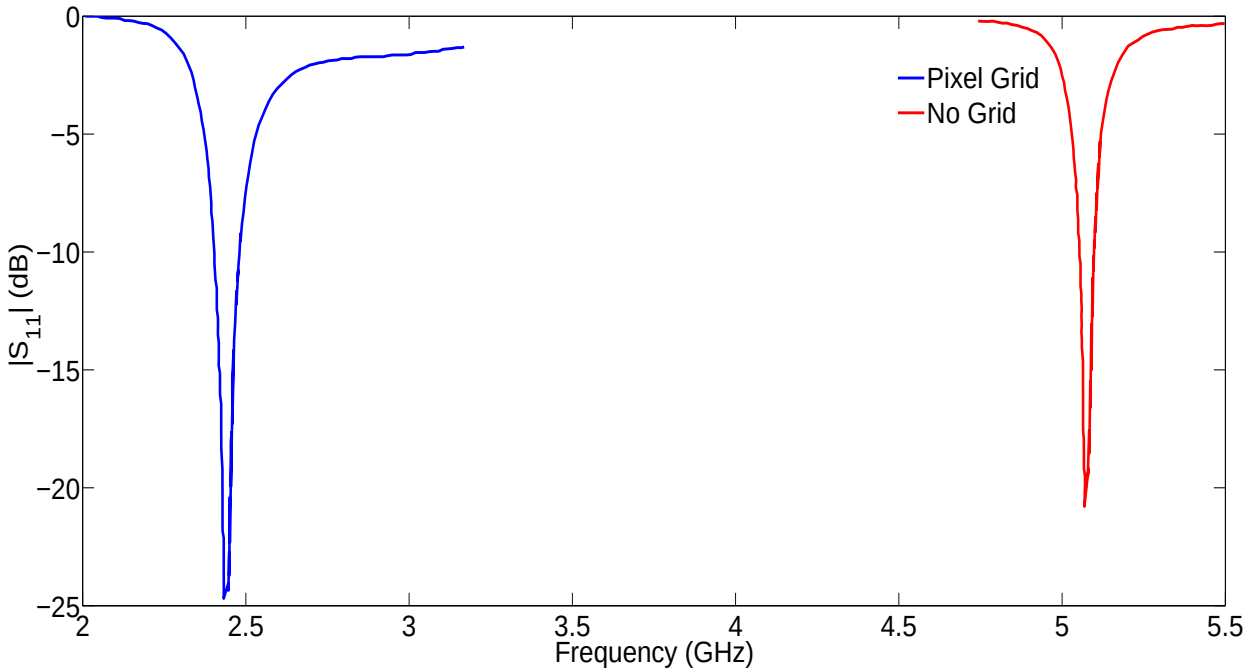

Figure 2.2 Reflection coefficient of monopole antenna with and without optimized pixel grid.

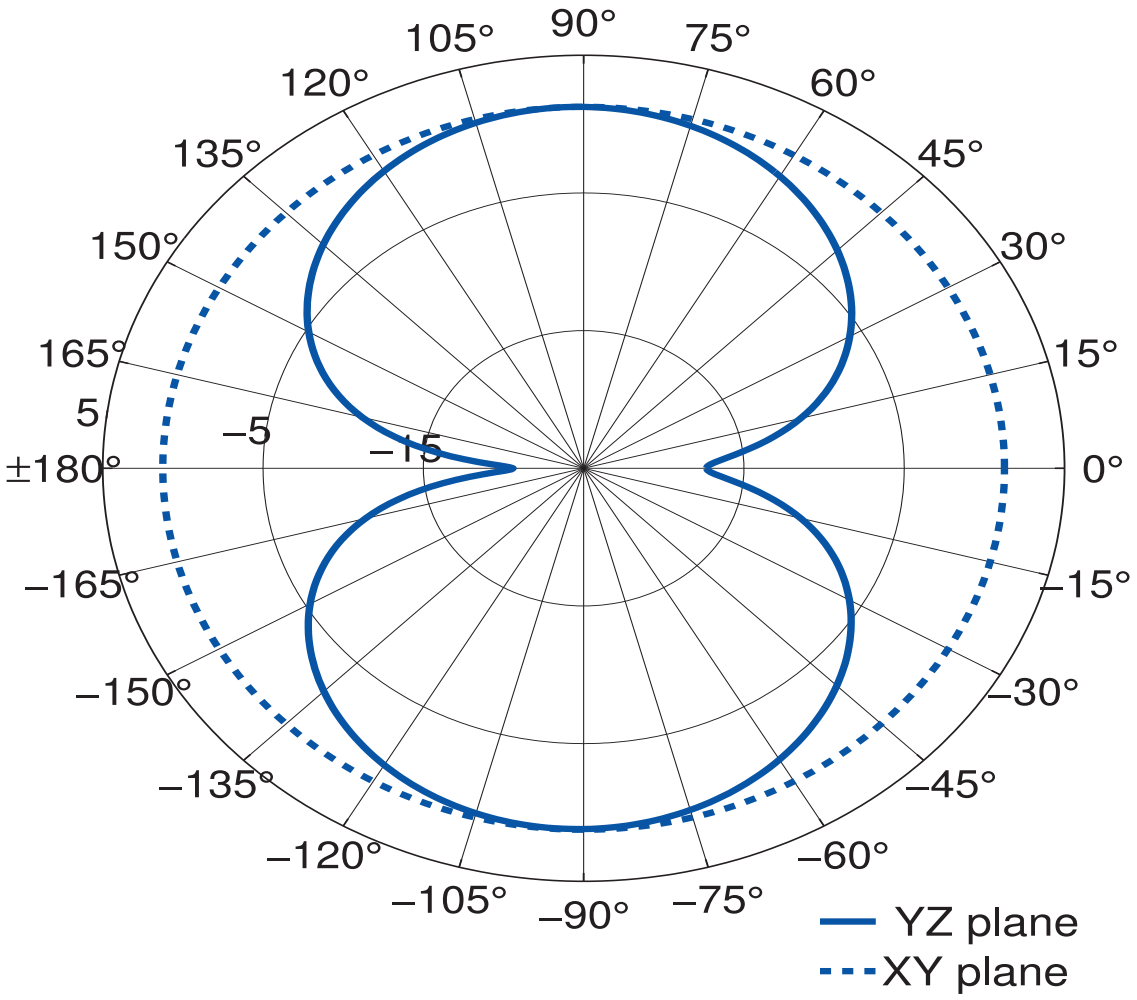

Figure 2.3 Simulated radiation patterns in the XY and YZ planes.

2.1.3 Fabrication and Measured Results

The antenna is fabricated using conventional micro-fabrication in a clean room environment. Care is taken so that the edges of the pixels are overlapping. If the pixels edges are simply left the same as in the simulations, undercut will cause the pixels to no longer be electrically connected. A small shorting pin between the pixels is added to the structure so that the electrical connection is maintained. Figure 2.4 shows the pixel structure under magnification, where the edges of the pixels can be seen. Without the shorting structure, it is clear that the pixels would no be electrically connected, although this method may slightly effect the measured results, it is a necessary step. A fabricated antenna designed for operation at 2.5 GHz is shown in Figure 2.5.

To properly characterize the antenna miniaturization, the reflection coefficient was measured using a Agilent N5227A network analyzer. The measured reflection coefficient of an antenna configuration at 2.5 GHz compared with the simulated result is shown in Figure 2.6. The results show very good agreement between measurement and simulations. The magnitude of the reflection coefficient matches very well, while the location is only shifted by approximately 100MHz. These slight discrepancies are most likely caused by the added structure between pixels to prevent undercut. Overall, this antenna presents many desired traits, such as a high amount of miniaturization, a strongly resonant reflection coefficient, and good agreement between simulations and measurement. However, as discussed in chapter 1, miniaturized antennas of this kind have very narrow bandwidth, requiring frequency tuning structures.

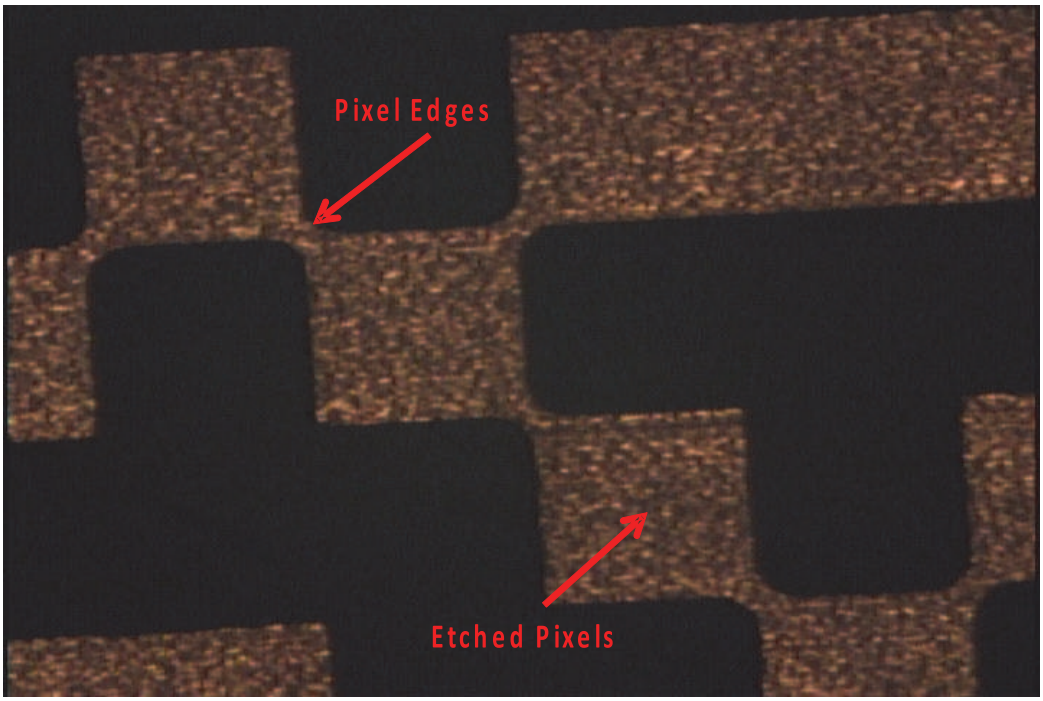

Figure 2.4 Fabricated pixel edges.

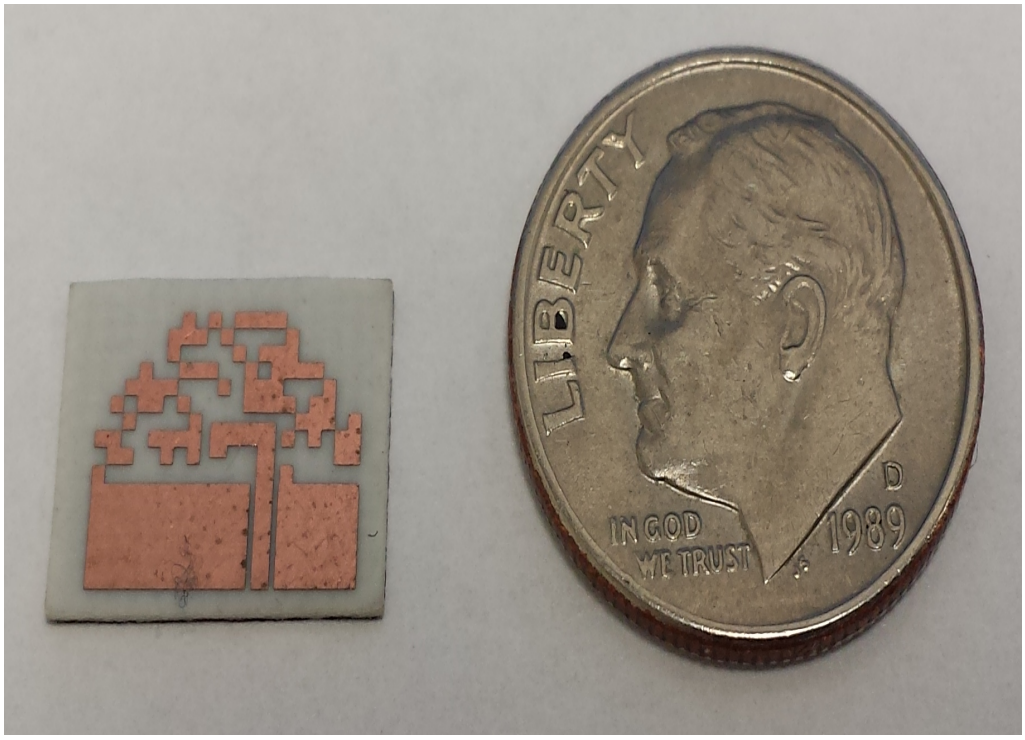

Figure 2.5 Fabricated antenna compared with a US dime.

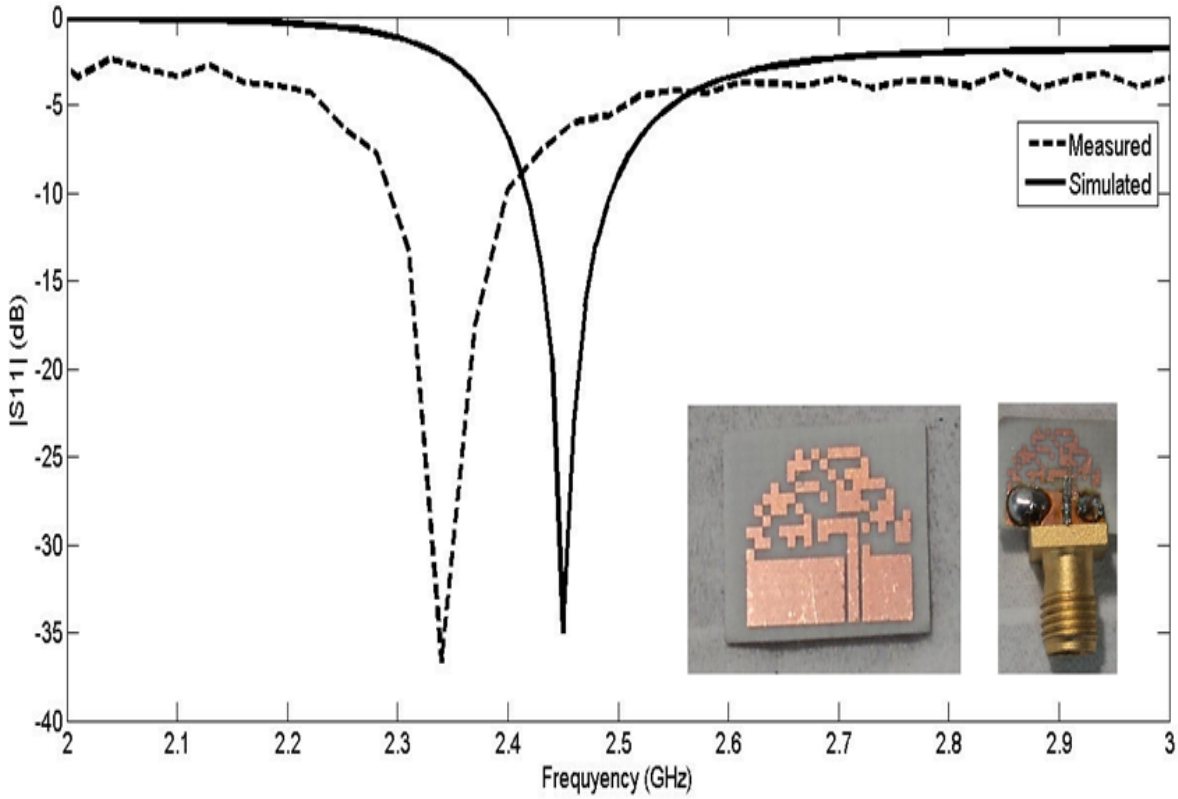

Figure 2.6 Simulated and measured reflection coefficient of miniaturized antenna.

2.2 Effects of a Second Tuning Layer on Antenna Characteristics

To use a second metamaterial structure as a tuning element for the antenna first requires a study of the effects this layer will have on the original antenna's characteristics. The effects of a second layer are first tested using a thin $25m$ piece of the same rogers material that the antenna was originally fabricated with. The effect of the layer itself, as well as multiple sample pixel combinations, are studied. The overall geometry and pixel setup is shown in Figure 2.7. The layer is covered in two pixel groups, labeled as pixels A and B. The simulated reflection coefficient with each combination is shown in Figure 2.8. The reflection coefficients show relatively little change between each combination in terms of the magnitude of the resonance, however, the location of the resonance is slightly shifted.

Two primary observations can be made from these results. The first is that little change is shown in the reflection coefficients between the adding of the pixels and the second layer and the original antenna. This is a desired results because if the resonance was greatly affected with just a few pixels than adding an entire pixel grid may completely change the characteristics of the antenna. Although it is more applicable to the radiation characteristics of the antenna, these observations are also applicable to the reflection coefficients as well. The second is that some tuning is shown between each pixel combination, meaning that pixels added on top of the layer have potential to be used as a tuning element.

The radiation patterns of the antenna are also studied with and without the dielectric layer. The patterns are studied in two primary planes, the azimuth and elevation plane. In this case, the azimuth plane refers to the XY plane, and the elevation plane refers to the YZ plane. In the azimuth plane, a monopole antenna is expected to exhibit a simple uni-directional antenna pattern (similar to a circle). Both the antenna with and without the layer added have very little differences in the radiation patterns in this plane. Similarly, in the elevation plane, the expected pattern for a monopole antenna is bi-directional in the

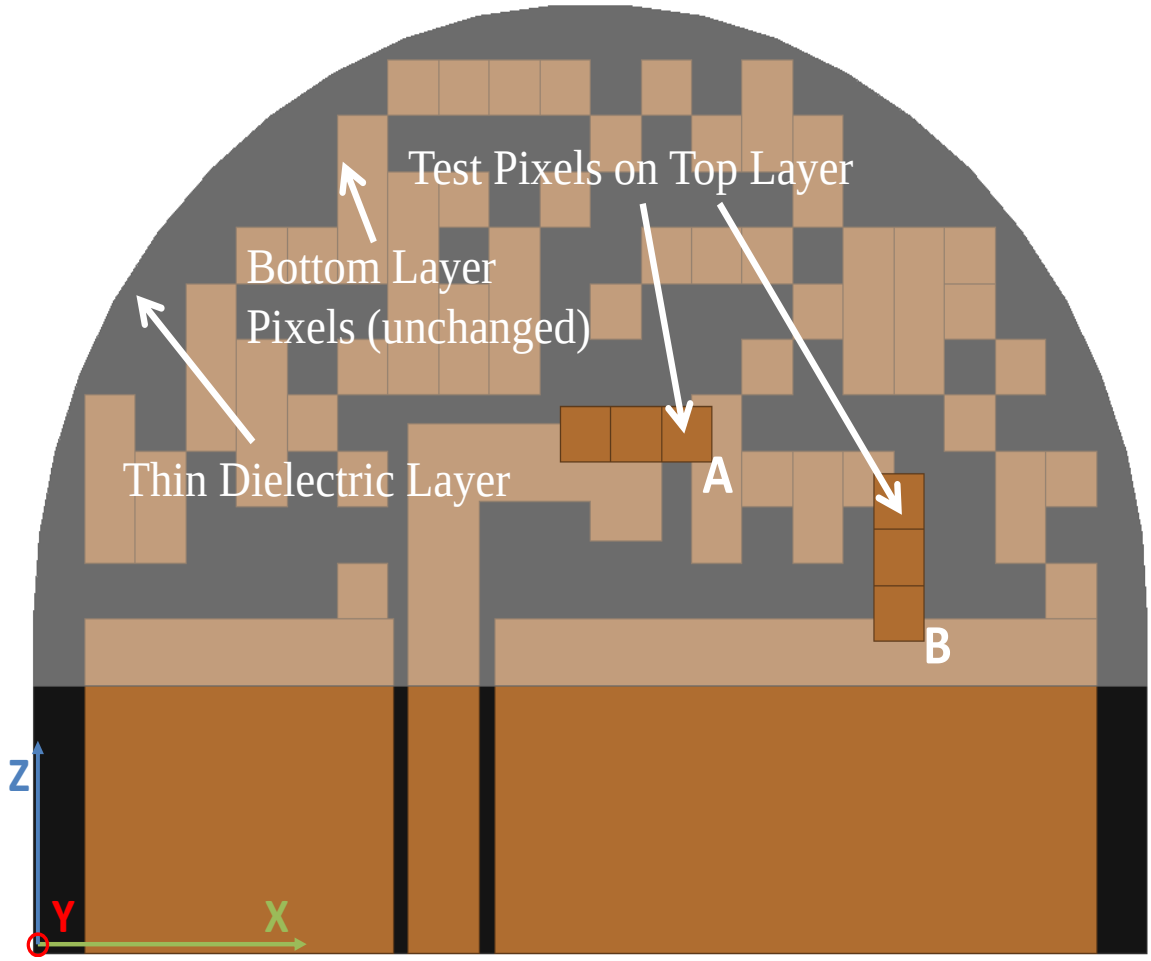

Figure 2.7 Miniaturized antenna with added dielectric layer and pixels.

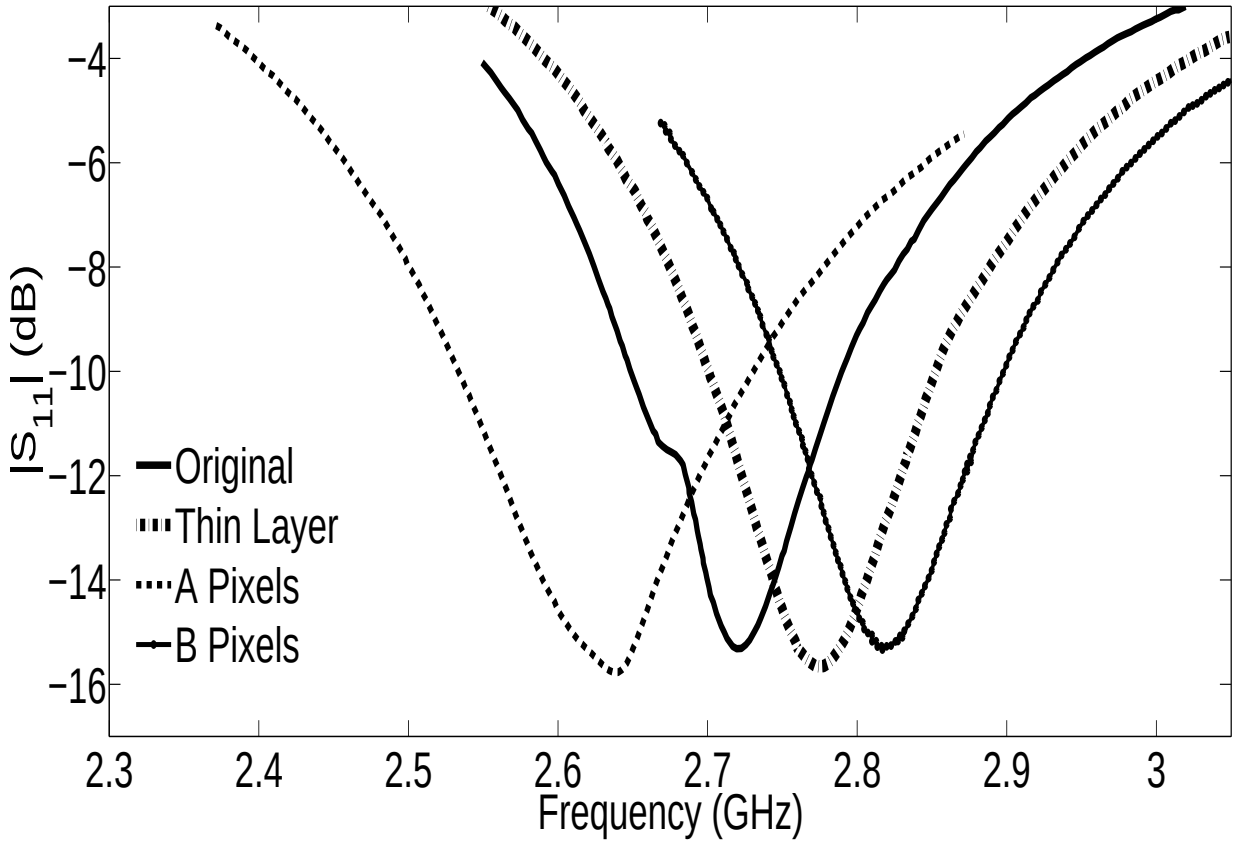

Figure 2.8 Effect of multiple pixel configurations of second layer on reflection coefficient of the antenna.

shape of a figure eight. In this plane, the results also match very well for both with and without the dielectric layer. These results are very encouraging as the radiation pattern is maintained in both planes despite the addition of the layer. This suggests that the pixelization, as well as the added dielectric layer, have little effect on the radiation characteristics of the monopole antenna.

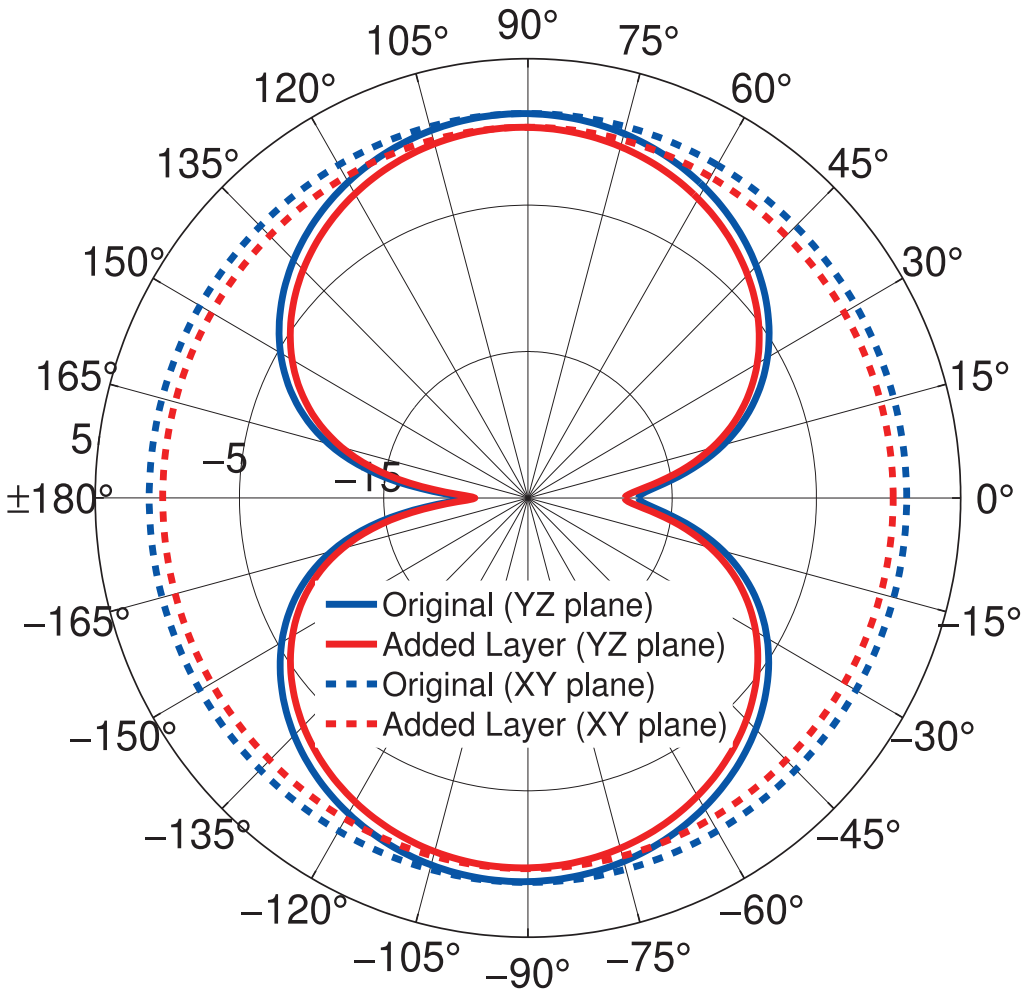

Figure 2.9 Comparison of the radiation patterns of the antenna with the added dielectric layer.

2.3 Design of Second Tuning Layer

2.3.1 Second Layer Configuration

As discussed in the previous section, the addition of a second layer to the antenna does not have negative impact on the radiation characteristics of the monopole. However, the location of the reflection coefficient is shown to shift with different pixel combinations. In order to exploit this shift in resonance, another pixelized patch is placed directly above the dielectric layer. In this thesis, this added layer will be commonly referred to as the top layer of the antenna, and the original miniaturized antenna will be referred to as the bottom layer of the antenna. The pixel size for the second layer is designed to be the same as the first layer, but the grid is no longer limited to the geometry surrounding the antenna. Thus, the pixel grid is extended to envelope the entire antenna, utilizing a 178 pixel grid, with 2^{178} possible combinations. The geometry of the antenna with the second pixel grid is shown in Figure 2.10.

To utilize the top layer as a tuning element, each pixel is made of a suitable material whose conductive properties can be changed in real time. This layer could be composed of an optically controlled semiconductor, or a phase change material. In the case of a semiconducting layer, each pixel can be configured to an "on" or "off" state through optical illumination to produce a configuration that is found from the GA optimization for a desired resonant frequency. To initially test the tuning layer, the pixels are modeled with the conductivity of copper.

The dielectric layer thickness between the two layers is chosen to be 25μm, and is again modeled with the same Rogers material as the bottom layer. The bottom layer of the antenna is maintained fixed throughout this work at the configuration shown in section 2.1 designed for a resonance at 2.5GHz. Changing the bottom layer of the antenna may change the possible tuning range of the second layer, as well as other characteristics of the antenna, but

is not explored in this work. While the bottom layer pixel configuration remains constant, the top layer of the antenna is optimized through a similar GA techniques used on the bottom layer.

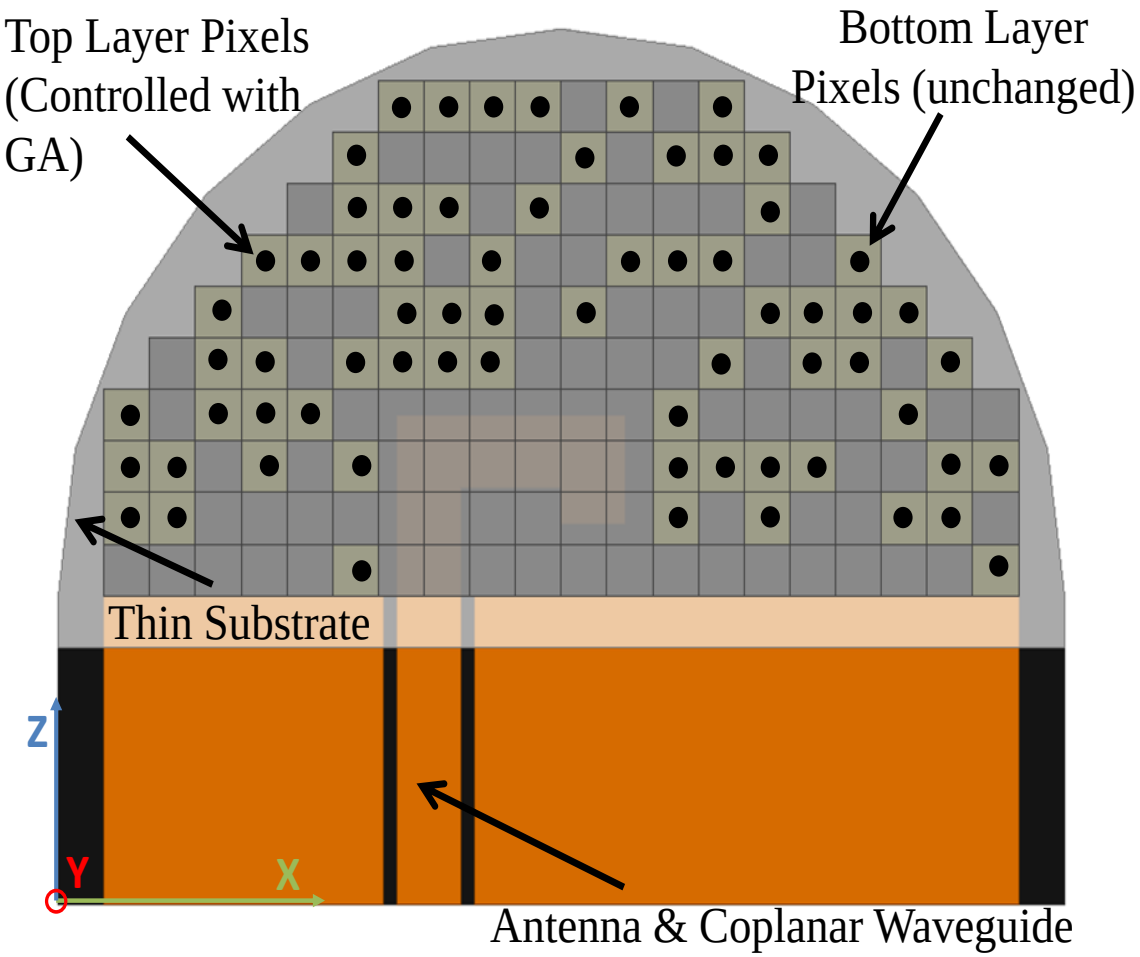

Figure 2.10 Antenna configuration with a second pixelized tuning grid.

2.3.2 GA Optimization of Tuning Layer

The GA optimization for the second layer is similar to the first layer, however, the number of pixel combinations are now higher due to a decrease in geometrical constraints on the new layer. The GA uses a tournament selection method with an initial population of 300 and a 10% selection rate. The initial population is increased for the second layer as a result of the increase in pixel combinations. Each chromosome is then 178 bits long, with a population matrix with 178 by 300 entries. The mutation rate is also set at 20%, with a 2-point crossover with an evolving single bit mutation. The GA is allowed to run for a maximum of three generations or until the desired results are met. The initial fitness function of the GA is the same as in equation 2.1, and the objective is to minimize the reflection coefficient at a desired frequency.

To feed the GA, a random search is first implemented where the chromosomes of the population matrix are randomly selected. This random selection is accomplished with the following matlab code.

```
for ip=1:popsize;
for jp = 1:ChromLength
    if rand() > 0.5
        Pop(ip,jp) = 1;
    else
        Pop(ip,jp) =0;
    end
end
```

The corresponding pixel arrangements on the second layer are then created one by one and passed to HFSS. The matlab code used to create each pixel and pass the geometry to HFSS is shown in the following code.

```
for i=1:m; NN=0;
        for j=1:n
            if Meta(j,i)==1;
                NN=1+ NN;
            end
          if NN>0
            if Meta(j,i)==0
                N=N+1;
                xp=(i)*Pw;
                yp=(j)*Pw;
                hfssRectangle(fid, sprintf('RecB%d',N), 'Y' , ...
                    [-xp+SRR_LX/2, -.025, yp-(1+NN)*Pw], Pw*NN, Pw,'mm');
                hfssAssignFiniteCond(fid, sprintf('RecBPEC%d',N), 0, ...
                    'um', {sprintf('RecB%d',N)})
                NN=0;
            end
             if j==n
                 if Meta(j,i)==1;
                N=N+1;
                xp=(i)*Pw;
                yp=(j)*Pw;
                hfssRectangle(fid, sprintf('RecB%d',N), 'Y', ...
                    [-xp+SRR_LX/2, -.025, yp-NN*Pw], Pw*NN, Pw,'mm');
                hfssAssignFiniteCond(fid, sprintf('RecBPEC%d',N), 0, ...
                    'um', {sprintf('RecB%d',N)})
                NN=0;
                                    end
             end
           end
                end
end
```

These random chromosomes are then evaluated with equation 2.1, and ranked from lowest to highest. During each iteration of both the random search and the GA, every antenna configuration is evaluated in HFSS and saved in a local directory. This allows for easy access to any configuration after the GA is finished, as opposed to only saving the pixel combinations and having to re-simulate each desired configuration. Once the random search is finished, the re-organized fitness function is passed to the GA portion of the code. First, the chromosomes to be kept are selected, which is accoumplished in the following way.

```
% Selection of chromozomes to be kept
indx=find(fitness≤mean(fitness));
% Determines the chroms with fitness < mean fitness
keep=ceil(selection*popsize); %Number of chrom to keep
fitkeep=fitness(indx);% fitnesses to keep
Popkeep=Pop(indx,:);%Chroms to keep
M1=ceil((popsize-keep)*.6);
 % Chromosomes to be replaced via Xover and Mutation for case 1
M2=ceil((popsize-keep)*.4);
% Chromosomes to be replaced via Xover and Mutation for case 2
```

Next, a random selection of possible parents is performed.

```
 for ic2=1:2:M2
%Random Selection of Parents
%first Parent
ma=ceil(keep*rand());% indicies of first parent
%Second parent
pa=ceil(keep*rand());% indicies of second parent
```

From here, a 2-point crossover is performed between parents to create two offspring.

```
%2pt Crossover
Xpt1=ceil(rand()*Nt/2);
Xpt2=Xpt1 + ceil(rand()*(Nt-1)/2);
Pop(keep+M1+ic2-1,:)=[Pop(ma,1:Xpt1) Pop(pa,Xpt1+1:Xpt2) ...
    Pop(ma,Xpt2+1:Nt)]; % Offspring 1
Pop(keep+M1+ic2,:)=[Pop(pa,1:Xpt1) Pop(ma,Xpt1+1:Xpt2) ...
    Pop(pa,Xpt2+1:Nt)];%Offspring 2
end
```

Then the best two individuals are selected and 2-point crossover is performed again.

```
%selection the best of 2 individual
%first Parent
rc=ceil(keep*rand(1,Ntourn)); %Randomly select 2 chroms among those kept
[c,ci]=min(fitness(rc)); % Select the chrom with lowest fitness
ma=rc(ci);  % indicies of first parent
%Second parent
rc=ceil(keep*rand(1,Ntourn));%%Randomly select 2 chroms among those kept
[c,ci]=min(fitness(rc)); % Select the chrom with lowest fitness
pa=rc(ci);  % indicies of second parent
```

Finally, single-bit mutations are performed based on the probability of mutation.

```
%mutation: keep best two and mutate a single bit on the other
%chromosomes based on mutating probability
  for iMu=keep:popsize
    if Muprob≥rand()
     Mupt=ceil(rand()*Nt);% bit to be mutated
     Pop(iMu,Mupt)=not(Pop(iMu,Mupt));
    end
  end
```

After the population matrix is refilled, the chromosomes are evaluated in the same way as the random search. Once all the possible pixel combinations are evaluated, the population matrix is passed back to the beginning of the GA and the process if repeated in a new generation. In the case of this work, the GA is allowed to optimize over 3 generations, corresponding to the simulation of 1200 different pixel configurations. At approximately 15 minutes per simulation, the optimization can take over a week to complete for a desired frequency. However, the results are also displayed in real-time, so if a configuration that meets the desired criteria is found, the GA can be stopped early. The entire code for the matlab-HFSS GA can be found in appendix A.

2.3.3 Simulated Reflection Coefficients of Selected Antenna Configurations

The second layer tuning element is first tested over a variety of possible frequency ranges. Figure 2.11 and 2.12 show some selected reflection coefficients in the 3-4GHz frequency range as well as the 5-6GHz frequency range. These antennas show just some of the possible configurations with reflection coefficients of less than -10dB. The gaps between reflection coefficients in these regions are only a result of computational time, as antennas with well defined resonances can also be found for those frequencies.

At the upper end of the 6GHz frequency range, the antenna is tuned in frequency by nearly 240 %.Compared with the methods introduced in sections 1.2 and 1.3.1, this is an extremely drastic tuning range. In addition, the magnitude of many of these antenna reflection coefficients are very large, and in some cases even better than the original antenna. From these results, the potential for a dynamically tunable antenna is clear, however, the conductivities of the pixels in this case are very high, correspond to copper. In the next section, similar antenan configurations will be investigated but with much lower conductivities for the second layer pixel grid.

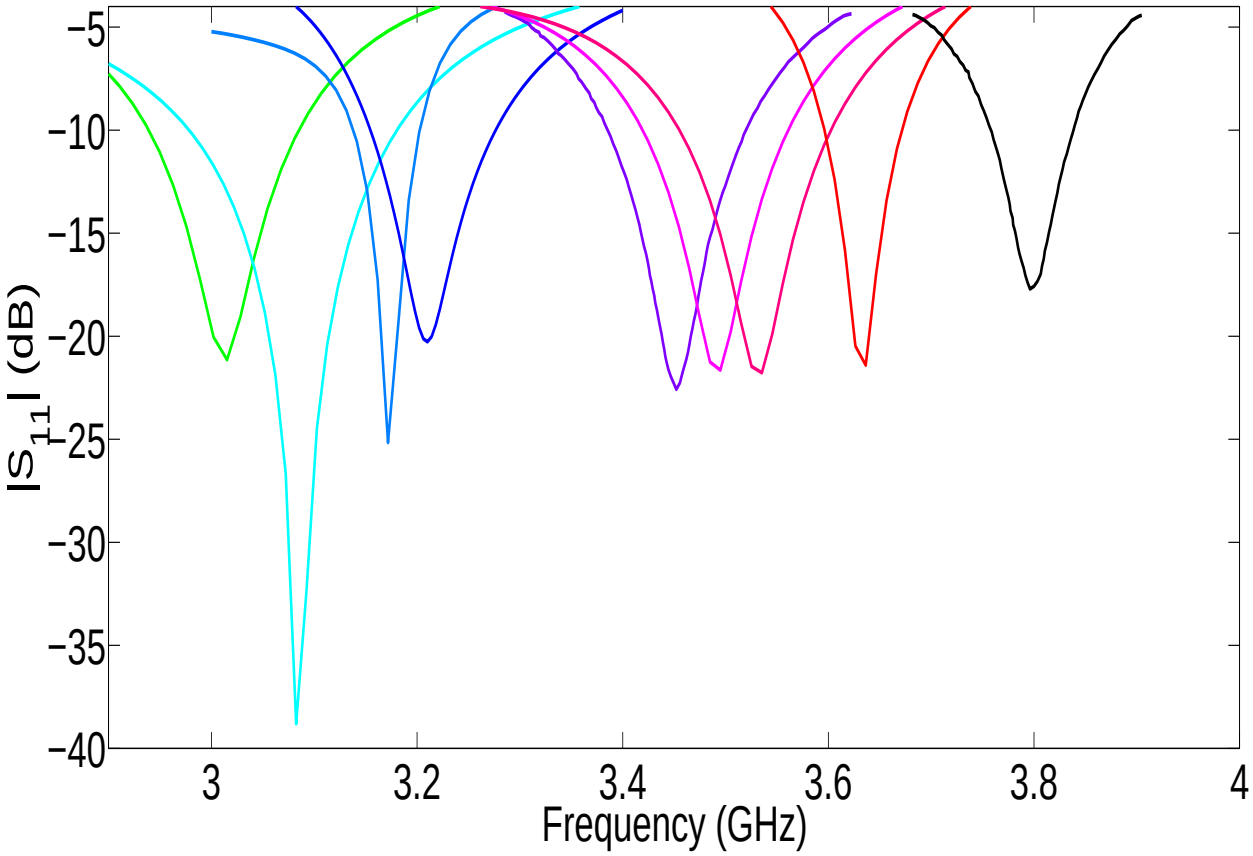

Figure 2.11 Reflection coefficients of some sample antenna configurations within the 3-4 GHz frequency range.

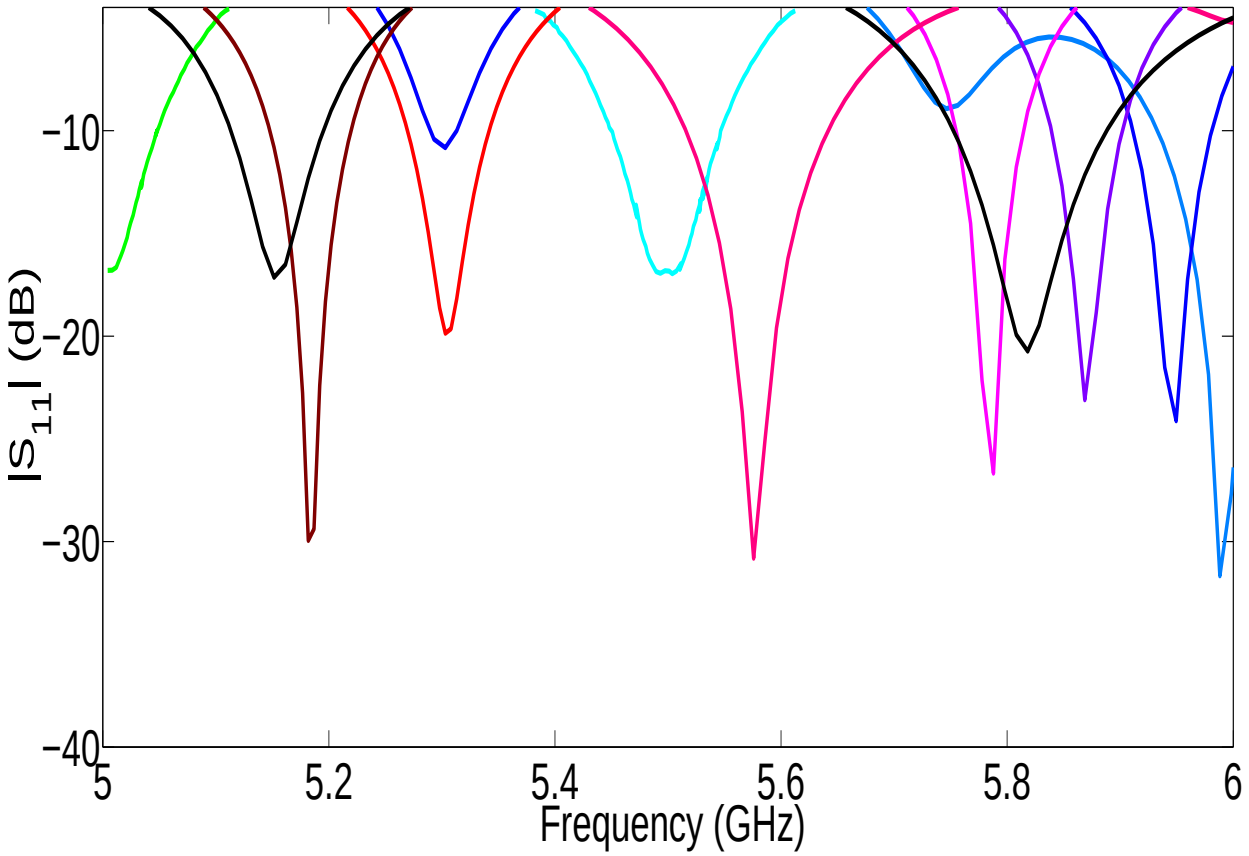

Figure 2.12 Reflection coefficients of some sample antenna configurations within the 5-6 GHz frequency range.

2.3.4 Investigation of Pixel Conductivities

While the previous analysis only takes into account highly conductive metals such as copper, the top layer pixels of the antenna are envisioned to be made of materials that may have a conductivity much less than typical metals. To investigate the effect of change in the conductivity of the pixels on the top layer, an antenna with a resonance at 3.8 GHz is chosen. The conductivity is varied from a value corresponding to a typical metal $5.9x10^7 S/m$ (copper), to an order of magnitude less than most metals. As the conductivity is decreased from the original conductivity the pixel states were optimized for, the reflection coefficient of the antenna grows, until at one point the antenna is no longer highly resonant. This trend is shown is shown for a variety of conductivities in Figure 2.13. While changing the conductivity of an already optimized pixel state increases the magnitude of the reflection coefficient of the antenna to a state where it is unusable, the conductivity can also be change prior to the original optimization of the second layer to dissipate this effect.

Two frequencies corresponding to antennas with pixel combinations made from much lower conductivities are optimized with the same GA parameters as previously shown. Figure 2.14 shows a pair of the best possible antennas found for each of the individual conductivities within the 3-4GHz band. One antenna corresponds to a pixel with conductivity of $2x10^5 S/m$, while the other corresponds to $2x10^4 S/m$. Clearly, antenna configurations can be found with conductivities much below common metals that are still highly resonant.

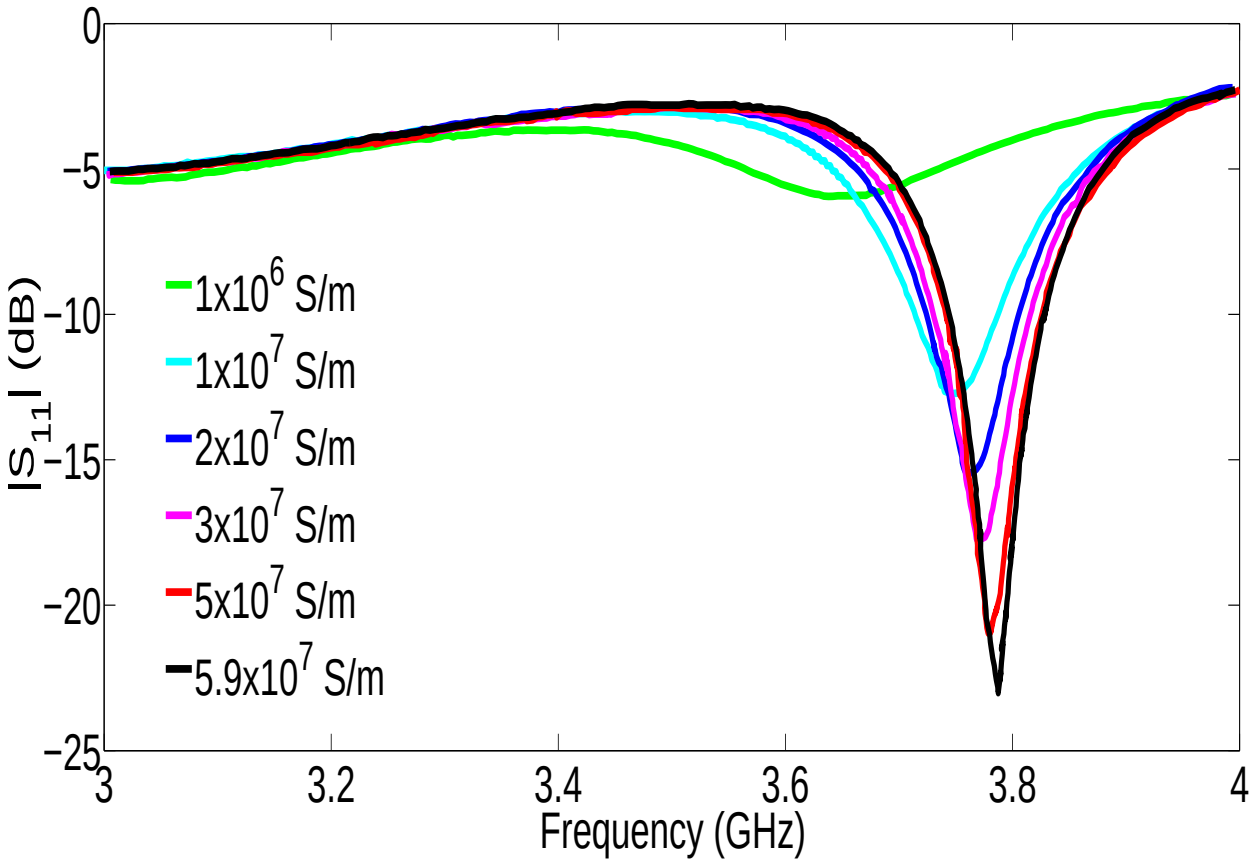

Figure 2.13 Effect of changing the top layer pixel conductivity on the reflection coefficient.

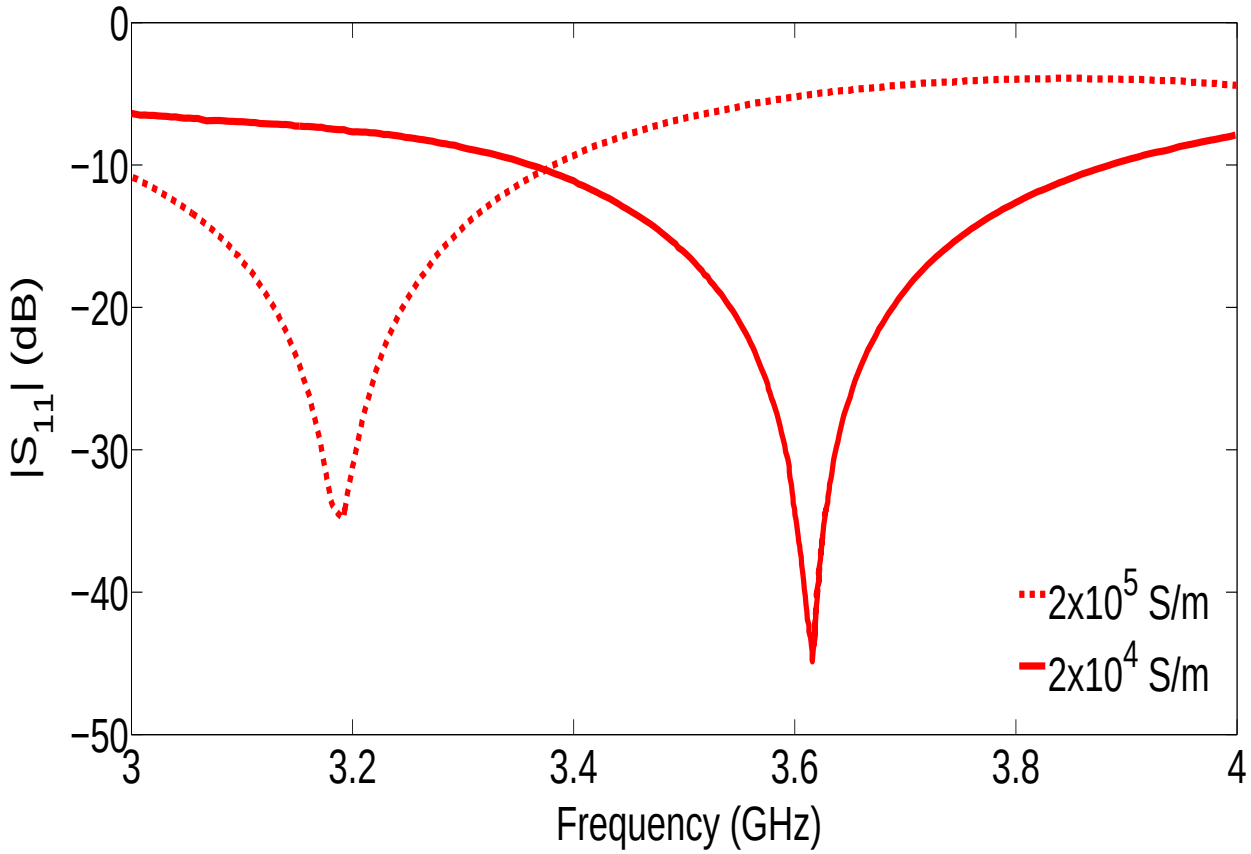

Figure 2.14 Reflection coefficient of optimized antenna configurations corresponding to very low top layer pixel conductivity.

2.4 Simultaneous Optimization of Radiation Efficiency and Reflection Coefficient

While these antenna configurations correspond to very good reflection coefficients at a wide range of possible frequencies, the radiation characteristics of the antenna are also important. However, the antenna with the highest reflection coefficient will not necessarily correspond to the best radiator. While some of these antennas could maintain an acceptable radiation pattern and efficiency, others could simply be acting as strongly resonant structures with little radiation. In order to properly ensure the device is acting as an antenna, the fitness function of the GA is altered to also weigh the radiation efficiency of the antenna. This is achieved by using the radiation efficiency(η) as a weighting function of the magnitude of the reflection coefficient which was initially minimized, i.e.

$$fitness = \eta * 20log_{10}(|S_{11}|) \tag{2.2}$$

In order to determine the antenna configuration that will correspond to the best fit for our desired results, the radiation efficiency and reflection coefficient are monitored for every optimized antenna state. From the trend between the two, a antenna configuration which has a tradeoff between a high radiation efficiency and a good reflection coefficient can be selected. In this case, any antenna with a reflection coefficient lower than -10dB can be thought of as a desirable antenna, so the highest radiation efficiency for any state meeting this reflection coefficient will be selected. Figures 2.15-2.18 show the radiation efficiency versus reflection coefficient for four discrete frequency antenna designs. Each graph shows the antenna configurations corresponding to the initial random search, as well as after the third generation of the GA. It can be seen that the antennas found after three generations have much better characteristics than the initial random search. This confirms that the GA

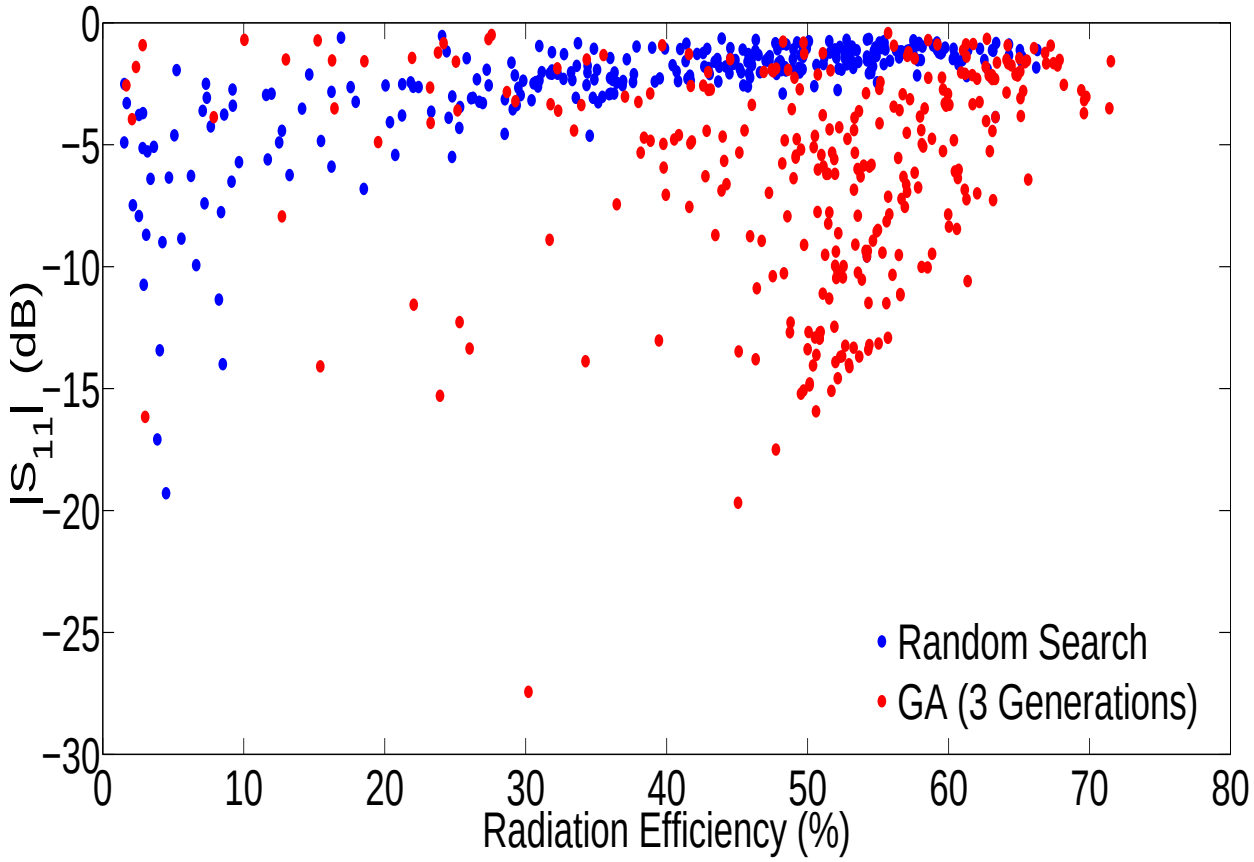

Figure 2.15 Reflection coefficient versus radiation efficiency for the random search and after 3 generations of GA optimization for 2.5 GHz.

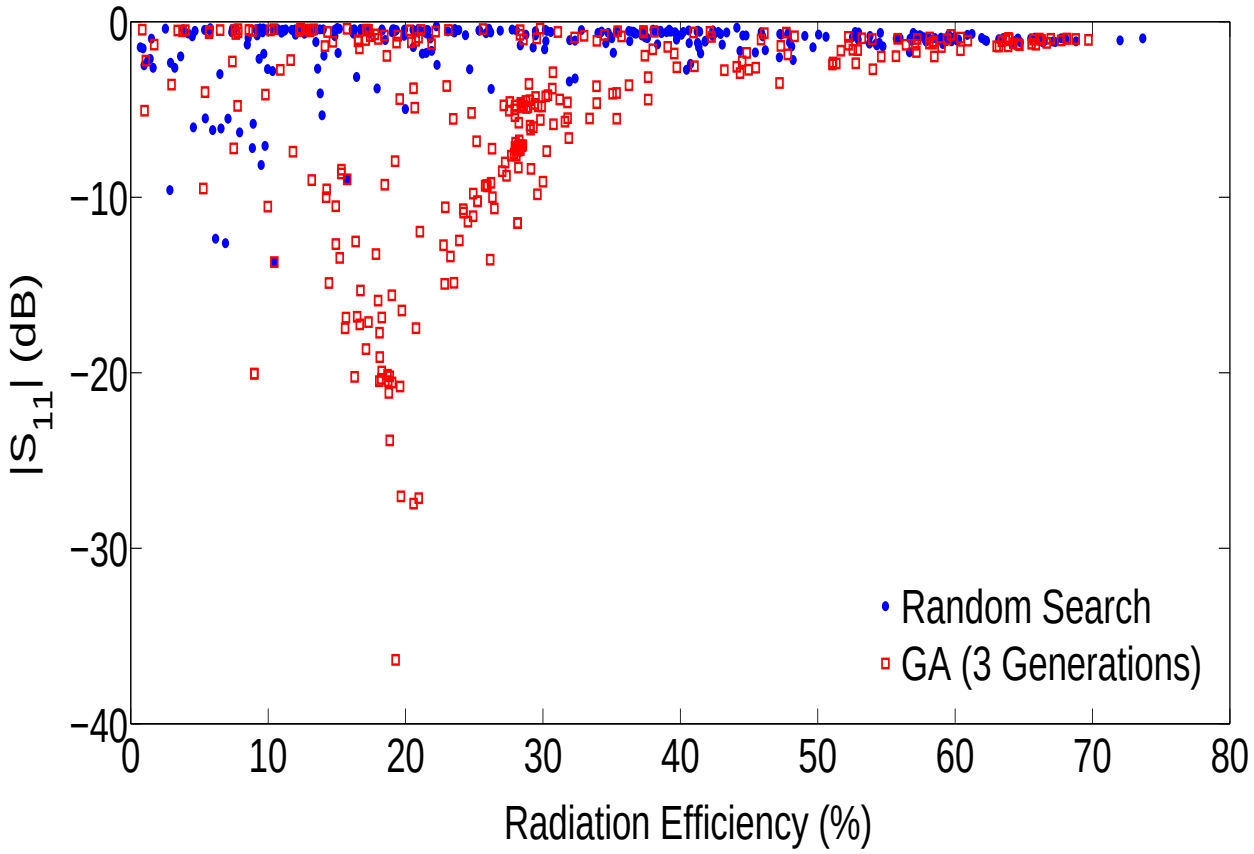

Figure 2.16 Reflection coefficient versus radiation efficiency for the random search and after 3 generations of GA optimization for 4 GHz.

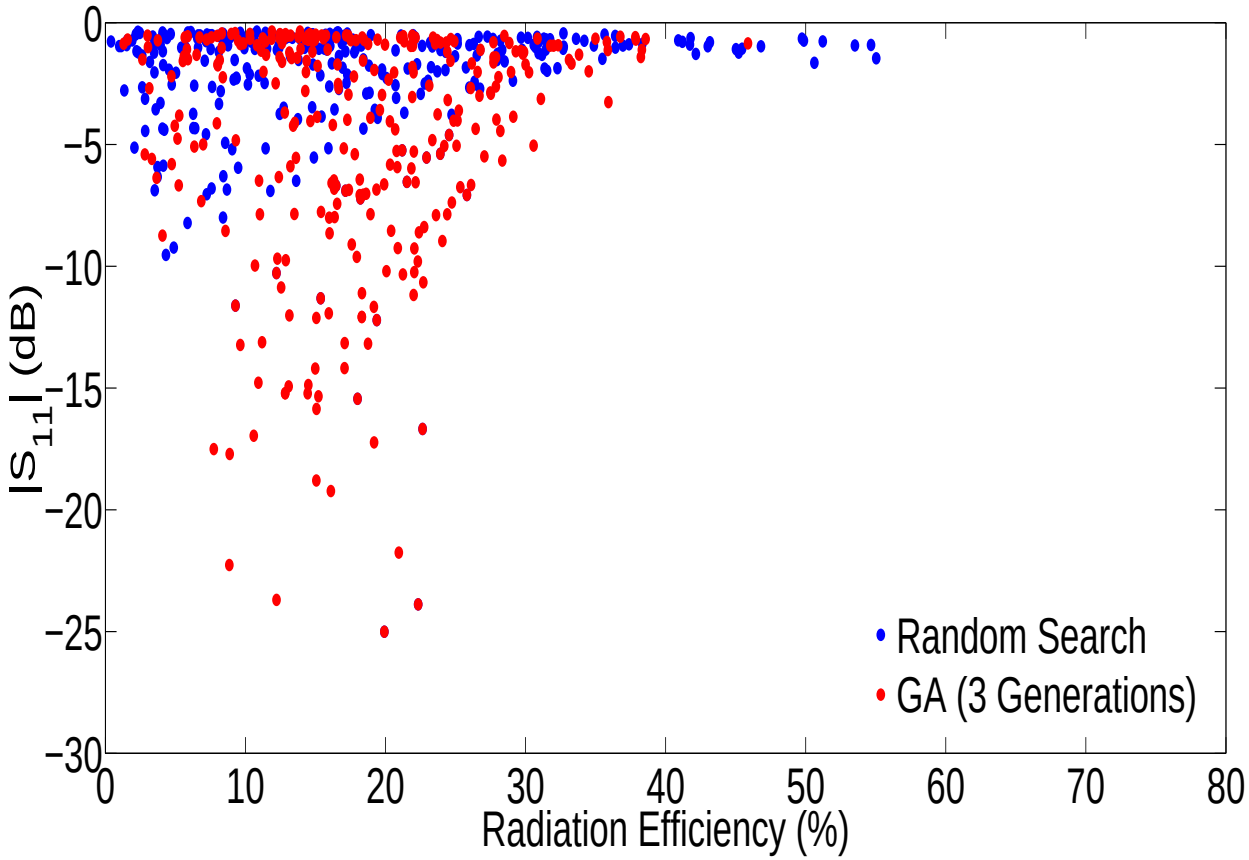

Figure 2.17 Reflection coefficient versus radiation efficiency for the random search and after 3 generations of GA optimization for 6 GHz.

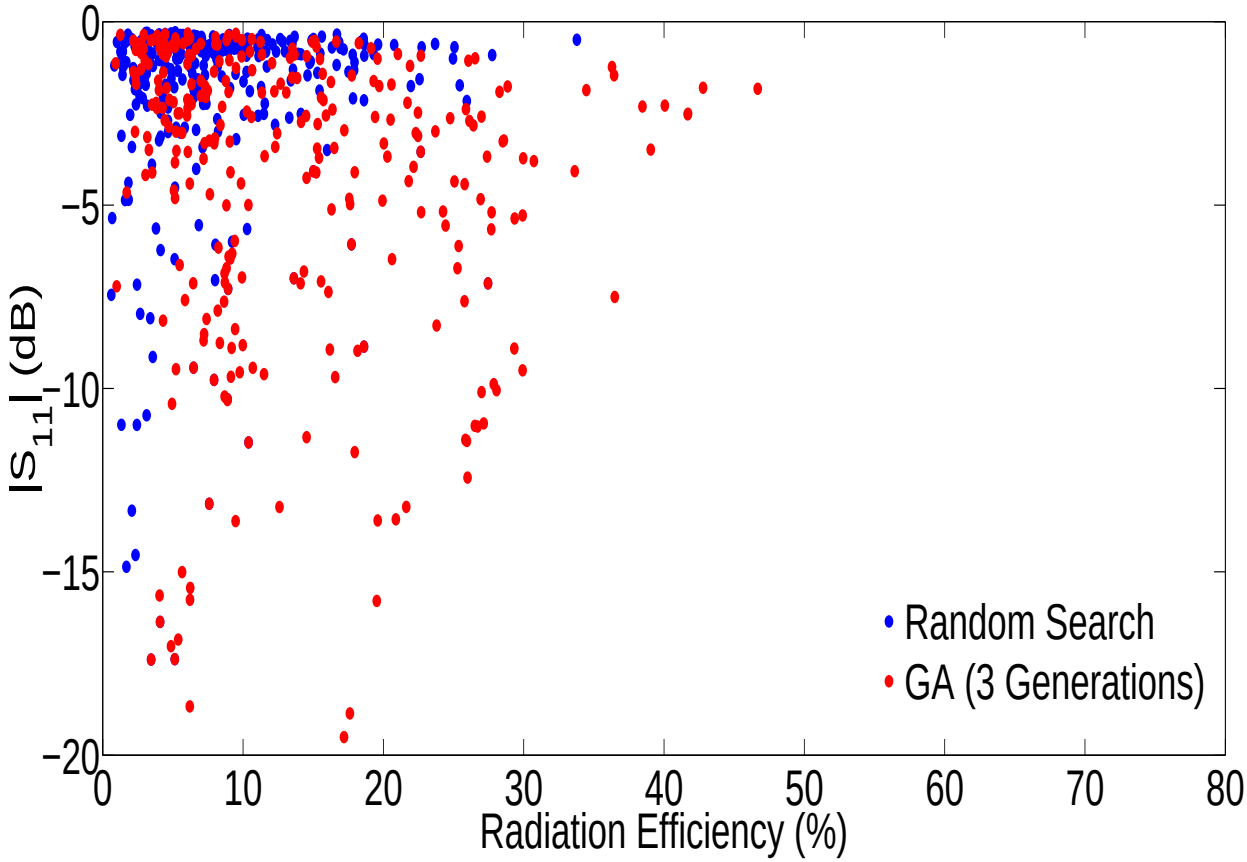

Figure 2.18 Reflection coefficient versus radiation efficiency for the random search and after 3 generations of GA optimization for 8 GHz.

can create much better results than a simple random search. From these results the theoretical tuning range of the antenna can begin to be discussed. At frequencies lower or higher than the tuning range of the antenna, some configurations may have a low reflection coefficient, but the radiation efficiency of the antenna will be near zero. To illustrate this, radiation efficiency and reflection coefficients are calculated over three GA generations for a very wide frequency range. This range goes from 1.5GHz to 18 GHz. The antenna corresponding to the best radiation efficiency and a reflection coefficient of -10dB at each frequency are then recorded. From these results, it can be observed that at 1.5 GHz there is essentially no radiation. As the frequency increases towards the resonance of the bottom layer, the efficiency increases and peaks locally at 2.5 GHz. From this point onward, the efficiency oscillates but does not drive downward towards zero. These results are shown in Figure 2.19, where the dotted line corresponds to the resonance of the bottom layer. The upper portion of the tuning is not clearly found in these results, however, as the frequency is increased, the size of the antenna structure becomes much larger with respect to the wavelength. While the antenna will still radiate efficiently at these frequencies, the radiation pattern becomes much more complex and the original pattern of the monopole can no longer be maintained.

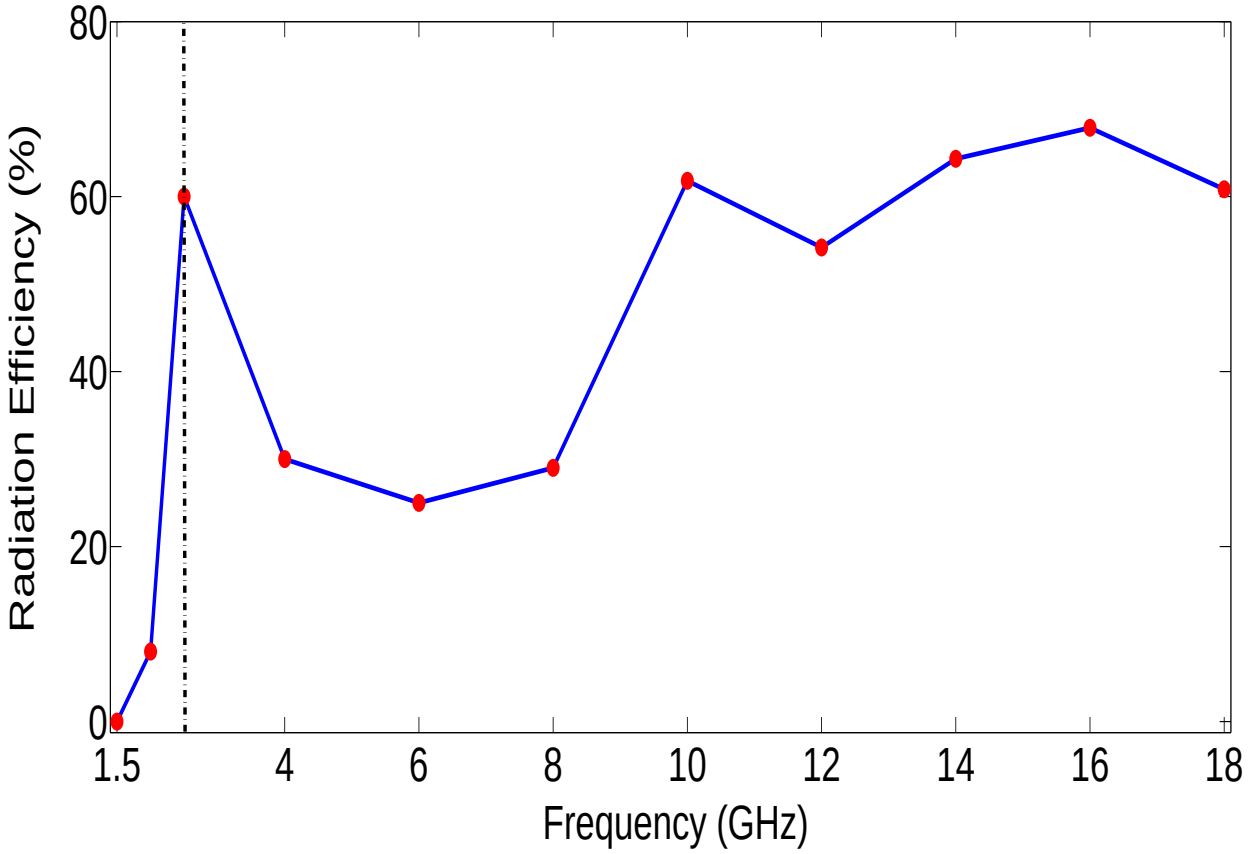

Figure 2.19 Best radiation efficiency corresponding to a reflection coefficient of at least -10dB for a variety of frequencies.

CHAPTER 3

Fabrication and Experimental Results

In this chapter, the fabrication and measurement of the antenna with the second tuning layer is presented. The second layer in this work is made of a metallic pixel grid in order to test the concept of the layer as a tuning element. First, the layer is constructed using thin PET films with the pixel grid etched on. The PET film is envisioned to be used as a hot swappable loading element that can be placed directly on the bottom layer of the antenna. The problem with this method is that the misalignment and airgap between the layers has a largely negative impact on the performance of the second layer. To solve these problems, a multi-layer fabrication process is developed which uses a simple photo resist as a dielectric layer. In this case, the photo resist used is a $25\mu m$ SU-8 layer. The SU-8 can be directly spun onto the bottom layer of the antenna, eliminating airgaps and reducing the misalignment. With this method, multiple antennas are fabricated over a wide frequency range. The reflection coefficient and radiation patterns of each of the antennas are measured, and each antenna configuration shows relatively good agreement with their simulated counterpart.

3.1 Fabrication of Second Layer Using PET Films

The first method implemented in the fabrication of the second layer is using PET thin films. The configuration of the antenna with the PET film layer is shown in Figure 3.1. The PET layer is envisioned to be placed directly on the bottom layer of the antenna. Each pixel configuration found through simulation can then be fabricated directly onto the PET film, and then placed directly on the antenna to act as the second layer. The PET film in this case is $25\mu m$ thick, and a thin layer of aluminum is deposited on the film. The desired pixel state is then etched onto the PET film, and the film is placed onto the bottom layer of the antenna. A number of pixel configurations corresponding to different resonant frequencies are fabricated using the PET layers. Figure 3.2 shows some a sample of some of the PET thin film states.

With the second layer fabricated, each pixel configuration is placed directly on the bottom layer to achieve frequency tuning. The antenna with and without the PET layer is shown in Figure 3.3. It is easy to observe that the alignment between the layers in this case is difficult to control. In addition, the layers do not adhere directly to the substrate, making airgap between the layers a possible problem. Each antenna is fed with a thin-pin SMA connector from Lighthouse technologies (part # LTI-SASF55ZGT-P2-4). These SMA connectors have a very thin center pin, making them ideal for this application, as the connector needs to be soldered directly on the monopole antenna. To characterize the antenna, the reflection coefficient of the antenna is measured with a Agilent N5227A network analyzer.

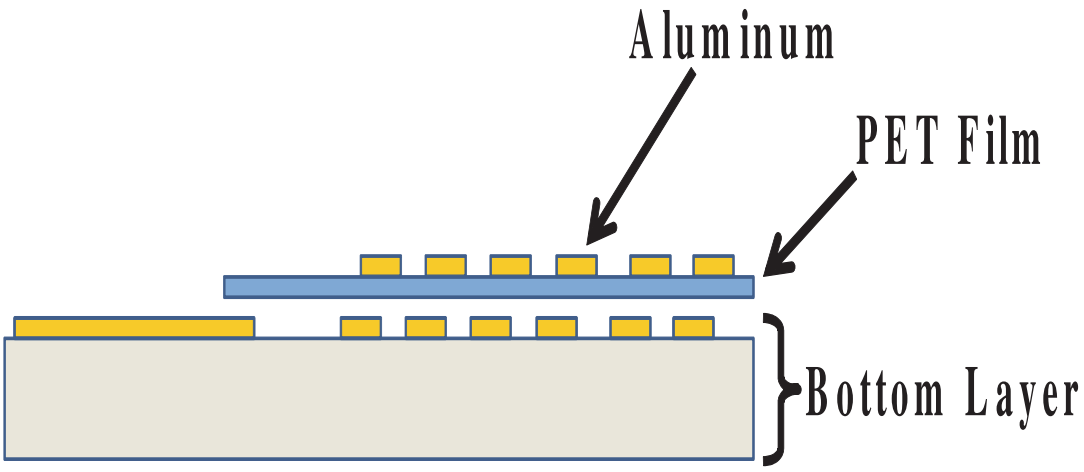

Figure 3.1 Antenna with PET layer setup.

Figure 3.2 Fabricated PET layers.

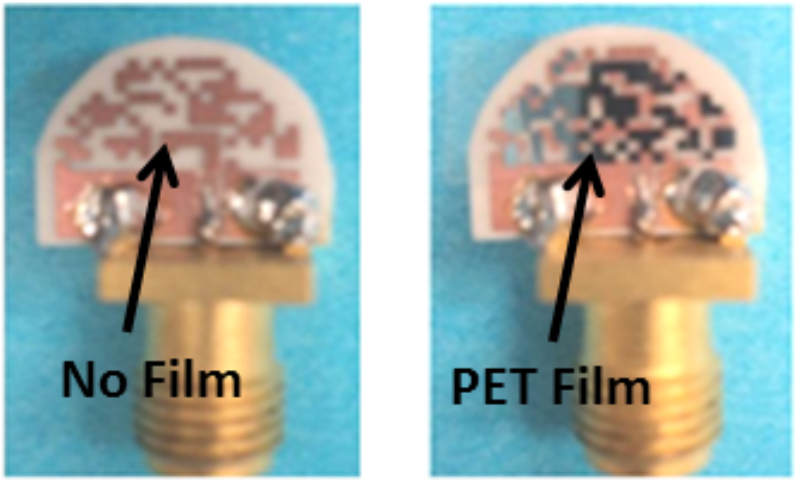

Figure 3.3 Antenna with and without PET layers.

Figure 3.4 shows the reflection coefficient for a antenna configuration chosen for a resonance of 3.75GHz. From these results we can see that the measured and simulated reflection coefficients have poor matching. The cause of this discrepancy is mostly attributed to the possible airgap between the layers, and the misalignment in the lateral directions of the antenna. The next section examines the effects of adding an airgap and misalignment between the top and bottom antenna layers.

3.1.1 Effects of Misalignment and Air Gap

First, the misalignment between the layers is studied. The top layer for a particular pixel configuration that produces a antenna resonance at 1.8GHz is chosen. The layer is moved in four directions along the lateral direction of the antenna. These correspond to shifts in the x and y directions of $250m$ and $500m$ each. Figure 3.5 shows the effect of misalignment on the reflection coefficient of the antenna. These misalignments correspond to both shifts in the location of the resonant frequency and alter the magnitude of the reflection coefficient. While there is not a direct relation between a shift in alignment and the effect it has on the reflection coefficient, it is noticeable that shifts in the y direction seem to alter the location of the resonance much more than in the x direction.

It is clear that the location of the resonance is shown to dramatically shift even with only slight misalignment. Although the exact level of misalignment in the fabricated antennas was not measured, levels similar to the above could easily be expected. While the misalignment between layers greatly alters the reflection coefficient, the amount of disagreement between the measured and simulated results presented in the previous section are not fully explained by just the misalignment.

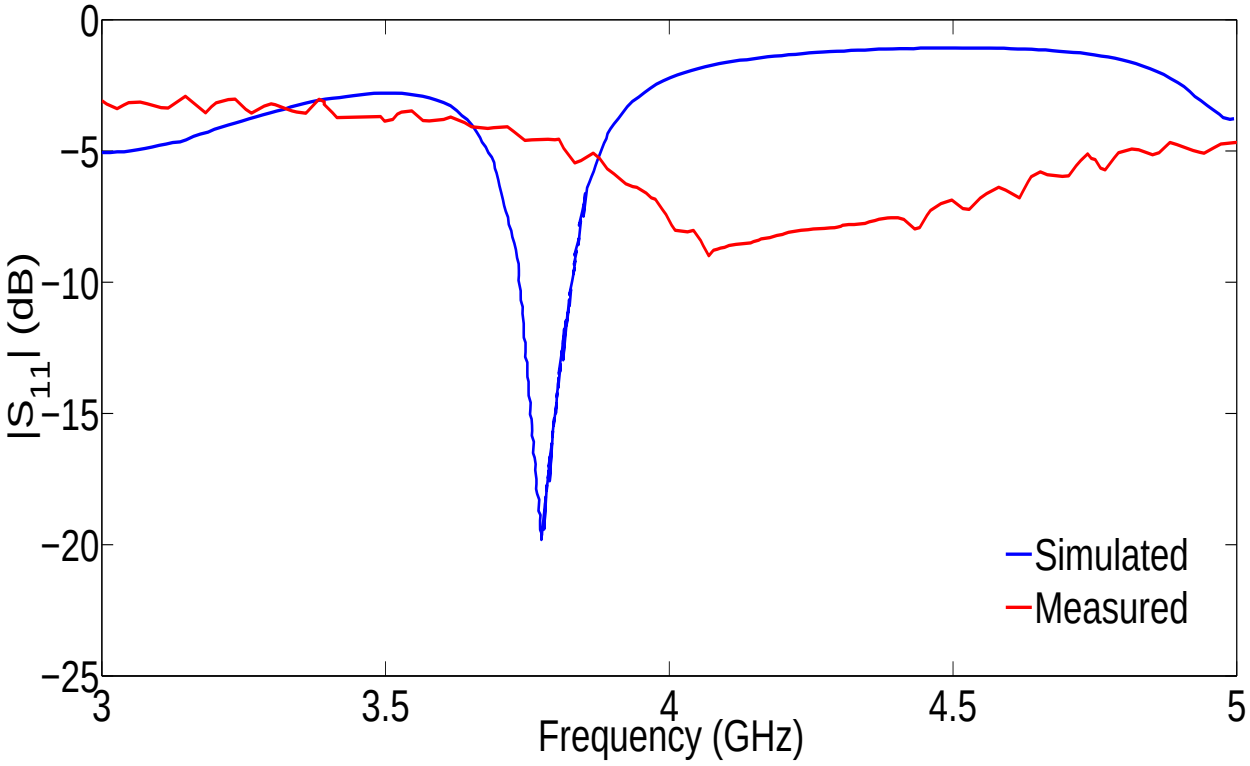

Figure 3.4 Reflection coefficient of antenna with PET layer at 3.75GHz.

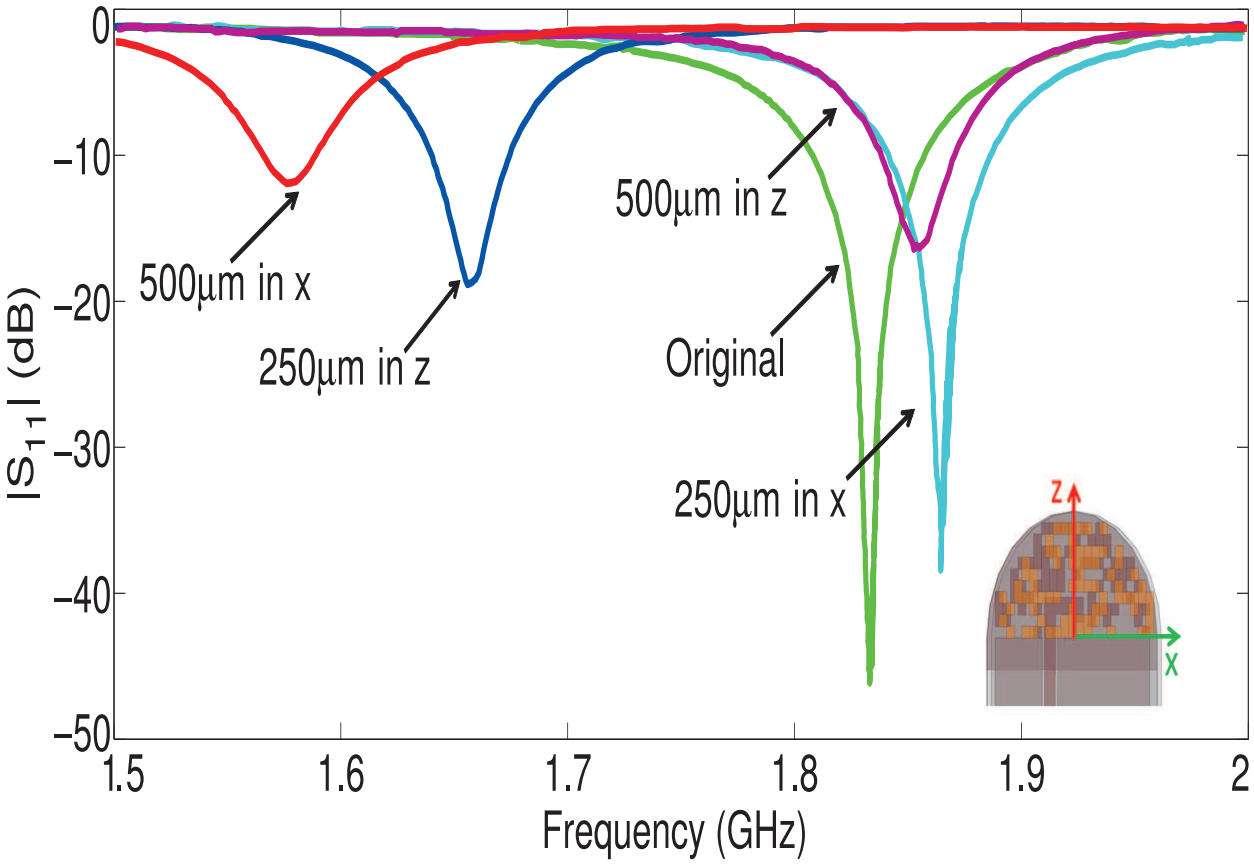

Figure 3.5 Effects of miss-alignment between layers on the reflection coefficient of the antenna.

The airgap between the layers can also be a major cause of disagreement in the measured results. Since the PET layers do not physically adhere to the bottom layer, some air can easily be trapped between the PET film and the antenna. To determine the effect of airgap between the tuning layer of the antenna, the antenna is simulated with a $10\mu m$ airgap between the PET film and the bottom layer of the antenna. Figure 3.6 shows the effect of this airgap in the reflection coefficient of the antenna. Obviously, the effect here is very dramatic and essentially destroys the performance of the antenna. However, as the exact airgap between the layers is unknown, this would most likely be the most extreme possibility.

Both of these effects hamper the performance of the antenna greatly. While the attractiveness of easily hot swappable PET films could provide many advantages, a more precise and permanent fabrication method must be used to ensure the antenna results match well with the simulated expectations.

3.2 Fabrication of Second Layer Using SU-8 Photoresist

In this section, a fabrication process is developed that eliminates the problems found in the attempt to use PET films for the second layer tuning element. In this case, a thin SU-8 photoresist is used as the dielectric layer between the bottom layer of the antenna and the tuning layer. This layer can be directly spin coated onto the antenna, eliminating any airgaps between the layers. Additionally, the thickness of the layer can be controlled within a few microns of the desired results. This method also treats the dielectric layer and second metallic layer with a mask aligner which allows the second tuning layer to be precisely aligned with the bottom layer of the antenna.

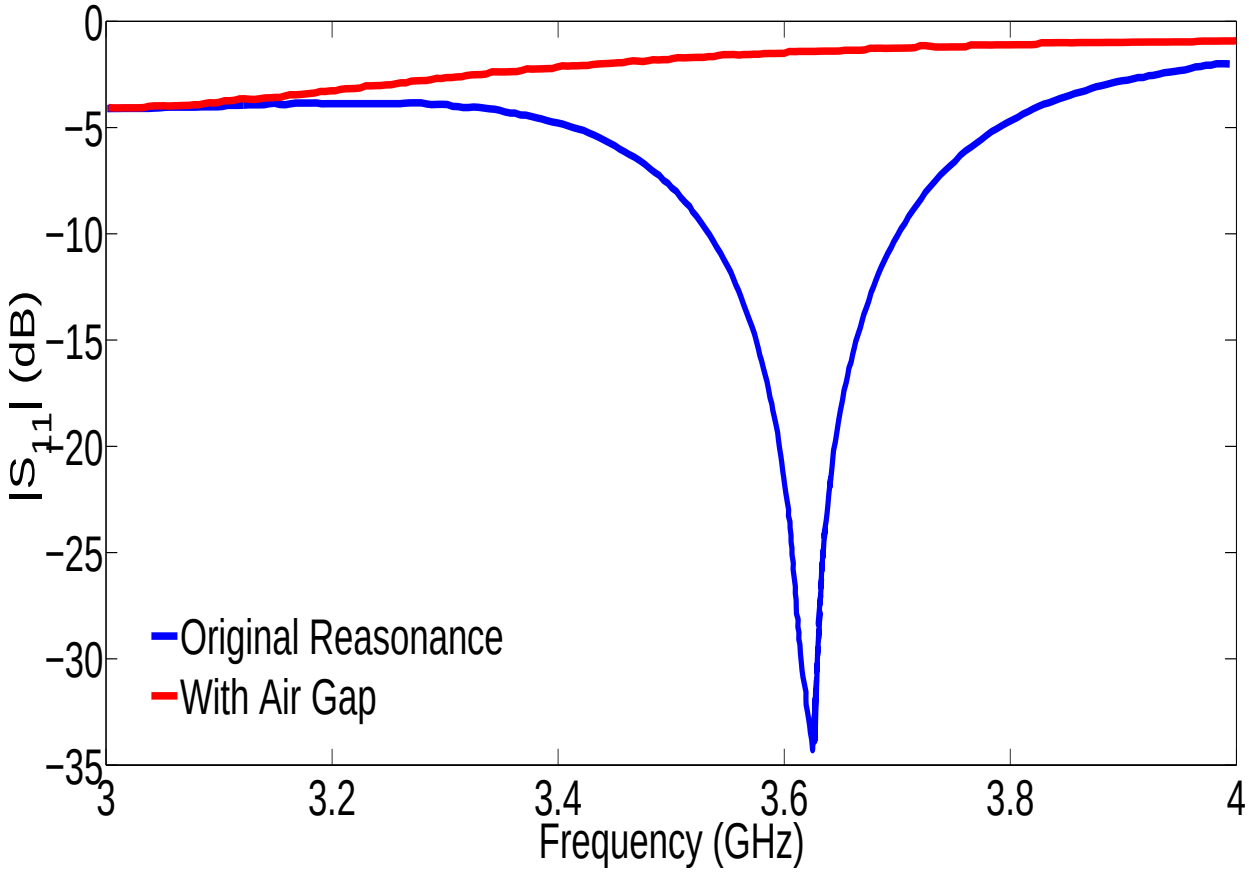

Figure 3.6 Effects of air-gap between layers on the reflection coefficient of the antenna.

3.2.1 Fabrication Process

To properly realize the antenna, a precise multi-layer fabrication process must be utilized. Slight miss-alignment between the top tuning layer and the bottom antenna can have dramatic effects due to the high sensitivity of the antenna. Additionally, small air gaps between the top layer and the antenna can negatively effect the antenna resonance. To ensure both of these problems are minimized as much as possible, the dielectric layer which hosts the tuning pixels is developed directly onto the antenna. In this case, a $25\mu m$ layer of SU-8 photo resist is used as the dielectric layer. The SU-8 layer has the properties of a relatively low loss material within the lower GHz spectrum, with $\epsilon_r = 3.28$ and $tan\delta = .015$ according to the Microchem data sheet.

The overall fabrication process is summarized in Figure 3.7. First, the bottom layer of the antenna is chemically etched onto a Rogers RO4003 substrate using a sodium persulfate etchant. After the patterning of the bottom layer is finished, the SU-8 is spun onto the antenna. In this case, the SU-8 used is developed by Microchem, and the product number is SU-8 25. For a $25\mu m$ thick layer, the SU-8 is spun onto the bottom layer with a Laurel 6" Photoresist Spinner at 2000 rpm. Before and after development, the SU-8 also requires a pre-bake and post-bake of 65 and $95^{\circ}C$, respectively. The SU-8 is aligned with the bottom layer using a Karl Suss MJB3 contact mask aligner. Alignment marks on the bottom layer made of copper are aligned with small SU-8 squares in the photomask to ensure proper alignment between the SU-8 and the bottom layer. A thin layer of titanium is then deposited on the SU-8 layer using a sputtering system to act as an adhesive layer for the copper. Next, a layer of copper ($\approx 1.5\mu m$) is sputtered onto the titanium layer using the same system. The copper is then patterned to the desired pixel configuration using the same wet-etching technique as the bottom antenna layer. Finally, the sample is then quickly dipped in hydrofluoric acid to remove the excess titanium.

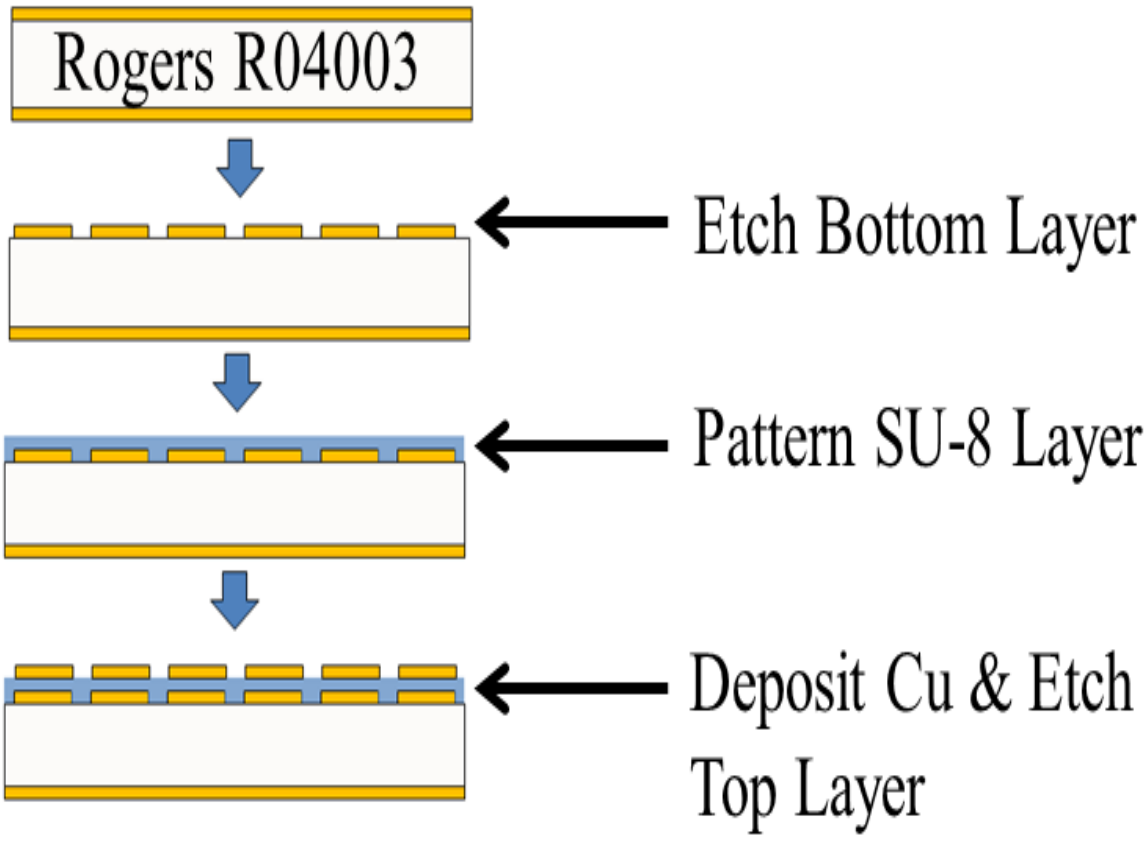

Figure 3.7 Overview of fabrication process.

3.2.2 Fabricated Antenna Samples

Using the previously described fabrication method, four antennas were fabricated and measured. The four antennas correspond to resonant frequencies of 2.5GHz, 4GHz, 5GHz, and 8GHz. A close up view of one of the fabricated antenna configurations is shown in Figure 3.8. In this case, the SU-8 layer is the semi-transparent layer shown between each metal. The metal on the top of the antenna is represented in black, while the bottom layer is the traditional copper color. Overall, the dimensions of the second layer and the antenna match well with the desired specifications. In addition, to the naked eye the layer appear to be very well aligned. Figure 3.9 shows the alignment marks between the SU-8 and the bottom copper layer. The SU-8 is represented by the semi-transparent layer which has a box shape that is placed around the metallic cross alignment mark for the bottom layer. From this figure, it is clear that the alignment between the layers is very good as the alignment marks match well.

However, the SU-8 is very difficult to spin evenly over the bottom layer of the antenna. Figure 3.10 shows the SU-8 one the antenna under high levels of magnification. Due to the uneven spread of the SU-8, ripples become prevalent along the surface of the antenna. These ripples essentially represent a difference in the thickness of the SU-8 at certain locations. In addition, along the edges of some spots of the second layer, excess copper can develop as the photoresist may have not fully developed. Figure 3.11 shows this excess copper for one pixel configuration along the edge of the SU-8 layer. This copper can be scraped off, but either way some will remain and may have a small effect on the antenna performance.

Each antenna is fed with a small SMC connector that is machined so that only the pin is exposed to prevent any further interference with the antenna. The ground connections are made with small wires from the sides of the SMC connector to the CPW feed. A picture of one of the final fabricated antennas with the SMC connector attached is shown in Figure 3.12.

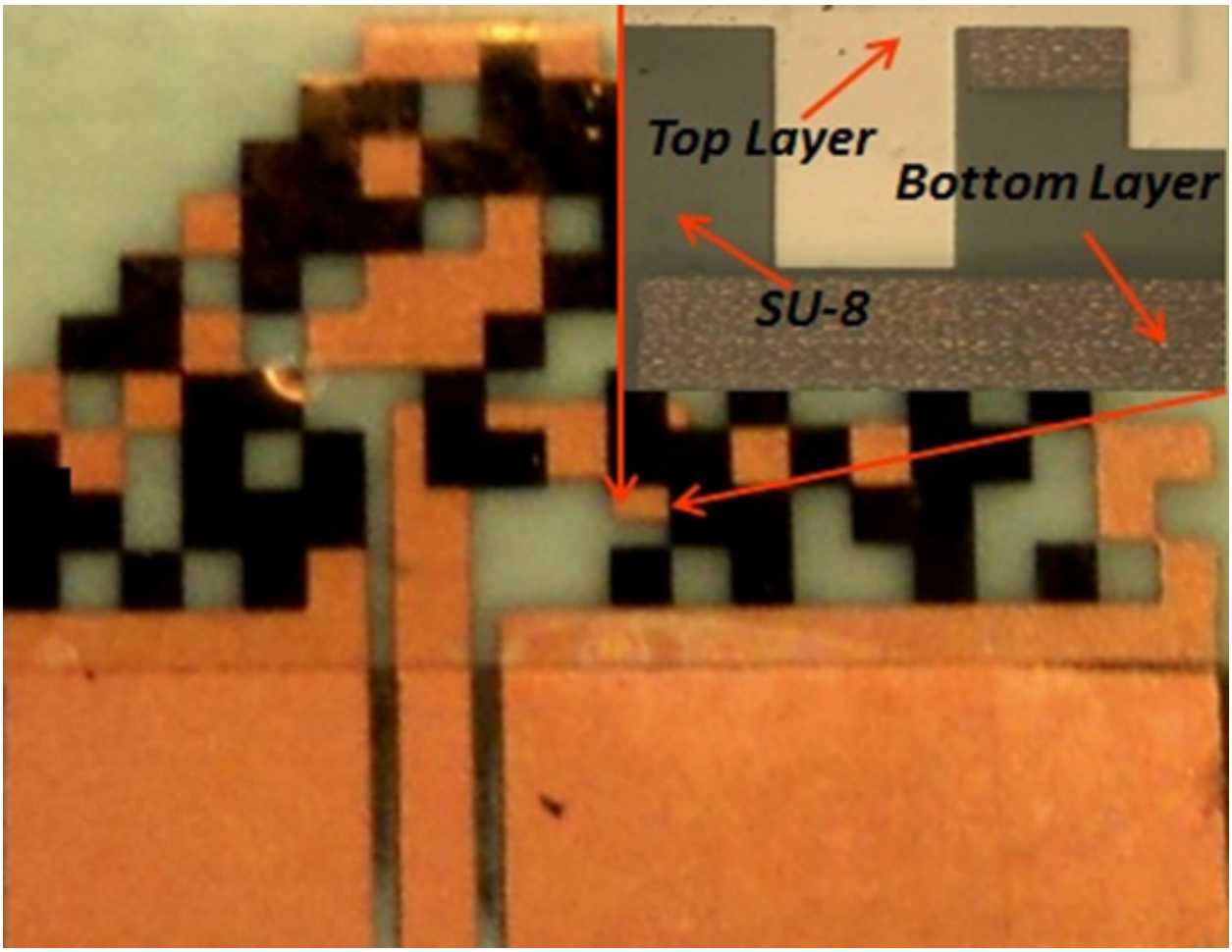

Figure 3.8 Close up of a fabricated antenna configuration.

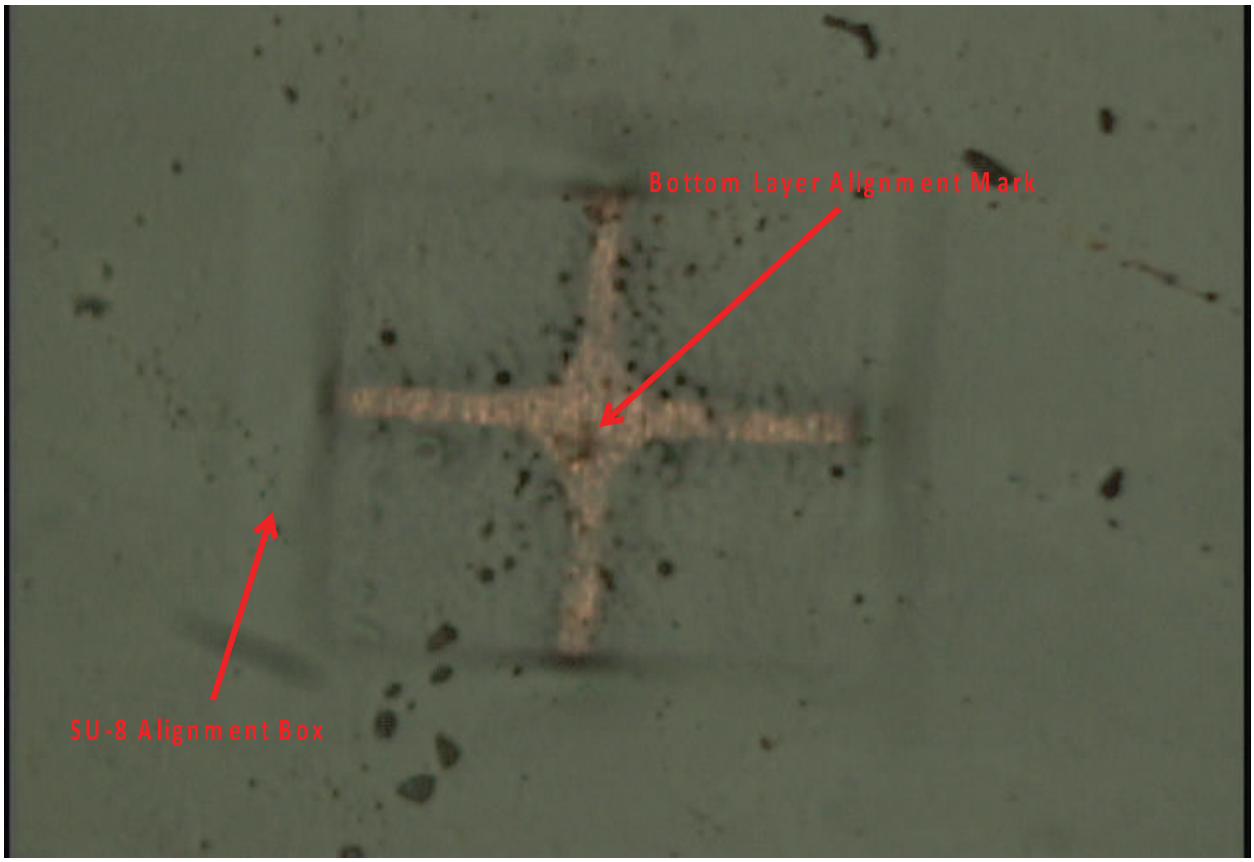

Figure 3.9 Alignment marks between SU-8 and bottom layer.

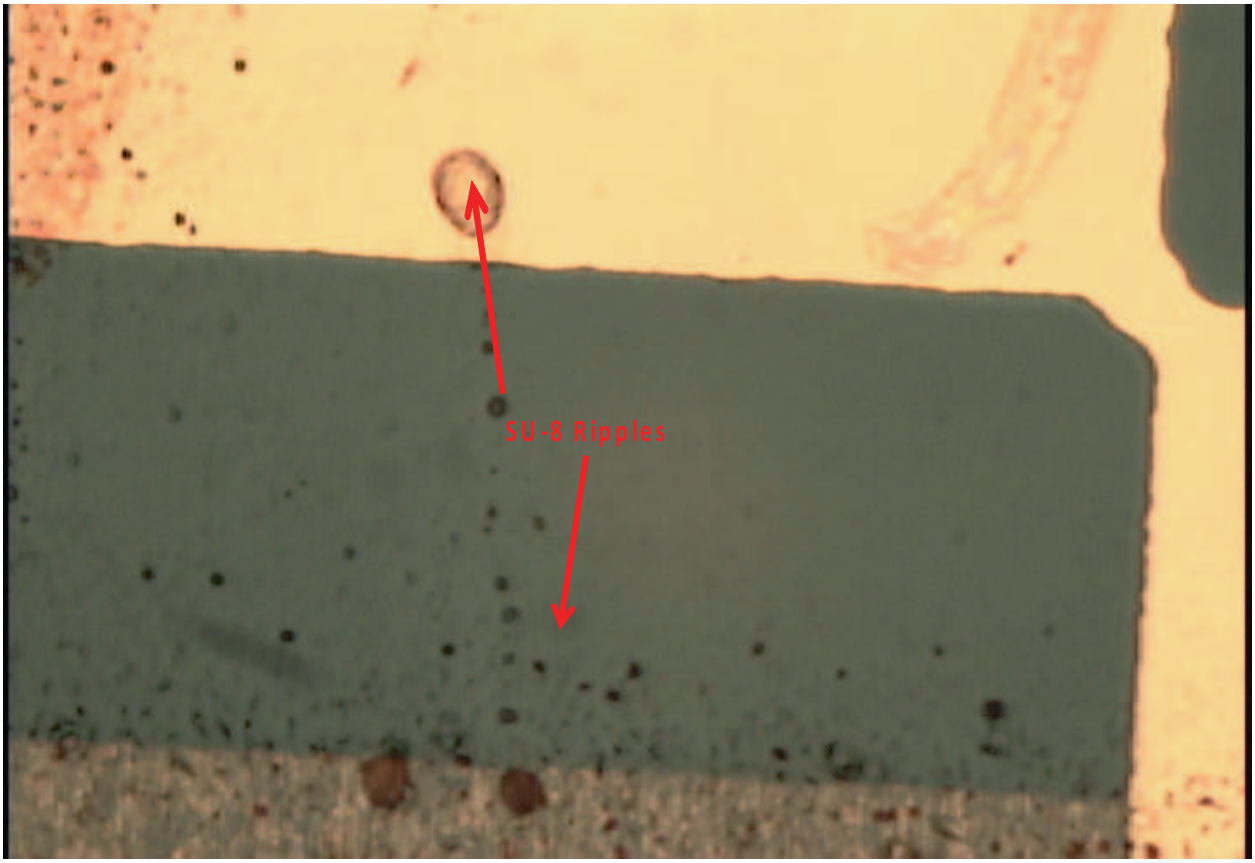

Figure 3.10 Non-uniformity of SU-8 layer.

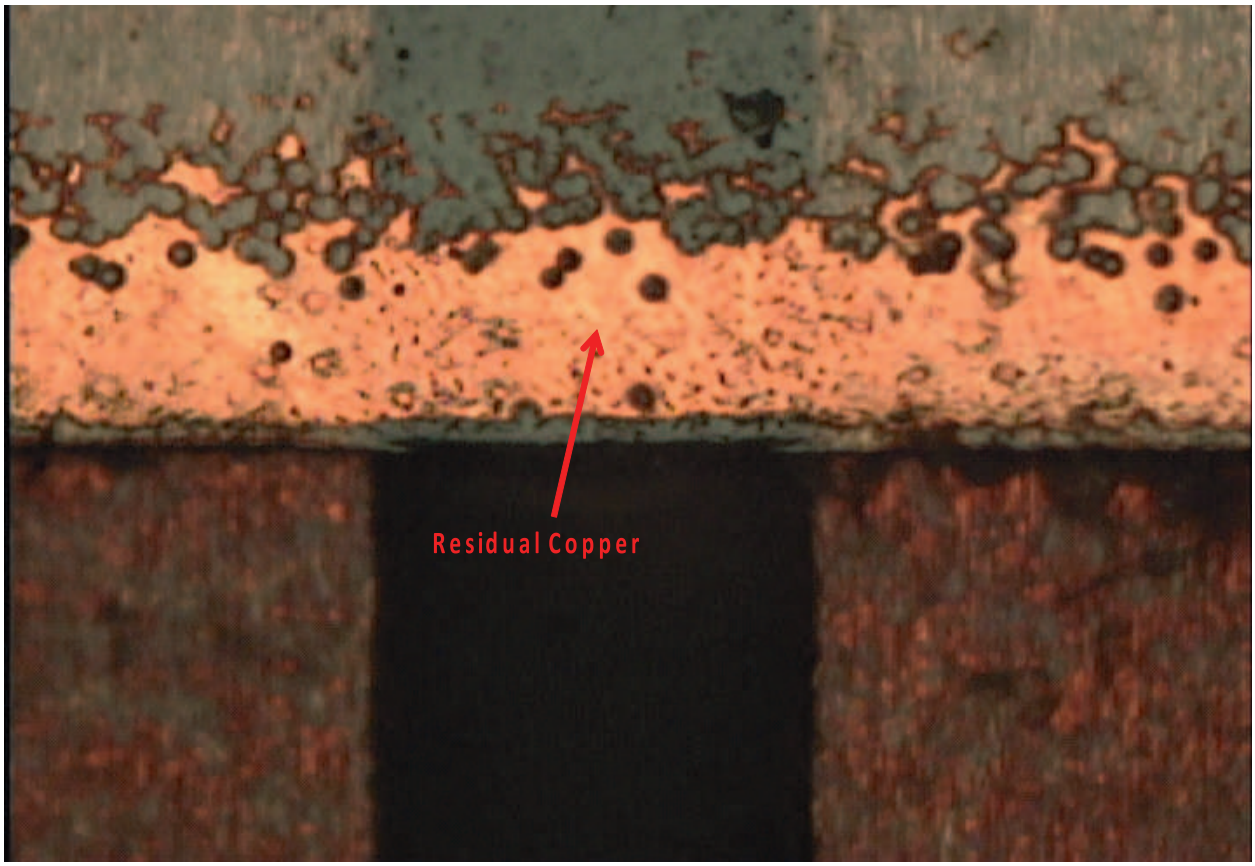

Figure 3.11 Excess copper on the second layer edges.

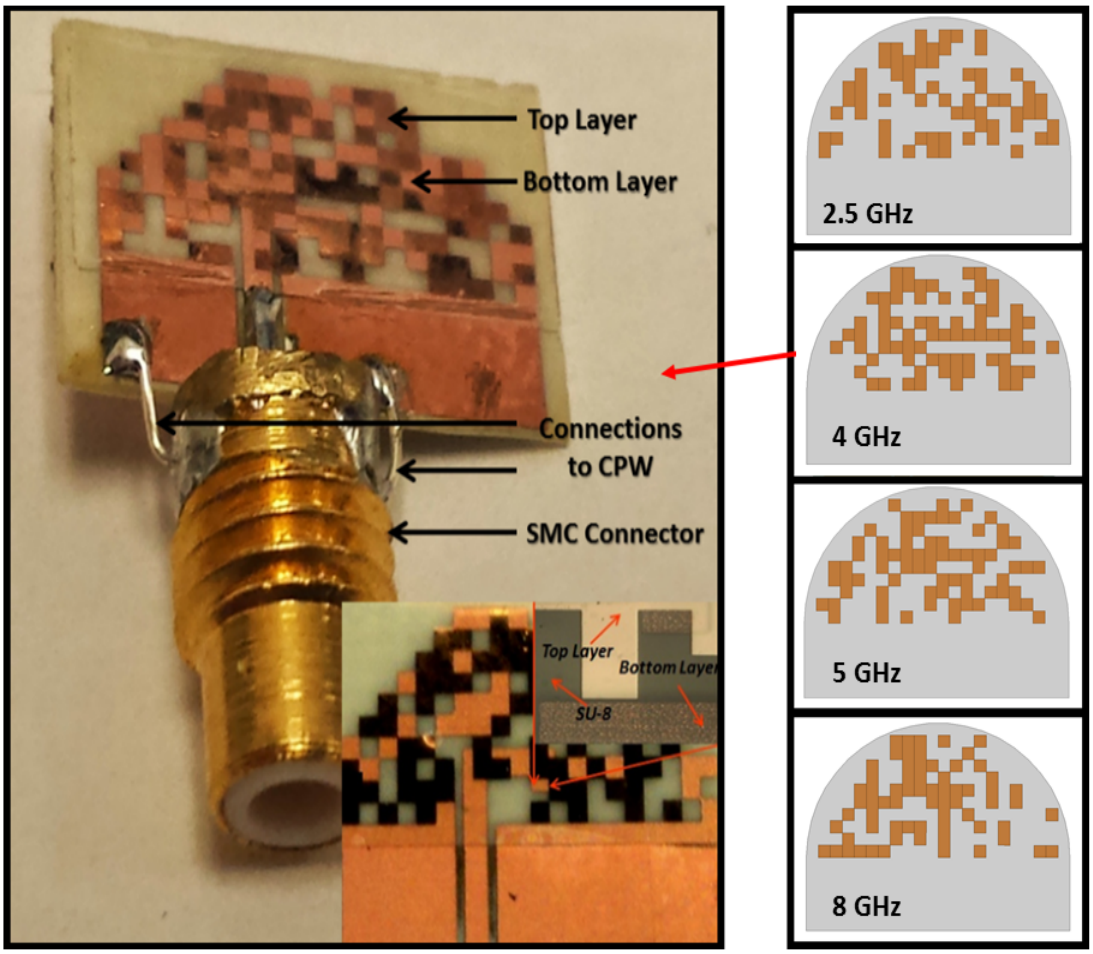

Figure 3.12 Example of one fabricated antenna configuration with a SMC connector attached. The simulated model of all pixel configurations are also shown for comparison.

3.3 Measurement of Antenna Reflection Coefficients

The reflection coefficients of the antennas are measured using a Agilent N5227A network analyzer. The reflection coefficients of antenna configurations corresponding to a resonance at 2.5, 4, 5, and 8GHz are measured. The measured reflection coefficient of each antenna as well as the simulated result are shown in Figures 3.13-3.16. The results show relatively good agreement with the simulations. However, the locations of the resonances are slightly shifted.

While a number of factors can contribute to this disagreement, the most likely cause is misalignment between the two antenna layers. Referencing Figure 3.5, resonance shifts similar to the ones displayed when misalignment is introduced are similar to the difference to the measured and simulated results shown here. Although the exact degree of misalignment in the fabricated antennas is unknown, levels similar to the above could easily be expected. Overall, the antenna resonance is within a reasonable range of the simulated values, especially considering the sensitivity of the antenna to misalignment. Figure 3.17 shows all four antenna configurations on the same frequency axis. From this figure it is clear that the tuning range of the antenna with the second layer is extremely dramatic, with a tuning range from 2.5GHz to 8GHz, or a tuning range of 320%.

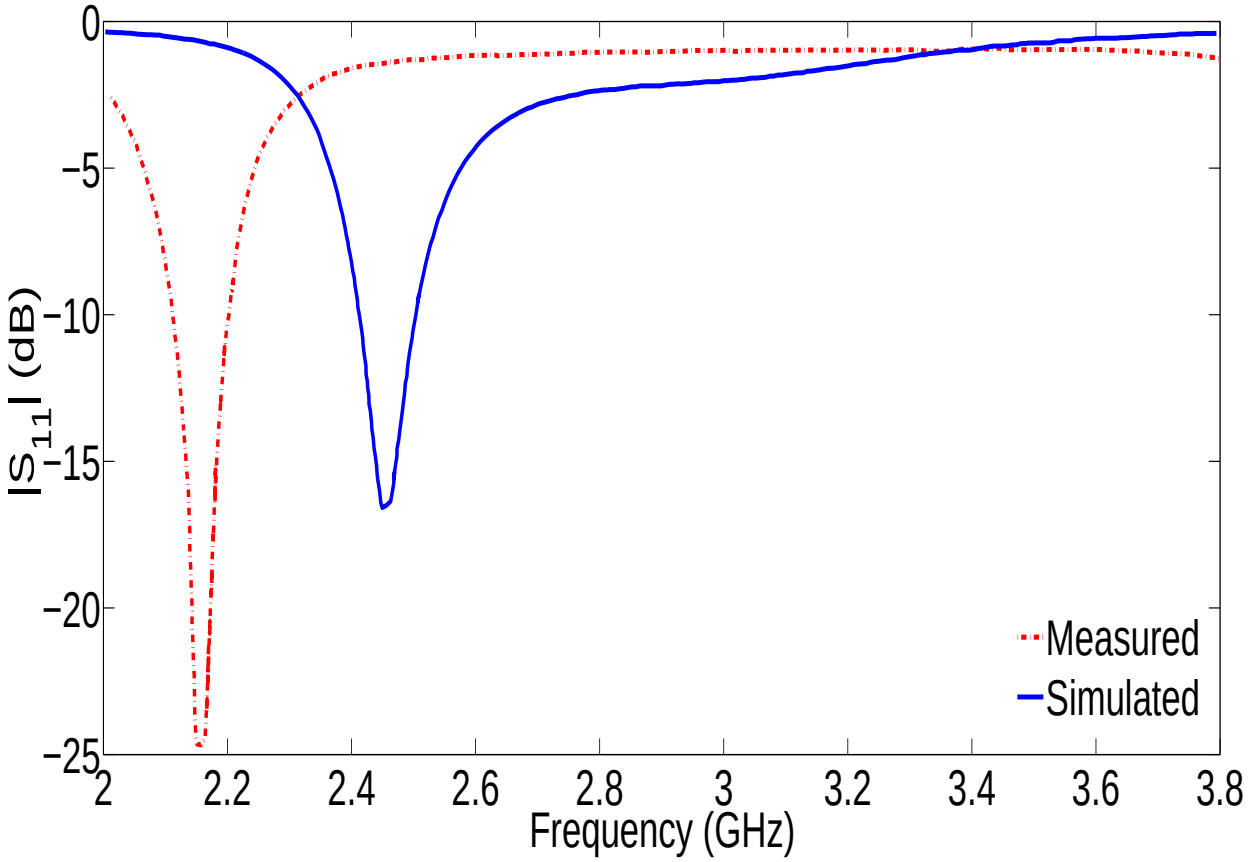

Figure 3.13 Measured and simulated reflection coefficients of one antenna configuration at 2.5GHz.

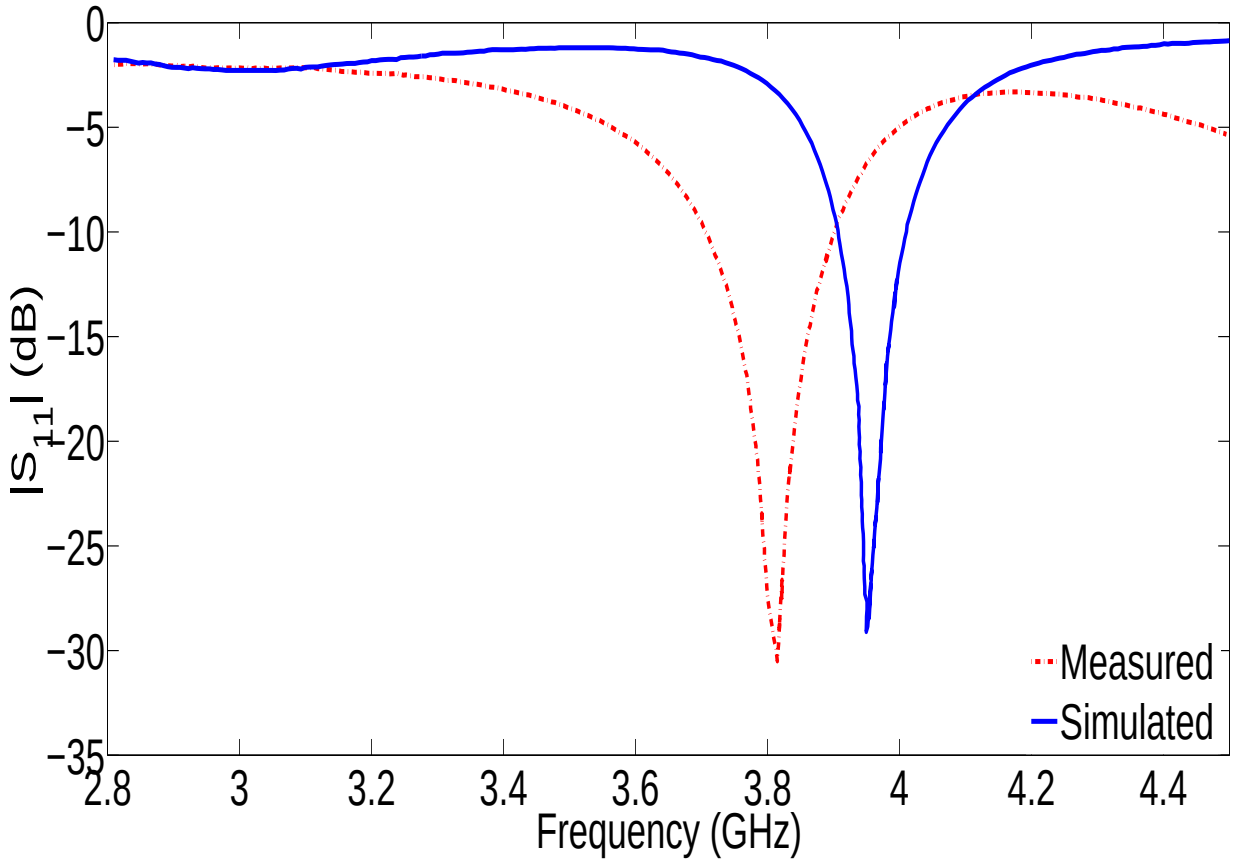

Figure 3.14 Measured and simulated reflection coefficients of one antenna configuration at at 4GHz.

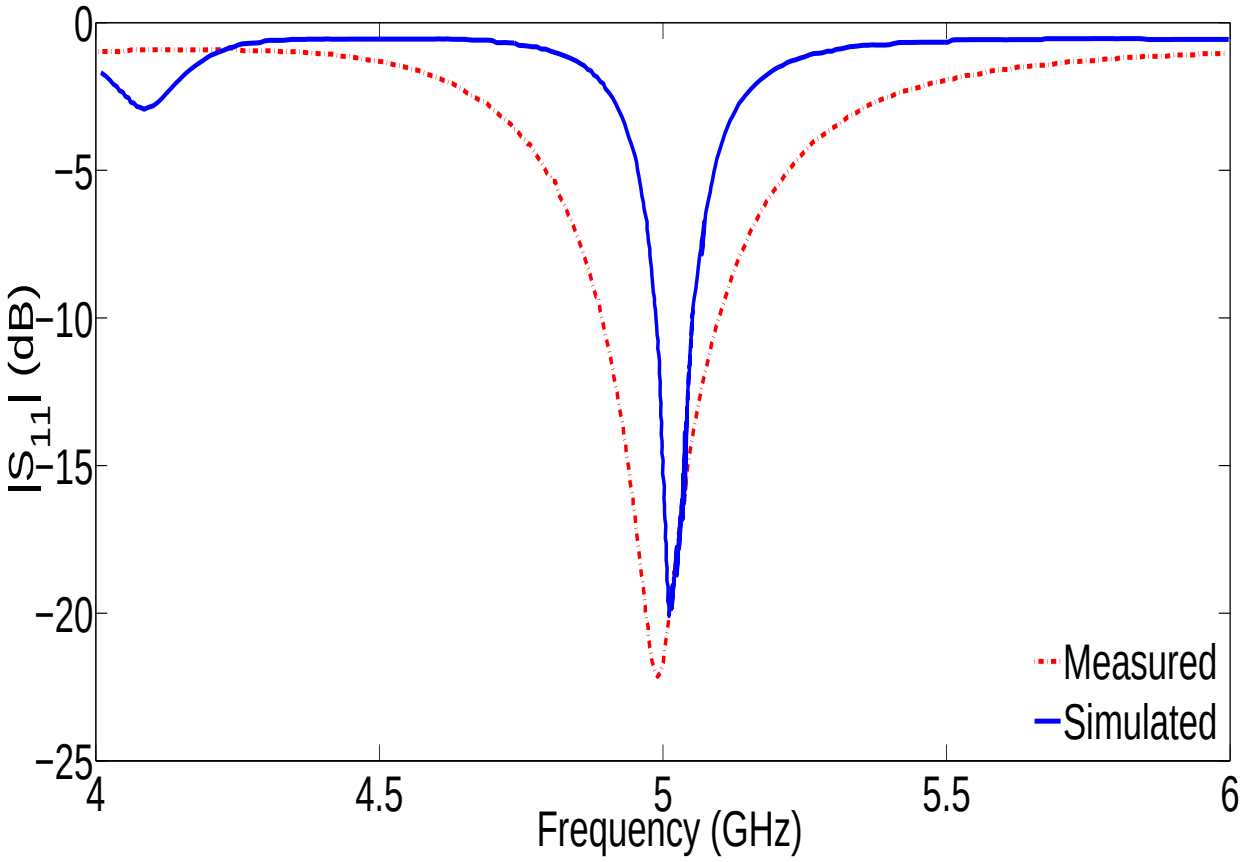

Figure 3.15 Measured and simulated reflection coefficients of one antenna configuration at at 5GHz.

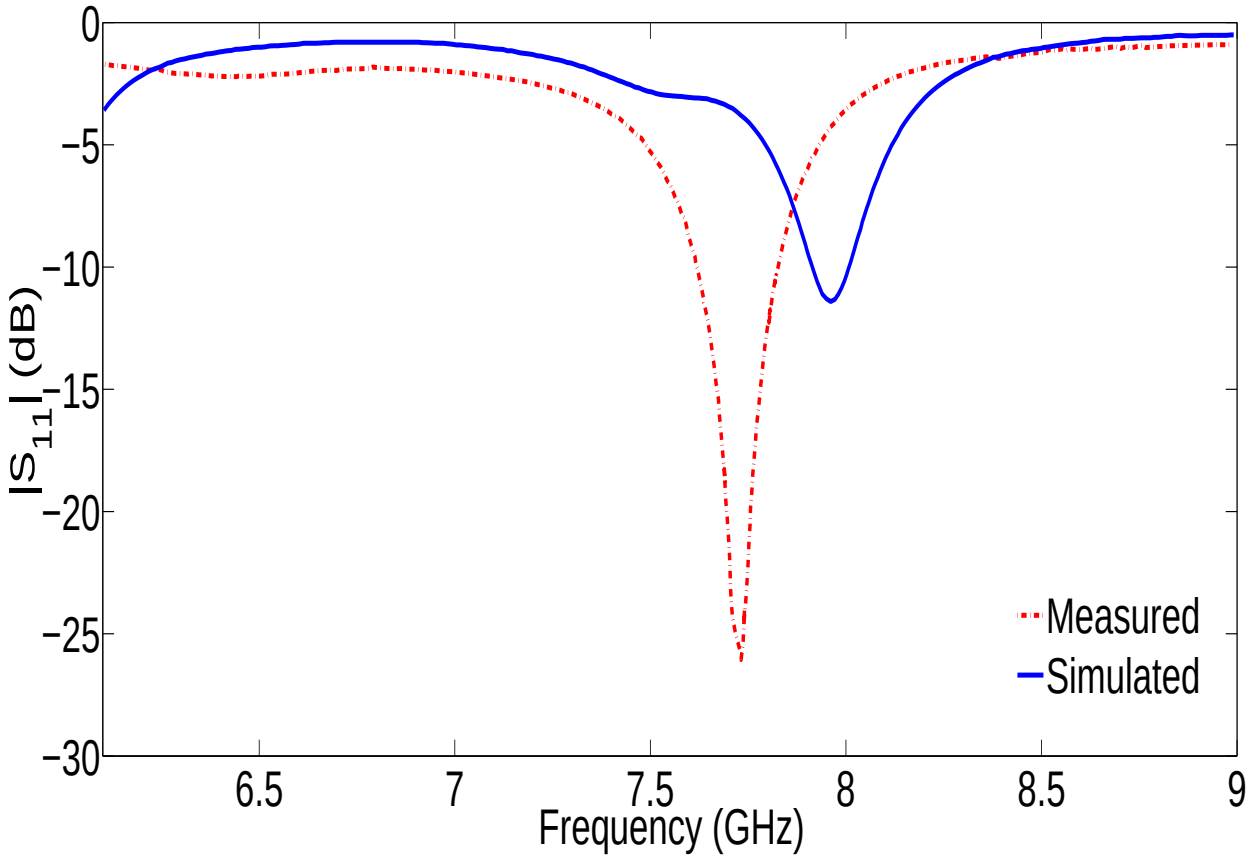

Figure 3.16 Measured and simulated reflection coefficients of one antenna configuration at at 8GHz.

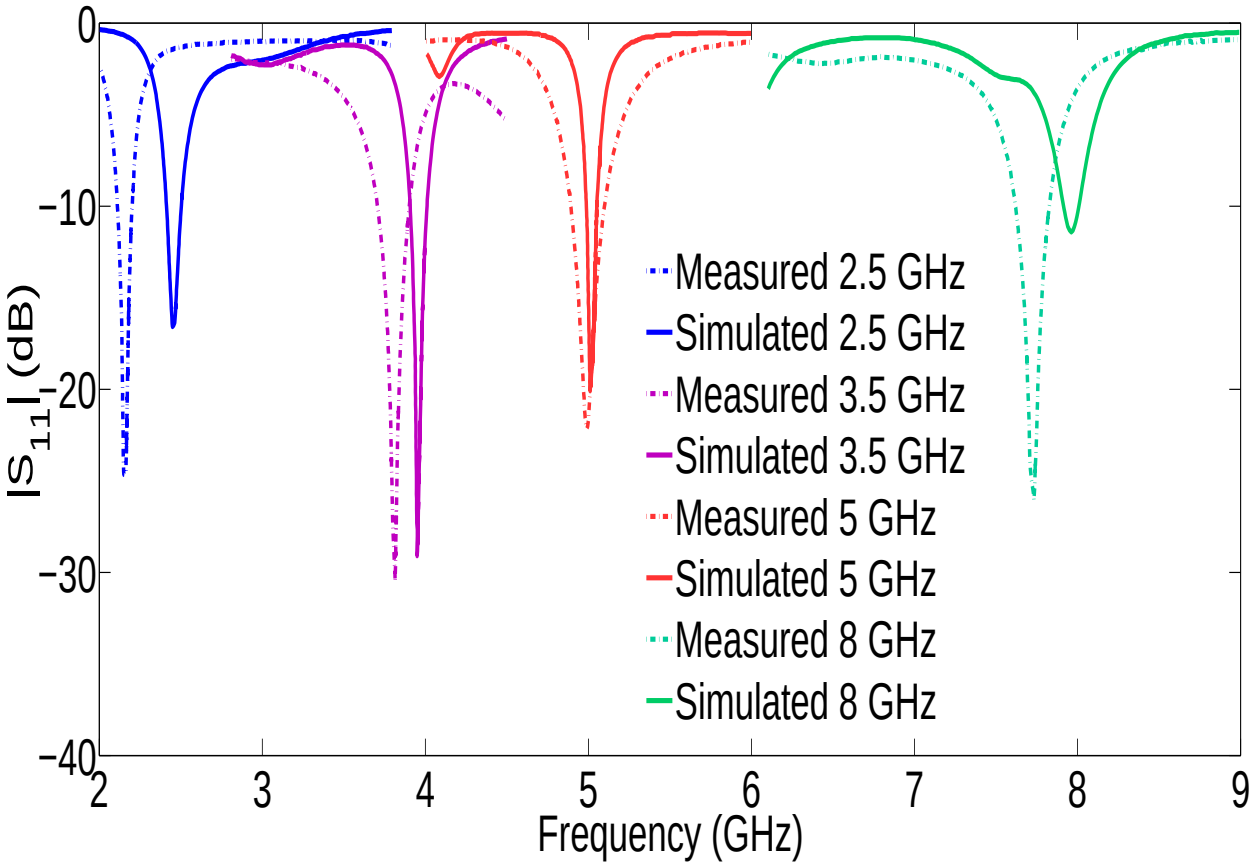

Figure 3.17 Measured and simulated reflection coefficients of all four antenna configurations.

3.4 Measurement of Antenna Radiation Parameters

The radiation characteristics of the antenna are also measured for three selected antenna configurations. The 2.5, 4, and 8GHz cases are measured using a SATIMO near-field measurement system. The radiation patterns are captured for both the azimuth (XY) and elevation (YZ) planes of the antenna. The antenna measurment setup is shown in Figure 3.18. The measured and simulated radiation patterns in both planes for the 2.5 GHz antenna are shown in Figures 3.19 and 3.20. The measured radiation patterns in both the azimuth and elevation planes match relatively well with the simulated results. Yet, in the elevation plane there is some disagreement in the back lobe of the pattern. Both patterns do however match well in terms of their maximum gain (directivity). In addition, the expected characteristics of the monopole are maintained, i.e. omnidirectional in the azimuth and bidirectional in the elevation plane.

Similar results are displayed for the patterns for the 4GHz plane, shown in Figures 3.21 and 3.22. However, in the azimuth plane, the pattern is further distorted than in the 2.5 GHz antenna, as there is an additional null in the pattern. Unfortunately, the measured results for the pattern of the 8GHz antenna do not match as well as the previous antennas. These results are shown in Figures 3.23 and 3.24. In the azimuth plane, many lobes are displayed in the measured results, as opposed to the omnidirectional pattern that is expected. The elevation plane matches slightly better than the azimuth, but neither show particularly good agreement with the simulated results.

These discrepancies are primary thought to be caused by the antenna becoming unbalanced at such a high frequency. In addition, at 8GHz the antenna is now much greater in wavelength than originally intended as the size is unchanged from the 2.5 GHz antenna configuration. While the radiation of the characteristics of the antenna do not match as well for the higher frequencies, most of the patterns match very well with the simulated results.

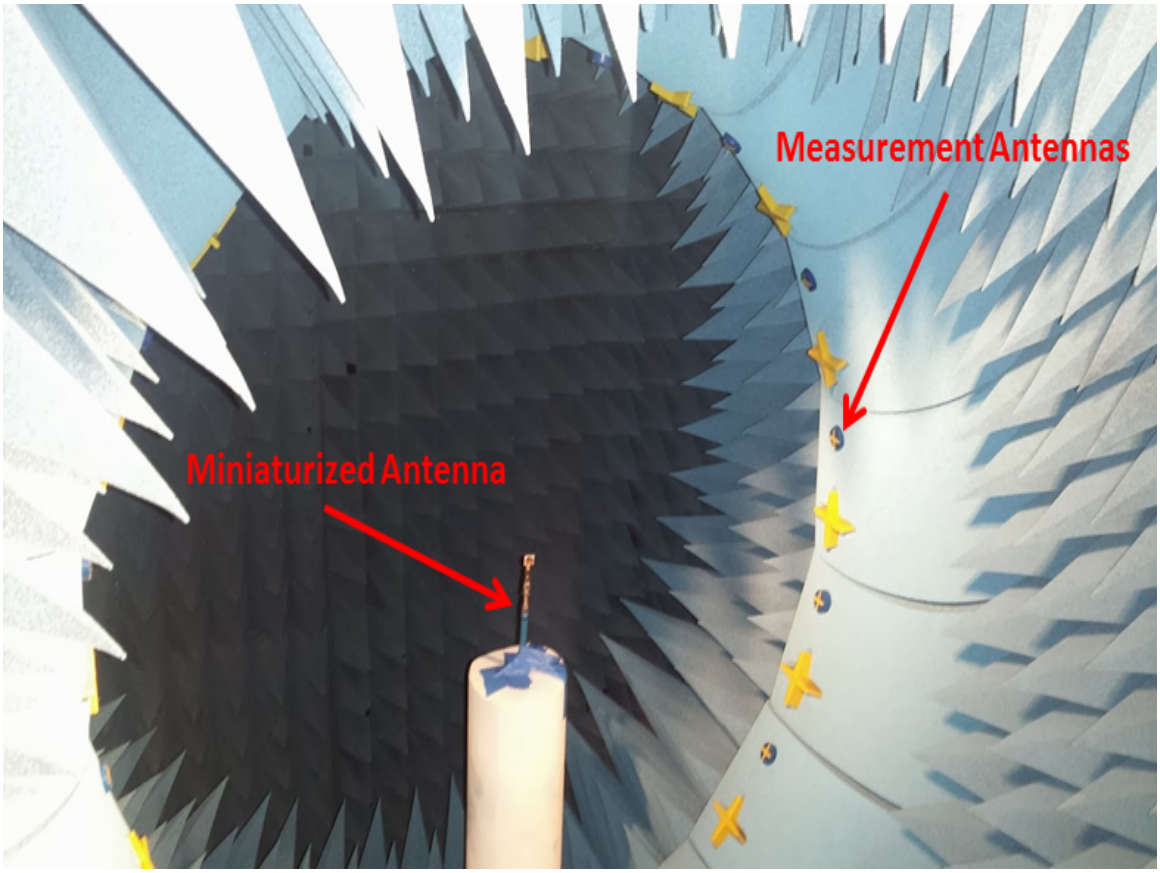

Figure 3.18 Antenna radiation pattern measurement setup.

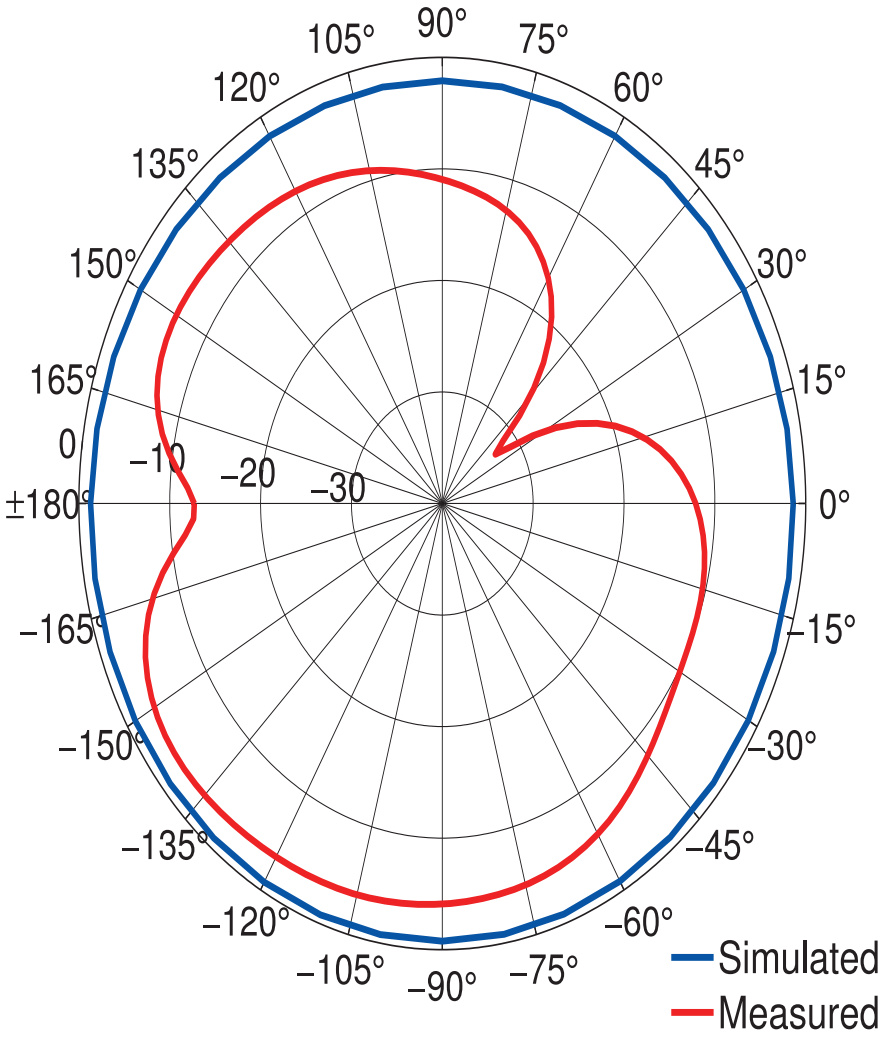

Figure 3.19 Measured and simulated radiation patterns in XY plane at 2.5 GHz.

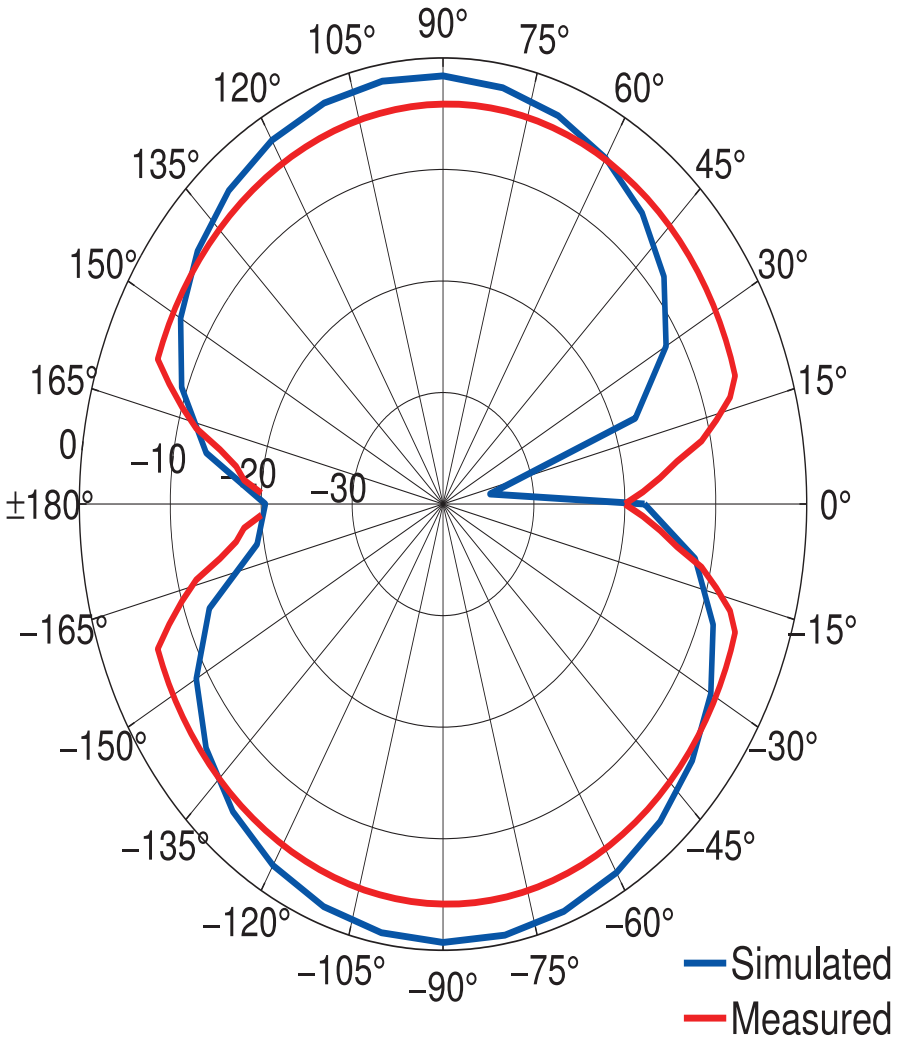

Figure 3.20 Measured and simulated radiation patterns in YZ plane at 2.5 GHz.

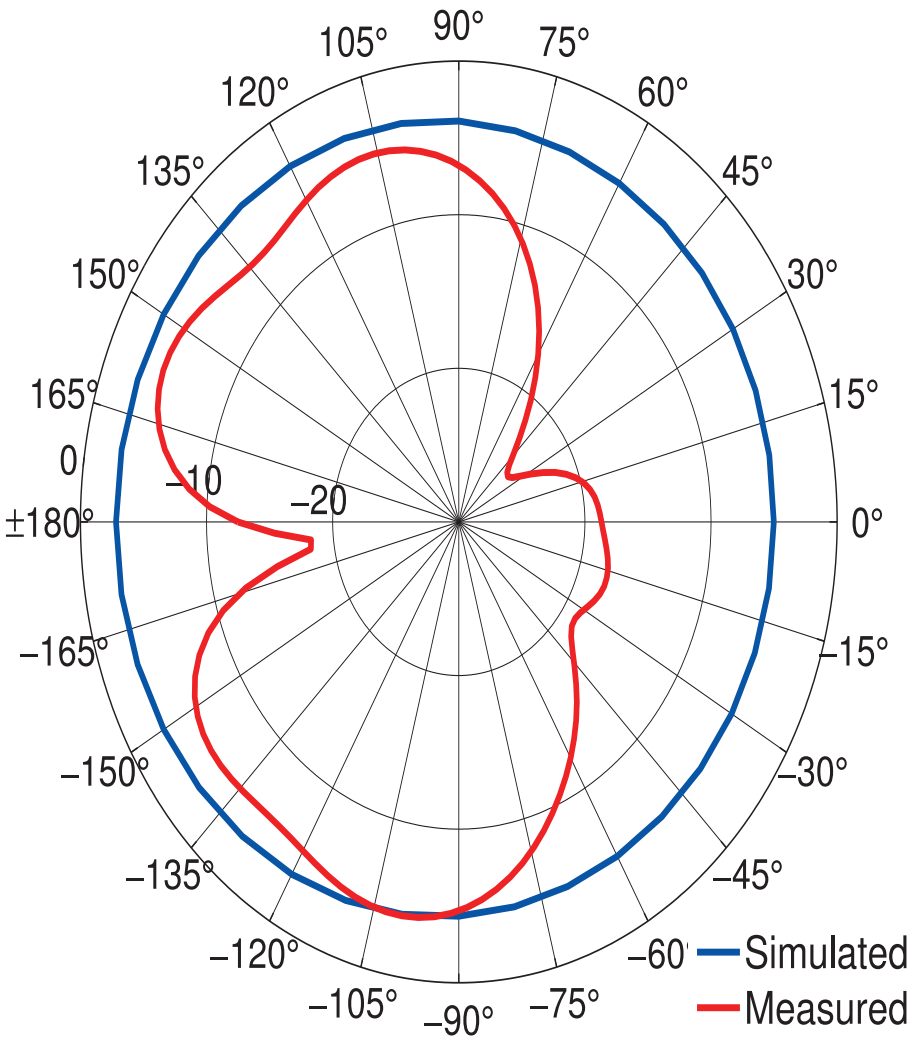

Figure 3.21 Measured and simulated radiation patterns in XY plane at 4 GHz.

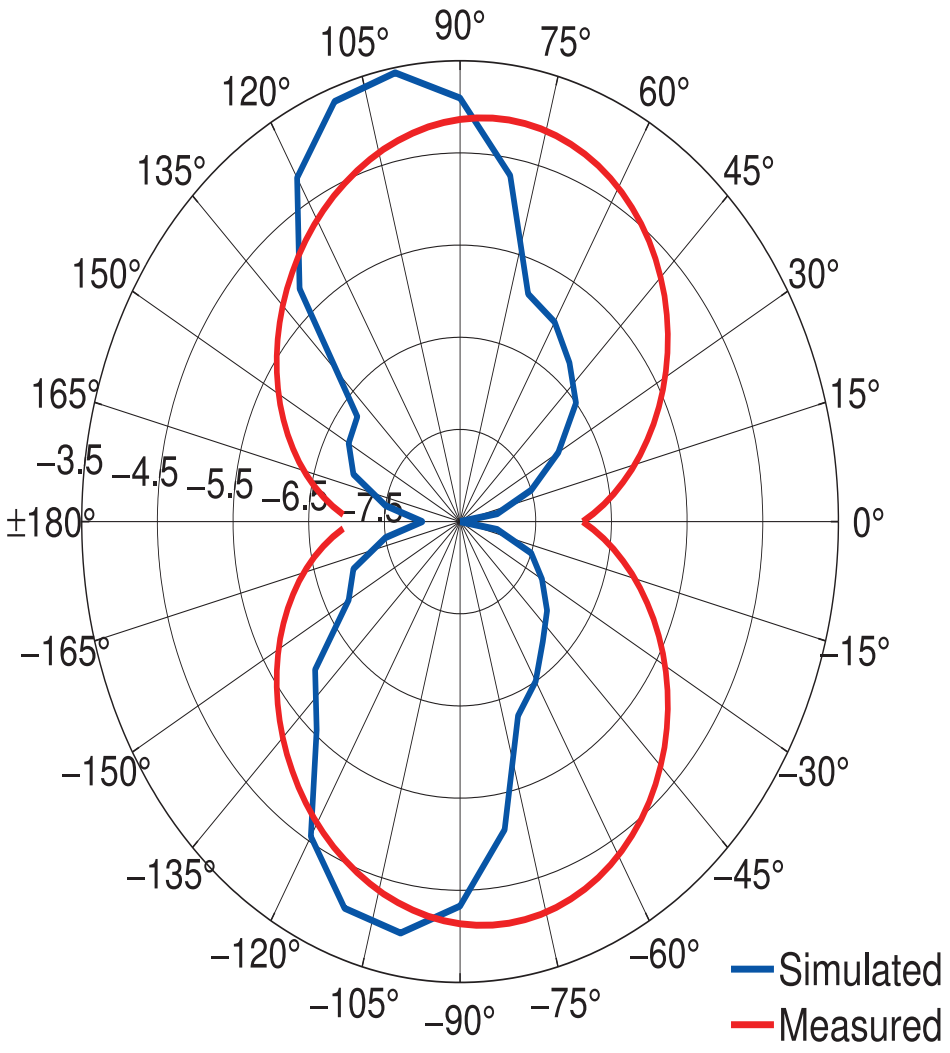

Figure 3.22 Measured and simulated radiation patterns in YZ plane at 4 GHz.

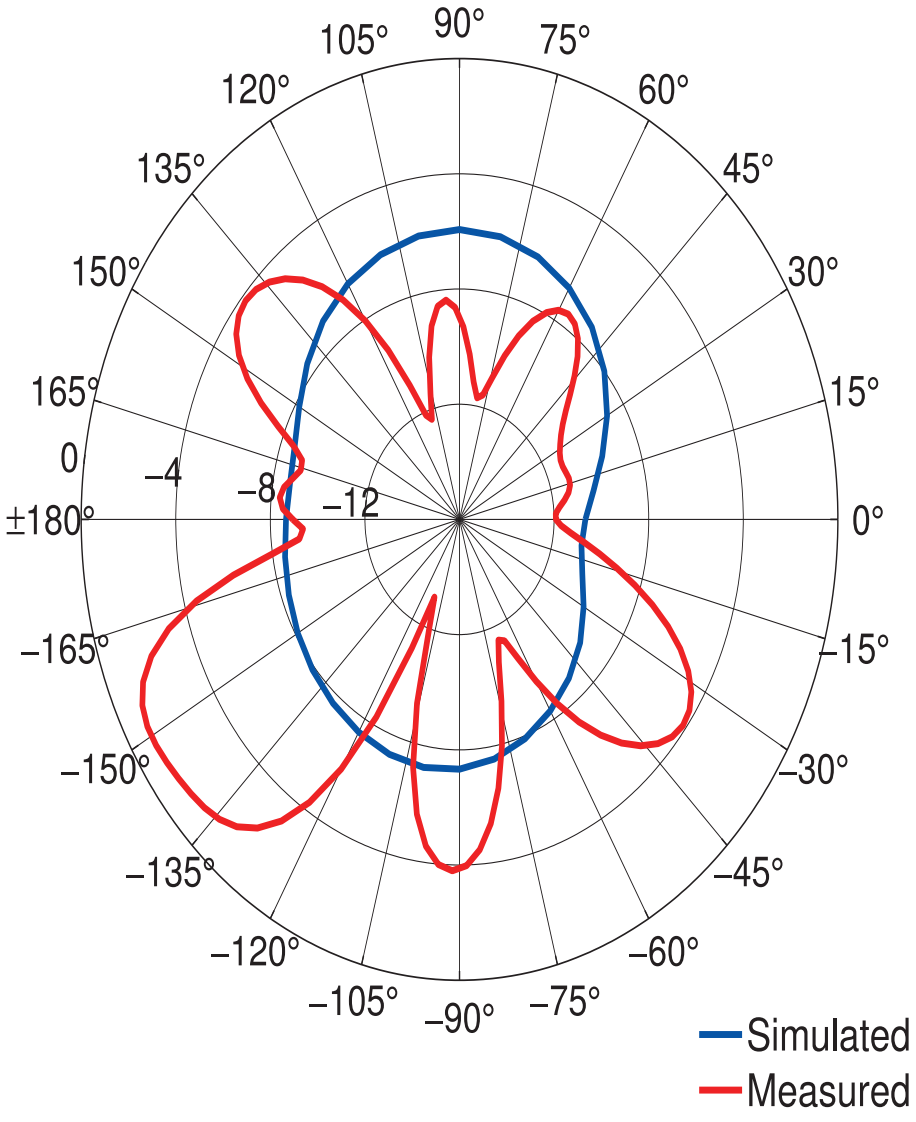

Figure 3.23 Measured and simulated radiation patterns in XY plane at 8 GHz.

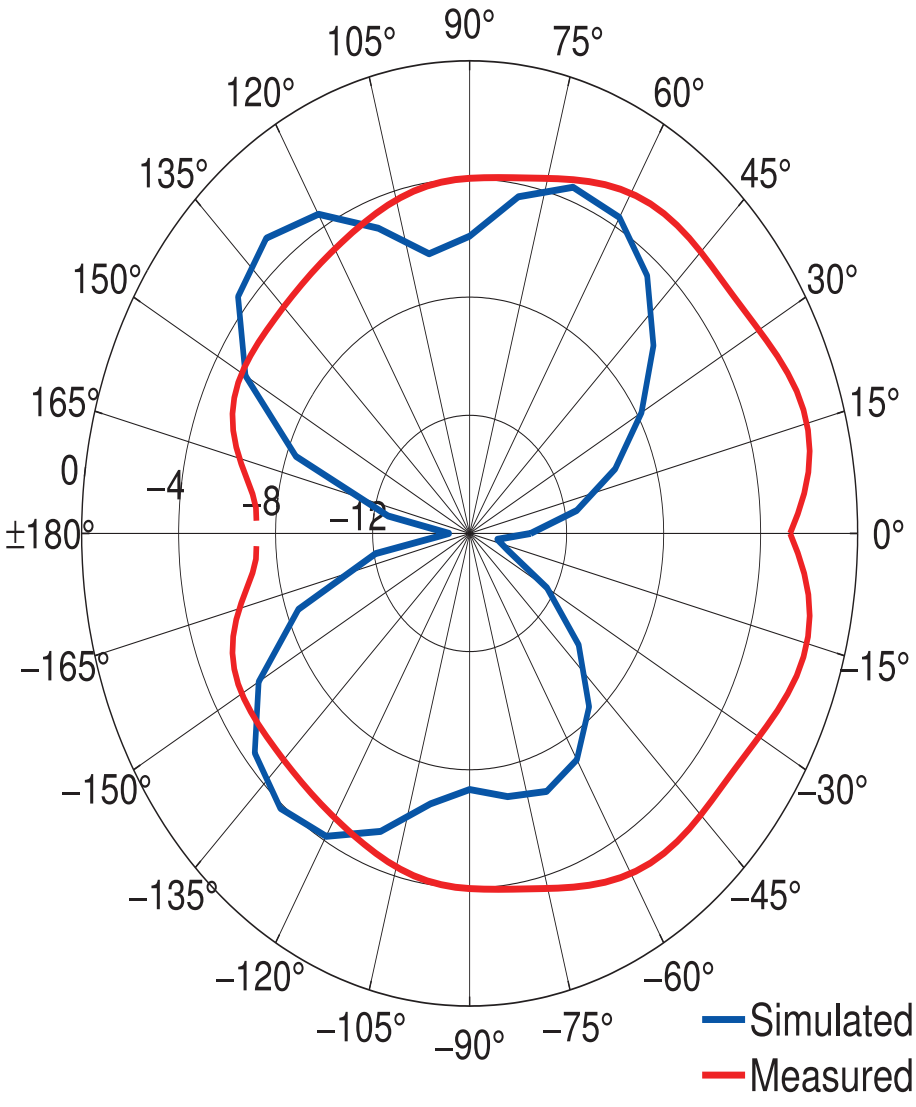

Figure 3.24 Measured and simulated radiation patterns in YZ plane at 8 GHz.

CHAPTER 4

Conclusions and Future Studies

A multi-layered metamaterial inspired antenna capable of dynamic tunability through a photoconductive pixel grid is introduced in this thesis. A GA optimization technique is used to tune the antenna with a second pixel grid that is placed directly on the miniaturized antenna layer. The GA design process is exlpained at length, and the simulated results show that many pixel combinations can be found which produce a large range of tuning. In addition, the radiation patterns of the antenna are shown to not be greatly affected by the second pixel tuning layer, and the radiation efficiency is optimized to produce the most efficient antenna possible. Further, a variety of conductivities are investigated to ensure the tuning layer will be useable with non-traditional conductors. Antenna states are fabricated with a metallic pixel grid to test the tuning ability of the antenna. Initially, PET thin films are investigated to be used as hot swappable loading elements, but the airgap and misalignment between layers are shown to be too large for this method to produce accurate results. A multi-layer fabrication method is then investigated which uses an SU-8 layer that can be precisely fabricated to eliminate the airgap and minimize the misalignment between layers. A large number of states are then fabricated using this method, and states corresponding to resonant frequencies of 2.5, 4, 5, and 8GHz are presented. The reflection coefficient for each antenna is measured and are shown to match extremely well with the

simulated results. Finally, the radiation patterns of each antenna were measured, which in the lower frequency spectrum show a good matching with the simulated results. These antennas show that a very large range of tuning can be achieved with this method. In comparison with the traditional tuning methods described in chapter one, this method provides at least 10 times the tuning capability achieved over the conventional approaches. If only the measured results are used as a measure of the possible tuning range of the antenna, a tuning range of approximately 320% is presented in this work. However, higher frequency antennas could easily be fabricated and this range could be extended much farther. Although in this case a metallic pixel grid is explored through fabrication, our expectations are that this second metal layer can be replaced by a photoconductor or phase change material to achieve real time tuning capability.

APPENDIX

Appendix: Genetic Algorithm Optimization Code

This particular GA is meant for use at a resonant frequency of 4 GHz. However, this frequency can easily be changed. To implement this code successfully, all of the local directories and paths need to be changed to fit the users desired setup.

```
1
2  clc
3  clear all;
4  format long
5  %START GA
6  %                        III. GA parameters
7  maxit=3;                     % max number of iterations
8  mincost=-10000;          % minimum cost
9  popsize=300;                    % set population size
10 Muprob=.2;              % set mutation rate
11 selection=0.1;              % fraction of population kept
12 m=20;                 %Number of bits per column
13 n=10 ;                %Number of bits per row
14 Nt=m*n;                         % number of bits in each chromosome
15 ChromLength=Nt;
16 keep=floor(selection*popsize);   % #population members that survive
17 iga=1;                   %INITIALIZE GENERATION COUNTER
```

```
18 bestfit=10000;
19 %-------------------------------------------------------------
20 %               Create the initial population for each individual
21
22
23 % Make folders for each generation and the random search hfss simulations
24 mkdir('Gen1')
25 mkdir('Gen2')
26 mkdir('Gen3')
27 mkdir('RandomSearch')
28
29
30 % add paths to the required m-files.
31 addpath('C:\AFRL_MAT\Efficiency4GHz\Files\');
32 FarFieldpath='C:\AFRL_MAT\Efficiency4GHz\farFieldEff.m' ;
33 % Frequency sweep parameters
34 eps_o=8.8541878176e-12;  %Epsilon
35 mu_o= 4*pi*1e-7;          %Mu
36 Co=1/sqrt(eps_o*mu_o); %Speed of light in free space
37 fLow =6e9;     %Simulation start point
38 fHigh =10e9;    %Simulation end point
39 nPoints = 1;  %frequency range discretization
40 np = 1;
41 fC =4e9;        % Frequency of Interest.
42 Wv = (Co/fC)*1000;  % Wavelength.
43
44 Pw=.5;           % Pixel Width
45 XL=m;          % Nuber of pixels in X direction
46 ZL=n; %Nuber of pixels in Y direction
47 SRR_LX=(Pw*XL); %Unit cells length X-direction
48 SRR_LZ=(Pw*ZL);  %Unit cell height Y direction
49
50 %Ground Plane
```

```
51 Gnd_X=Wv/2;
52 Gnd_Y=Wv/2;
53 Gnd_Z=3*Pw+3*Pw;
54
55 X_sp=Pw/3;
56 Z_sp=X_sp/2;
57
58 %Antenna Parameter
59 PwL=Pw;
60 LoopW=5*PwL;
61 P_X=1*PwL;
62 P_Z=3.5*PwL;
63 P_w=PwL*1.4;
64 P_sx=P_X-P_w;
65 P_sz=P_Z-0.5*P_w;
66 sub_P=P_Z/3-PwL;
67 Gndgap=P_w+.3;
68
69 %Substrate Dimensions
70 Sub_X= SRR_LX+2*Pw;   %Substrate length
71 Sub_Y=-.5 ;%Substrate width
72 Sub2_Y=-.5;
73 Sub_Z= SRR_LZ;%SRR_LZ %54.6100;%Substrate height
74 Cir_Sub_Y=-.3;
75 %Feed parameters
76 R_oc=2.6/2;
77 Th_oc=R_oc-.1;
78 Hi_oc=30;
79 R_feed=.635/2;
80 Hi_feed=Hi_oc;
81 R_tf=Th_oc; %R_oc-.1;
82 Th_tf=R_feed;
83 Feed=(-P_X+P_w/2)/2;
```

```
84 Deembed=Hi_feed;
85 FX=-2.5*Pw-.2;
86 CapZ=1;
87  % Airbox Dimensions
88 G_R =Wv/3+SRR_LX*2 ;       %Waveguide length
89 G_H = Wv/2+SRR_LX+Hi_oc;    %Waveguide height
90
91 Cop_Th=.017;
92
93 % HFSS Executable Path.
94 hfssExePath = 'C:\"Program Files (x86)"\Ansoft\HFSS13.0\hfss.exe';
95
96
97 for ip=1:popsize;
98     tic
99
100 for jp = 1:ChromLength
101     if rand() > 0.5
102         Pop(ip,jp) = 1;
103     else
104         Pop(ip,jp) =0;
105     end
106 end
107
108
109 Meta=(reshape(Pop(ip,:),n,m));
110  tt=0;
111   for ix=1:6
112       for iy=1:5
113       Meta(n-iy+tt,ix)=0;
114       end
115       tt=tt+1;
116   end
```

```
117
118   tt=0;
119   for ix=1:6
120      for iy=1:5
121      Meta(n-iy+tt,m-ix+1)=0;
122      end
123      tt=tt+1;
124   end
125  % Temp Files.
126
127
128 tmpPrjFile = 'C:\AFRL_MAT\Efficiency4GHz\GALoop.hfss';
129 tmpDataFile = 'C:\AFRL_MAT\Efficiency4GHz\GALoopData.m';
130 tmpScriptFile = 'C:\AFRL_MAT\Efficiency4GHz\GALoopScript.vbs';
131
132
133     % Create a new temporary HFSS script file.
134     fid = fopen(tmpScriptFile, 'wt');
135
136     % Create a new HFSS Project and insert a new design.
137     hfssNewProject(fid);
138     hfssInsertDesign(fid, 'GA_Loop');
139
140
141   %Draw AirBox
142 hfssCylinder(fid, 'Air_Box', 'Z', [0, 0, -(Hi_oc+Gnd_Z+CapZ+10)], G_R, ...
      G_H, 'mm');
143 hfssAssignRadiation(fid, 'Box_Rad', 'Air_Box');
144 hfssSetTransparency(fid, {'Air_Box'}, 0.95);
145   %Draw Feed (Outer Conductor)
146   hfssHollowCylinder(fid, 'Outer_C', 'Z', [FX, 0, -(Hi_oc+Gnd_Z)], ...
         Th_oc, R_oc, (Hi_oc), 'mm');
147   hfssAssignPE(fid, 'PEC_oc',  {'Outer_C'});
```

```
148 %   Teflon
149   hfssHollowCylinder(fid, 'Tef', 'Z', [FX, 0, -(Hi_oc+Gnd_Z)], Th_tf, ...
          R_tf, (Hi_oc), 'mm');
150    hfssAssignMaterial(fid, 'Tef', 'Neltec NX9294 (tm)');
151 %     Inner Conductor
152   hfssCylinder(fid, 'Inner_C', 'Z', [FX, 0, -(Hi_oc+Gnd_Z)], R_feed, ...
          (Hi_oc), 'mm');
153   hfssAssignPE(fid, 'PEC_Ic',  {'Inner_C'});
154 %Draw waveport
155     hfssCircularPort(fid, 'LPort', 'port1', 'Z', [FX, 0, ...
            -(Hi_oc+Gnd_Z)], R_tf,Deembed, 'mm');
156     hfssCylinder(fid, 'PortCup1', 'Z', [FX, 0, -(Hi_oc+Gnd_Z)], R_oc, ...
            -CapZ, 'mm');
157 hfssAssignMaterial(fid, 'PortCup1', 'pec');
158
159
160 %Draw Ground plane
161 %Ground 1
162 hfssRectangle(fid, 'Gnd', 'Y', [-Sub_X/2+Pw, 0, ...
       -Gnd_Z],Gnd_Z,Sub_X-2*Pw, 'mm');
163 hfssRectangle(fid, 'Gnd_Sub', 'Y', [-Gndgap/2+FX, 0, -Gnd_Z], Gnd_Z, ...
       Gndgap, 'mm');
164 hfssSubtract(fid, {'Gnd'}, {'Gnd_Sub'});
165 hfssAssignFiniteCond(fid, 'PEC_Gnd', 0, 'um', {'Gnd'});
166
167
168 %Circuitry
169 hfssRectangle(fid, 'Circuit1', 'Y', [-Sub_X/2, -Sub_Y, ...
       -Gnd_Z+1.62],Gnd_Z-1.62,Sub_X, 'mm');
170 hfssCircle(fid, 'Circuit2', 'Y', [0, -Sub_Y, 0],Sub_X/2, 'mm');
171 hfssRectangle(fid, 'Circuit2Sub', 'Y', [-Sub_X/2, -Sub_Y, ...
       0],-Sub_X/2,Sub_X, 'mm');
172 hfssSubtract(fid, {'Circuit2'}, {'Circuit2Sub'});
```

```
hfssUnite(fid, 'Circuit1','Circuit2');
hfssAssignFiniteCond(fid, 'PEC_Circuit1', 0, 'um', {'Circuit1'});


%Draw Substrate
hfssBox(fid, 'Substrate', [-Sub_X/2, 0, -Gnd_Z], [Sub_X, -Sub_Y, ...
    Gnd_Z], 'mm');
hfssAssignMaterial(fid, 'Substrate', 'Rogers RO4003 (tm)');
hfssSetColor(fid, 'Substrate', [0, 128, 0]);
hfssSetTransparency(fid, {'Substrate'}, 0.8);
hfssCylinder(fid, 'Sub2', 'Y', [0, 0, 0], Sub_X/2, -Sub_Y, 'mm');
hfssBox(fid, 'Sub2sub', [-Sub_X/2, 0, -Sub_X/2], [Sub_X, -Sub_Y, ...
    Sub_X/2], 'mm');
hfssSubtract(fid, {'Sub2'}, {'Sub2sub'});
hfssUnite(fid, 'Substrate','Sub2');

%Draw Extra Layer Substrate
hfssBox(fid, 'Layer', [-Sub_X/2, 0, -Gnd_Z], [Sub_X, .025, Gnd_Z], 'mm');
hfssAssignMaterial(fid, 'Layer', 'GIL MC5 (tm)');
hfssSetColor(fid, 'Layer', [0, 900, 0]);
hfssSetTransparency(fid, {'Layer'}, 0.8);
hfssCylinder(fid, 'Sub0', 'Y', [0, 0, 0], Sub_X/2, .025, 'mm');
hfssBox(fid, 'Sub2sub0', [-Sub_X/2, 0, -Sub_X/2], [Sub_X, .025, ...
    Sub_X/2], 'mm');
hfssSubtract(fid, {'Sub0'}, {'Sub2sub0'});
hfssUnite(fid, 'Layer','Sub0');
hfssMove(fid, {'Layer'}, [0, -.025, 0], 'mm');

%Draw Folded Monopole
hfssRectangle(fid, 'mono', 'Y', [-P_w/2+FX, 0, -Gnd_Z], Gnd_Z, P_w,'mm');
hfssRectangle(fid, 'Loop', 'Y', [-P_w/2+FX, 0, 0], P_Z, LoopW,'mm');
hfssRectangle(fid, 'Loopsub', 'Y', [FX+P_w/2, 0, 0], P_Z-P_w, ...
    LoopW-2*P_w,'mm');
```

```
202 hfssRectangle(fid, 'Loopsub2', 'Y', [FX+LoopW-3*P_w/2, 0, 0], P_w*1, ...
        P_w,'mm');
203 hfssAssignFiniteCond(fid, 'PEC_Loop', 0, 'um', {'mono'});
204 hfssSubtract(fid, {'Loop'}, {'Loopsub'});
205  hfssSubtract(fid, {'Loop'}, {'Loopsub2'});
206 hfssUnite(fid, 'mono','Loop');
207
208 % Draw Bottom Substrate pads
209  hfssRectangle(fid, 'Pad1', 'Y' , [-2.5,0,0], .5, .5,'mm');
210  hfssAssignFiniteCond(fid, 'Pad1', 0, 'um', {'Pad1'})
211 hfssRectangle(fid, 'Pad2', 'Y' , [-5,0,.5], 1.5, .5,'mm');
212  hfssAssignFiniteCond(fid, 'Pad2', 0, 'um', {'Pad2'})
213 hfssRectangle(fid, 'Pad3', 'Y' , [-4.5,0,.5], 1, .5,'mm');
214  hfssAssignFiniteCond(fid, 'Pad3', 0, 'um', {'Pad3'})
215 hfssRectangle(fid, 'Pad4', 'Y' , [-4,0,1.5], 1.5, .5,'mm');
216  hfssAssignFiniteCond(fid, 'Pad4', 0, 'um', {'Pad4'})
217 hfssRectangle(fid, 'Pad5', 'Y' , [-3.5,0,1], 1.5, .5,'mm');
218  hfssAssignFiniteCond(fid, 'Pad5', 0, 'um', {'Pad5'})
219 hfssRectangle(fid, 'Pad6', 'Y' , [-3,0,1.5], .5, .5,'mm');
220  hfssAssignFiniteCond(fid, 'Pad6', 0, 'um', {'Pad6'})
221 hfssRectangle(fid, 'Pad7', 'Y' , [-2.5,0,1], .5, .5,'mm');
222  hfssAssignFiniteCond(fid, 'Pad7', 0, 'um', {'Pad7'})
223 hfssRectangle(fid, 'Pad8', 'Y' , [-2.5,0,2], .5, .5,'mm');
224  hfssAssignFiniteCond(fid, 'Pad8', 0, 'um', {'Pad8'})
225 hfssRectangle(fid, 'Pad9', 'Y' , [-3.5,0,3], .5, .5,'mm');
226  hfssAssignFiniteCond(fid, 'Pad9', 0, 'um', {'Pad9'})
227 hfssRectangle(fid, 'Pad10', 'Y' , [-3,0,3], .5, .5,'mm');
228  hfssAssignFiniteCond(fid, 'Pad10', 0, 'um', {'Pad10'})
229 hfssRectangle(fid, 'Pad11', 'Y' , [-2.5,0,3], 1.5, .5,'mm');
230  hfssAssignFiniteCond(fid, 'Pad11', 0, 'um', {'Pad11'})
231 hfssRectangle(fid, 'Pad12', 'Y' , [-2,0,2], 2, .5,'mm');
232  hfssAssignFiniteCond(fid, 'Pad12', 0, 'um', {'Pad12'})
233 hfssRectangle(fid, 'Pad13', 'Y' , [-2,0,4.5], .5, .5,'mm');
```

```
234  hfssAssignFiniteCond(fid, 'Pad13', 0, 'um', {'Pad13'})
235 hfssRectangle(fid, 'Pad14', 'Y' , [-1.5,0,2], 1, .5,'mm');
236  hfssAssignFiniteCond(fid, 'Pad14', 0, 'um', {'Pad14'});
237  hfssRectangle(fid, 'Pad15', 'Y' , [-1.5,0,3.5], .5, .5,'mm');
238  hfssAssignFiniteCond(fid, 'Pad15', 0, 'um', {'Pad15'});
239  hfssRectangle(fid, 'Pad16', 'Y' , [-1.5,0,4.5], .5, .5,'mm');
240  hfssAssignFiniteCond(fid, 'Pad16', 0, 'um', {'Pad16'});
241  hfssRectangle(fid, 'Pad17', 'Y' , [-1,0,2], 1.5, .5,'mm');
242  hfssAssignFiniteCond(fid, 'Pad17', 0, 'um', {'Pad17'});
243  hfssRectangle(fid, 'Pad18', 'Y' , [-1,0,4.5], .5, .5,'mm');
244  hfssAssignFiniteCond(fid, 'Pad18', 0, 'um', {'Pad18'});
245  hfssRectangle(fid, 'Pad19', 'Y' , [-.5,0,3.5], .5, .5,'mm');
246  hfssAssignFiniteCond(fid, 'Pad19', 0, 'um', {'Pad19'});
247  hfssRectangle(fid, 'Pad20', 'Y' , [-.5,0,4.5], .5, .5,'mm');
248  hfssAssignFiniteCond(fid, 'Pad20', 0, 'um', {'Pad20'});
249  hfssRectangle(fid, 'Pad21', 'Y' , [0,0,2.5], .5, .5,'mm');
250  hfssAssignFiniteCond(fid, 'Pad21', 0, 'um', {'Pad21'});
251  hfssRectangle(fid, 'Pad22', 'Y' , [0,0,4], .5, .5,'mm');
252  hfssAssignFiniteCond(fid, 'Pad22', 0, 'um', {'Pad22'});
253  hfssRectangle(fid, 'Pad23', 'Y' , [.5,0,3], .5, .5,'mm');
254  hfssAssignFiniteCond(fid, 'Pad23', 0, 'um', {'Pad23'});
255  hfssRectangle(fid, 'Pad24', 'Y' , [.5,0,4.5], .5, .5,'mm');
256  hfssAssignFiniteCond(fid, 'Pad24', 0, 'um', {'Pad24'});
257  hfssRectangle(fid, 'Pad25', 'Y' , [1,0,3], .5, .5,'mm');
258  hfssAssignFiniteCond(fid, 'Pad25', 0, 'um', {'Pad25'});
259  hfssRectangle(fid, 'Pad26', 'Y' , [1,0,4], .5, .5,'mm');
260  hfssAssignFiniteCond(fid, 'Pad26', 0, 'um', {'Pad26'});
261  hfssRectangle(fid, 'Pad27', 'Y' , [1.5,0,3], .5, .5,'mm');
262  hfssAssignFiniteCond(fid, 'Pad27', 0, 'um', {'Pad27'});
263  hfssRectangle(fid, 'Pad28', 'Y' , [1.5,0,4], 1, .5,'mm');
264  hfssAssignFiniteCond(fid, 'Pad28', 0, 'um', {'Pad28'});
265  hfssRectangle(fid, 'Pad29', 'Y' , [2,0,3.5], 1, .5,'mm');
266  hfssAssignFiniteCond(fid, 'Pad29', 0, 'um', {'Pad29'});
```

```
267  hfssRectangle(fid, 'Pad30', 'Y' , [1,0,.5], 1.5, .5,'mm');
268   hfssAssignFiniteCond(fid, 'Pad30', 0, 'um', {'Pad30'});
269  hfssRectangle(fid, 'Pad31', 'Y' , [1.5,0,1], .5, .5,'mm');
270   hfssAssignFiniteCond(fid, 'Pad31', 0, 'um', {'Pad31'});
271  hfssRectangle(fid, 'Pad32', 'Y' , [1.5,0,2], .5, .5,'mm');
272   hfssAssignFiniteCond(fid, 'Pad32', 0, 'um', {'Pad32'});
273  hfssRectangle(fid, 'Pad33', 'Y' , [2,0,.5], 1, .5,'mm');
274   hfssAssignFiniteCond(fid, 'Pad33', 0, 'um', {'Pad33'});
275  hfssRectangle(fid, 'Pad34', 'Y' , [2,0,2.5], .5, .5,'mm');
276   hfssAssignFiniteCond(fid, 'Pad34', 0, 'um', {'Pad34'});
277  hfssRectangle(fid, 'Pad35', 'Y' , [2.5,0,1], .5, .5,'mm');
278   hfssAssignFiniteCond(fid, 'Pad35', 0, 'um', {'Pad35'});
279  hfssRectangle(fid, 'Pad36', 'Y' , [2.5,0,2], 1.5, .5,'mm');
280   hfssAssignFiniteCond(fid, 'Pad36', 0, 'um', {'Pad36'});
281  hfssRectangle(fid, 'Pad37', 'Y' , [3,0,2], 1.5, .5,'mm');
282   hfssAssignFiniteCond(fid, 'Pad37', 0, 'um', {'Pad37'});
283  hfssRectangle(fid, 'Pad38', 'Y' , [3.5,0,3], .5, .5,'mm');
284   hfssAssignFiniteCond(fid, 'Pad38', 0, 'um', {'Pad38'});
285  hfssRectangle(fid, 'Pad39', 'Y' , [3.5,0,1.5], .5, .5,'mm');
286   hfssAssignFiniteCond(fid, 'Pad39', 0, 'um', {'Pad39'});
287  hfssRectangle(fid, 'Pad40', 'Y' , [3.5,0,2.5], .5, .5,'mm');
288   hfssAssignFiniteCond(fid, 'Pad40', 0, 'um', {'Pad40'});
289  hfssRectangle(fid, 'Pad41', 'Y' , [4,0,.5], 1,.5,'mm');
290   hfssAssignFiniteCond(fid, 'Pad41', 0, 'um', {'Pad41'});
291  hfssRectangle(fid, 'Pad42', 'Y' , [4,0,2], .5, .5,'mm');
292   hfssAssignFiniteCond(fid, 'Pad42', 0, 'um', {'Pad42'});
293  hfssRectangle(fid, 'Pad43', 'Y' , [4.5,0,0], .5, .5,'mm');
294   hfssAssignFiniteCond(fid, 'Pad43', 0, 'um', {'Pad43'});
295  hfssRectangle(fid, 'Pad44', 'Y' , [4.5,0,1], .5, .5,'mm');
296   hfssAssignFiniteCond(fid, 'Pad44', 0, 'um', {'Pad44'});
297
298 N=1;
299  for i=1:m
```

```
300         NN=0;
301         for j=1:n
302             if Meta(j,i)==1;
303                 NN=1+ NN;
304             end
305         if NN>0
306             if Meta(j,i)==0
307                 N=N+1;
308                 xp=(i)*Pw;
309                 yp=(j)*Pw;
310                 hfssRectangle(fid, sprintf('RecB%d',N), 'Y' , ...
                        [-xp+SRR_LX/2, -.025, yp-(1+NN)*Pw], Pw*NN, Pw,'mm');
311                 hfssAssignFiniteCond(fid, sprintf('RecBPEC%d',N), 0, ...
                        'um', {sprintf('RecB%d',N)})
312                 NN=0;
313             end
314              if j==n
315                  if Meta(j,i)==1;
316                 N=N+1;
317                 xp=(i)*Pw;
318                 yp=(j)*Pw;
319                 hfssRectangle(fid, sprintf('RecB%d',N), 'Y', ...
                        [-xp+SRR_LX/2, -.025, yp-NN*Pw], Pw*NN, Pw,'mm');
320                 hfssAssignFiniteCond(fid, sprintf('RecBPEC%d',N), 0, ...
                        'um', {sprintf('RecB%d',N)})
321                 NN=0;
322                  end
323              end
324          end
325         end
326 end
327     % Add a Solution Setup.
328     hfssInsertSolution(fid, 'Setup', fC/1e9, 0.02,20);
```

```
329     % Save the project to a temporary file and solve it.
330     hfssSaveProject(fid, tmpPrjFile, true);
331     hfssSolveSetup(fid, 'Setup');
332     hfssInsertFarField(fid, 'Infinite Sphere1',0,0,0,0,0,0,'deg')
333     % Export the Network data as an m-file.
334     hfssExportNetworkData(fid, tmpDataFile, 'Setup', 'LastAdaptive');
335      FFc=fC*(1e-9);
336      hfssCreateReportDualComp(fid,FarFieldpath, FFc, 'GHz');
337     hfssCreateReport(fid, FFc, 'GHz');
338
339     % Close the HFSS Script File.
340     fclose(fid);
341     % Execute the Script by starting HFSS.
342     disp('Solving using HFSS ..');
343     hfssExecuteScript(hfssExePath, tmpScriptFile);
344
345     % Load the data by running the exported matlab file.
346
347  run(tmpDataFile);
348
349     [heffi2, RadEff] = hdrload('farFieldEff.m');
350     radF=RadEff(:,1);
351     RE=RadEff(:,2);
352
353
354     for np=1:nPoints
355     S1r(np)=20*log10(abs(S(np,:,:)));
356     end
357
358
359
360
361 fitness(ip)= RE*S1r;
```

```
362 Sfc(ip) = S1r;
363 Rfc(ip) = RE;
364 % min(S1r) and rad efficiency
365
366
367
368 Name = ...
       sprintf('C:\\AFRL_MAT\\Efficiency4GHz\\RandomSearch\\Name%d.hfss',ip);
369      movefile('GALoop.hfss',Name)
370
371   if ip == popsize
372  figure
373  scatter(Rfc,Sfc)
374  axis([ 0 1 -40 0])
375  set(gca,'FontSize',17);
376  xlabel('Efficiency')
377  ylabel('|S11| (dB)')
378  title('Random Search 4GHZ')
379     savefile = 'Sfc.mat';
380         save(savefile, 'Sfc');
381         savefile = 'Rfc.mat';
382         save(savefile, 'Rfc');
383   end
384
385
386
387 end
388
389
390
391 [fitness,ind]=sort(fitness) ;   %Sort fitness such that the lowest is ...
       at ind 1
392 Pop=Pop(ind,:);   % sorts population with lowest fitness placed at ind 1
```

```
393 Sfc = Sfc(:,ind);
394 Rfc = Rfc(:,ind);
395 minc(1)=min(fitness);% find min of the population
396 max(1)=max(fitness);   % find max of the population
397 meanc(1)=mean(fitness); %find mean of the population
398
399 Nt=ChromLength;
400 h = 1;
401
402 % %Start Iterating through generations
403   while iga≤maxit
404       tic
405       NewPop=Pop;  %store the previous population for reference
406       Muprob=.2;               % set mutation rate
407 selection=0.2;             % fraction of population kept
408
409 %    %I) Selection of chromozomes to be kept
410 indx=find(fitness≤mean(fitness));% Determines the chroms with fitness < ...
       mean fitness
411 keep=ceil(selection*popsize); %Number of chrom to keep
412 fitkeep=fitness(indx);% fitnesses to keep
413 Popkeep=Pop(indx,:);%Chroms to keep
414 M1=ceil((popsize-keep)*.6); % Chromosomes to be replaced via Xover and ...
       Mutation for case 1
415 M2=ceil((popsize-keep)*.4); % Chromosomes to be replaced via Xover and ...
       Mutation for case 2
416
417 %II) Pairing Chromozomes for Xover/Mutation
418 %Case I: random selection of 2 individual
419
420 Ntourn=2;
421  for ic2=1:2:M2
422       %Random Selection of Parents
```

```
423 %first Parent
424 ma=ceil(keep*rand());  % indicies of first parent
425 %Second parent
426 pa=ceil(keep*rand());  % indicies of second parent
427
428 if ic2≤ceil(M2/3)
429 %1pt Crossover
430 ma=1;
431 Xpt=ceil(rand()*(Nt-1));
432 Pop(keep+M1+ic2-1,:)=[Pop(ma,1:Xpt) Pop(pa,Xpt+1:Nt)]; % Offspring 1
433 Pop(keep+M1+ic2,:)=[Pop(pa,1:Xpt) Pop(ma,Xpt+1:Nt)];%Offspring 2
434 end
435 if ic2≥ceil(M2/3) && ic2≤ceil(2*M2/3)
436 %2pt Crossover
437 Xpt1=ceil(rand()*Nt/2);
438 Xpt2=Xpt1 + ceil(rand()*(Nt-1)/2);
439 Pop(keep+M1+ic2-1,:)=[Pop(ma,1:Xpt1) Pop(pa,Xpt1+1:Xpt2) ...
       Pop(ma,Xpt2+1:Nt)]; % Offspring 1
440 Pop(keep+M1+ic2,:)=[Pop(pa,1:Xpt1) Pop(ma,Xpt1+1:Xpt2) ...
       Pop(pa,Xpt2+1:Nt)];%Offspring 2
441 end
442 if ic2≥ceil(M2/3)
443 %3pt Crossover
444 Xpt1=ceil(rand()*Nt/3);
445 Xpt2=Xpt1 + ceil(rand()*(Nt)/3);
446 Xpt3=Xpt2 + ceil(rand()*(Nt-1)/3);
447 Pop(keep+M1+ic2-1,:)=[Pop(ma,1:Xpt1) Pop(pa,Xpt1+1:Xpt2) ...
       Pop(ma,Xpt2+1:Xpt3) Pop(pa,Xpt3+1:Nt)]; % Offspring 1
448 Pop(keep+M1+ic2,:)=[Pop(pa,1:Xpt1) Pop(ma,Xpt1+1:Xpt2) ...
       Pop(pa,Xpt2+1:Xpt3) Pop(ma,Xpt3+1:Nt)];%Offspring 2
449 end
450  end
451
```

```
452   %Case I:  selection the best of 2 individual
453   for ic=1:2:M1
454 %first Parent
455 rc=ceil(keep*rand(1,Ntourn)); %Randomly select 2 chroms among those kept
456 [c,ci]=min(fitness(rc)); % Select the chrom with lowest fitness
457 ma=rc(ci);  % indicies of first parent
458 %Second parent
459 rc=ceil(keep*rand(1,Ntourn));%%Randomly select 2 chroms among those kept
460 [c,ci]=min(fitness(rc)); % Select the chrom with lowest fitness
461 pa=rc(ci);  % indicies of second parent
462 if ic≤ceil(M1/5)
463 %1pt Crossover
464 Xpt=ceil(rand()*(Nt-1));
465 Pop(keep+ic-1,:)=[Pop(ma,1:Xpt) Pop(pa,Xpt+1:Nt)]; % Offspring 1
466 Pop(keep+ic,:)=[Pop(pa,1:Xpt) Pop(ma,Xpt+1:Nt)];%Offspring 2
467 end
468 if ic≥ceil(M1/5) && ic≤ceil(4*M1/5)
469 %2pt Crossover
470 Xpt1=ceil(rand()*Nt/2);
471 Xpt2=Xpt1 + ceil(rand()*(Nt-1)/2);
472 Pop(keep+ic-1,:)=[Pop(ma,1:Xpt1) Pop(pa,Xpt1+1:Xpt2) ...
       Pop(ma,Xpt2+1:Nt)]; % Offspring 1
473 Pop(keep+ic,:)=[Pop(pa,1:Xpt1) Pop(ma,Xpt1+1:Xpt2) ...
       Pop(pa,Xpt2+1:Nt)];%Offspring 2
474 end
475 if ic≥ceil(4*M1/5)
476 %3pt Crossover
477 Xpt1=ceil(rand()*Nt/3);
478 Xpt2=Xpt1 + ceil(rand()*(Nt)/3);
479 Xpt3=Xpt2 + ceil(rand()*(Nt-1)/3);
480 Pop(keep+ic-1,:)=[Pop(ma,1:Xpt1) Pop(pa,Xpt1+1:Xpt2) ...
       Pop(ma,Xpt2+1:Xpt3) Pop(pa,Xpt3+1:Nt)]; % Offspring 1
481 Pop(keep+ic,:)=[Pop(pa,1:Xpt1) Pop(ma,Xpt1+1:Xpt2) Pop(pa,Xpt2+1:Xpt3) ...
```

```
    Pop(ma,Xpt3+1:Nt)];%Offspring 2
end
  end


%III) mutation: keep best two and mutate a single bit on the other
%chromosomes based on mutating probability

    for iMu=keep:popsize
    if Muprob≥rand()
Mupt=ceil(rand()*Nt);% bit to be mutated
Pop(iMu,Mupt)=not(Pop(iMu,Mupt));
    end
    end



CurrentChrom=keep;
for ip = keep:popsize

    %Added so that repeated structures are not analyzed
    for ipp=1:popsize
        if Pop(ip,:)==NewPop(ipp,:)
            for ipp1=1:Nt
                if Muprob≥rand()
        Pop(ip,ipp1)=not(Pop(ip,ipp1));
                end
            end
        end
    end

Meta=(reshape(Pop(ip,:),n,m));

```

```
514  tt=0;
515   for ix=1:6
516      for iy=1:5
517      Meta(n-iy+tt,ix)=0;
518      end
519      tt=tt+1;
520   end
521
522   tt=0;
523   for ix=1:6
524      for iy=1:5
525      Meta(n-iy+tt,m-ix+1)=0;
526      end
527      tt=tt+1;
528   end
529
530  % Temp Files.
531 tmpPrjFile = 'C:\AFRL_MAT\Efficiency4GHz\GALoopGA.hfss';
532 tmpDataFile = 'C:\AFRL_MAT\Efficiency4GHz\GALoopData.m';
533 tmpScriptFile = 'C:\AFRL_MAT\Efficiency4GHz\GALoopScript.vbs';
534
535     % Create a new temporary HFSS script file.
536     fid = fopen(tmpScriptFile, 'wt');
537
538     % Create a new HFSS Project and insert a new design.
539     hfssNewProject(fid);
540     hfssInsertDesign(fid, 'GA_Loop');
541
542
543    %Draw AirBox
544 hfssCylinder(fid, 'Air_Box', 'Z', [0, 0, -(Hi_oc+Gnd_Z+CapZ+10)], G_R, ...
       G_H, 'mm');
545 hfssAssignRadiation(fid, 'Box_Rad', 'Air_Box');
```

```
546 hfssSetTransparency(fid, {'Air_Box'}, 0.95);
547   %Draw Feed (Outer Conductor)
548   hfssHollowCylinder(fid, 'Outer_C', 'Z', [FX, 0, -(Hi_oc+Gnd_Z)], ...
        Th_oc, R_oc, (Hi_oc), 'mm');
549   hfssAssignPE(fid, 'PEC_oc',  {'Outer_C'});
550 %   Teflon
551   hfssHollowCylinder(fid, 'Tef', 'Z', [FX, 0, -(Hi_oc+Gnd_Z)], Th_tf, ...
        R_tf, (Hi_oc), 'mm');
552    hfssAssignMaterial(fid, 'Tef', 'Neltec NX9294 (tm)');
553 %     Inner Conductor
554   hfssCylinder(fid, 'Inner_C', 'Z', [FX, 0, -(Hi_oc+Gnd_Z)], R_feed, ...
        (Hi_oc), 'mm');
555   hfssAssignPE(fid, 'PEC_Ic',  {'Inner_C'});
556 %Draw waveport
557     hfssCircularPort(fid, 'LPort', 'port1', 'Z', [FX, 0, ...
          -(Hi_oc+Gnd_Z)], R_tf,Deembed, 'mm');
558     hfssCylinder(fid, 'PortCup1', 'Z', [FX, 0, -(Hi_oc+Gnd_Z)], R_oc, ...
          -CapZ, 'mm');
559 hfssAssignMaterial(fid, 'PortCup1', 'pec');
560
561
562 %Draw Ground plane
563 %Ground 1
564 hfssRectangle(fid, 'Gnd', 'Y', [-Sub_X/2+Pw, 0, ...
      -Gnd_Z],Gnd_Z,Sub_X-2*Pw, 'mm');
565 hfssRectangle(fid, 'Gnd_Sub', 'Y', [-Gndgap/2+FX, 0, -Gnd_Z], Gnd_Z, ...
      Gndgap, 'mm');
566 hfssSubtract(fid, {'Gnd'}, {'Gnd_Sub'});
567 hfssAssignFiniteCond(fid, 'PEC_Gnd', 0, 'um', {'Gnd'});
568
569
570 %Circuitry
571 hfssRectangle(fid, 'Circuit1', 'Y', [-Sub_X/2, -Sub_Y, ...
```

```
    -Gnd_Z+1.62],Gnd_Z-1.62,Sub_X, 'mm');
572 hfssCircle(fid, 'Circuit2', 'Y', [0, -Sub_Y, 0],Sub_X/2, 'mm');
573 hfssRectangle(fid, 'Circuit2Sub', 'Y', [-Sub_X/2, -Sub_Y, ...
    0],-Sub_X/2,Sub_X, 'mm');
574 hfssSubtract(fid, {'Circuit2'}, {'Circuit2Sub'});
575 hfssUnite(fid, 'Circuit1','Circuit2');
576 hfssAssignFiniteCond(fid, 'PEC_Circuit1', 0, 'um', {'Circuit1'});
577
578
579 %Draw Substrate
580 hfssBox(fid, 'Substrate', [-Sub_X/2, 0, -Gnd_Z], [Sub_X, -Sub_Y, ...
    Gnd_Z], 'mm');
581 hfssAssignMaterial(fid, 'Substrate', 'Rogers RO4003 (tm)');
582 hfssSetColor(fid, 'Substrate', [0, 128, 0]);
583 hfssSetTransparency(fid, {'Substrate'}, 0.8);
584 hfssCylinder(fid, 'Sub2', 'Y', [0, 0, 0], Sub_X/2, -Sub_Y, 'mm');
585 hfssBox(fid, 'Sub2sub', [-Sub_X/2, 0, -Sub_X/2], [Sub_X, -Sub_Y, ...
    Sub_X/2], 'mm');
586 hfssSubtract(fid, {'Sub2'}, {'Sub2sub'});
587 hfssUnite(fid, 'Substrate','Sub2');
588
589 %Draw Extra Layer Substrate
590 hfssBox(fid, 'Layer', [-Sub_X/2, 0, -Gnd_Z], [Sub_X, .025, Gnd_Z], 'mm');
591 hfssAssignMaterial(fid, 'Layer', 'GIL MC5 (tm)');
592 hfssSetColor(fid, 'Layer', [0, 900, 0]);
593 hfssSetTransparency(fid, {'Layer'}, 0.8);
594 hfssCylinder(fid, 'Sub0', 'Y', [0, 0, 0], Sub_X/2, .025, 'mm');
595 hfssBox(fid, 'Sub2sub0', [-Sub_X/2, 0, -Sub_X/2], [Sub_X, .025, ...
    Sub_X/2], 'mm');
596 hfssSubtract(fid, {'Sub0'}, {'Sub2sub0'});
597 hfssUnite(fid, 'Layer','Sub0');
598 hfssMove(fid, {'Layer'}, [0, -.025, 0], 'mm');
599
```

```
%Draw Folded Monopole
hfssRectangle(fid, 'mono', 'Y', [-P_w/2+FX, 0, -Gnd_Z], Gnd_Z, P_w,'mm');
hfssRectangle(fid, 'Loop', 'Y', [-P_w/2+FX, 0, 0], P_Z, LoopW,'mm');
hfssRectangle(fid, 'Loopsub', 'Y', [FX+P_w/2, 0, 0], P_Z-P_w, ...
    LoopW-2*P_w,'mm');
hfssRectangle(fid, 'Loopsub2', 'Y', [FX+LoopW-3*P_w/2, 0, 0], P_w*1, ...
    P_w,'mm');
hfssAssignFiniteCond(fid, 'PEC_Loop', 0, 'um', {'mono'});
hfssSubtract(fid, {'Loop'}, {'Loopsub'});
 hfssSubtract(fid, {'Loop'}, {'Loopsub2'});
hfssUnite(fid, 'mono','Loop');

% Draw Bottom Substrate pads
 hfssRectangle(fid, 'Pad1', 'Y' , [-2.5,0,0], .5, .5,'mm');
 hfssAssignFiniteCond(fid, 'Pad1', 0, 'um', {'Pad1'})
hfssRectangle(fid, 'Pad2', 'Y' , [-5,0,.5], 1.5, .5,'mm');
 hfssAssignFiniteCond(fid, 'Pad2', 0, 'um', {'Pad2'})
hfssRectangle(fid, 'Pad3', 'Y' , [-4.5,0,.5], 1, .5,'mm');
 hfssAssignFiniteCond(fid, 'Pad3', 0, 'um', {'Pad3'})
hfssRectangle(fid, 'Pad4', 'Y' , [-4,0,1.5], 1.5, .5,'mm');
 hfssAssignFiniteCond(fid, 'Pad4', 0, 'um', {'Pad4'})
hfssRectangle(fid, 'Pad5', 'Y' , [-3.5,0,1], 1.5, .5,'mm');
 hfssAssignFiniteCond(fid, 'Pad5', 0, 'um', {'Pad5'})
hfssRectangle(fid, 'Pad6', 'Y' , [-3,0,1.5], .5, .5,'mm');
 hfssAssignFiniteCond(fid, 'Pad6', 0, 'um', {'Pad6'})
hfssRectangle(fid, 'Pad7', 'Y' , [-2.5,0,1], .5, .5,'mm');
 hfssAssignFiniteCond(fid, 'Pad7', 0, 'um', {'Pad7'})
hfssRectangle(fid, 'Pad8', 'Y' , [-2.5,0,2], .5, .5,'mm');
 hfssAssignFiniteCond(fid, 'Pad8', 0, 'um', {'Pad8'})
hfssRectangle(fid, 'Pad9', 'Y' , [-3.5,0,3], .5, .5,'mm');
 hfssAssignFiniteCond(fid, 'Pad9', 0, 'um', {'Pad9'})
hfssRectangle(fid, 'Pad10', 'Y' , [-3,0,3], .5, .5,'mm');
 hfssAssignFiniteCond(fid, 'Pad10', 0, 'um', {'Pad10'})
```

```
631 hfssRectangle(fid, 'Pad11', 'Y' , [-2.5,0,3], 1.5, .5,'mm');
632  hfssAssignFiniteCond(fid, 'Pad11', 0, 'um', {'Pad11'})
633 hfssRectangle(fid, 'Pad12', 'Y' , [-2,0,2], 2, .5,'mm');
634  hfssAssignFiniteCond(fid, 'Pad12', 0, 'um', {'Pad12'})
635 hfssRectangle(fid, 'Pad13', 'Y' , [-2,0,4.5], .5, .5,'mm');
636  hfssAssignFiniteCond(fid, 'Pad13', 0, 'um', {'Pad13'})
637 hfssRectangle(fid, 'Pad14', 'Y' , [-1.5,0,2], 1, .5,'mm');
638  hfssAssignFiniteCond(fid, 'Pad14', 0, 'um', {'Pad14'});
639  hfssRectangle(fid, 'Pad15', 'Y' , [-1.5,0,3.5], .5, .5,'mm');
640  hfssAssignFiniteCond(fid, 'Pad15', 0, 'um', {'Pad15'});
641  hfssRectangle(fid, 'Pad16', 'Y' , [-1.5,0,4.5], .5, .5,'mm');
642  hfssAssignFiniteCond(fid, 'Pad16', 0, 'um', {'Pad16'});
643  hfssRectangle(fid, 'Pad17', 'Y' , [-1,0,2], 1.5, .5,'mm');
644  hfssAssignFiniteCond(fid, 'Pad17', 0, 'um', {'Pad17'});
645  hfssRectangle(fid, 'Pad18', 'Y' , [-1,0,4.5], .5, .5,'mm');
646  hfssAssignFiniteCond(fid, 'Pad18', 0, 'um', {'Pad18'});
647  hfssRectangle(fid, 'Pad19', 'Y' , [-.5,0,3.5], .5, .5,'mm');
648  hfssAssignFiniteCond(fid, 'Pad19', 0, 'um', {'Pad19'});
649  hfssRectangle(fid, 'Pad20', 'Y' , [-.5,0,4.5], .5, .5,'mm');
650  hfssAssignFiniteCond(fid, 'Pad20', 0, 'um', {'Pad20'});
651  hfssRectangle(fid, 'Pad21', 'Y' , [0,0,2.5], .5, .5,'mm');
652  hfssAssignFiniteCond(fid, 'Pad21', 0, 'um', {'Pad21'});
653  hfssRectangle(fid, 'Pad22', 'Y' , [0,0,4], .5, .5,'mm');
654  hfssAssignFiniteCond(fid, 'Pad22', 0, 'um', {'Pad22'});
655  hfssRectangle(fid, 'Pad23', 'Y' , [.5,0,3], .5, .5,'mm');
656  hfssAssignFiniteCond(fid, 'Pad23', 0, 'um', {'Pad23'});
657  hfssRectangle(fid, 'Pad24', 'Y' , [.5,0,4.5], .5, .5,'mm');
658  hfssAssignFiniteCond(fid, 'Pad24', 0, 'um', {'Pad24'});
659  hfssRectangle(fid, 'Pad25', 'Y' , [1,0,3], .5, .5,'mm');
660  hfssAssignFiniteCond(fid, 'Pad25', 0, 'um', {'Pad25'});
661  hfssRectangle(fid, 'Pad26', 'Y' , [1,0,4], .5, .5,'mm');
662  hfssAssignFiniteCond(fid, 'Pad26', 0, 'um', {'Pad26'});
663  hfssRectangle(fid, 'Pad27', 'Y' , [1.5,0,3], .5, .5,'mm');
```

```
664  hfssAssignFiniteCond(fid, 'Pad27', 0, 'um', {'Pad27'});
665  hfssRectangle(fid, 'Pad28', 'Y' , [1.5,0,4], 1, .5,'mm');
666  hfssAssignFiniteCond(fid, 'Pad28', 0, 'um', {'Pad28'});
667  hfssRectangle(fid, 'Pad29', 'Y' , [2,0,3.5], 1, .5,'mm');
668  hfssAssignFiniteCond(fid, 'Pad29', 0, 'um', {'Pad29'});
669  hfssRectangle(fid, 'Pad30', 'Y' , [1,0,.5], 1.5, .5,'mm');
670   hfssAssignFiniteCond(fid, 'Pad30', 0, 'um', {'Pad30'});
671  hfssRectangle(fid, 'Pad31', 'Y' , [1.5,0,1], .5, .5,'mm');
672   hfssAssignFiniteCond(fid, 'Pad31', 0, 'um', {'Pad31'});
673  hfssRectangle(fid, 'Pad32', 'Y' , [1.5,0,2], .5, .5,'mm');
674   hfssAssignFiniteCond(fid, 'Pad32', 0, 'um', {'Pad32'});
675  hfssRectangle(fid, 'Pad33', 'Y' , [2,0,.5], 1, .5,'mm');
676   hfssAssignFiniteCond(fid, 'Pad33', 0, 'um', {'Pad33'});
677  hfssRectangle(fid, 'Pad34', 'Y' , [2,0,2.5], .5, .5,'mm');
678   hfssAssignFiniteCond(fid, 'Pad34', 0, 'um', {'Pad34'});
679  hfssRectangle(fid, 'Pad35', 'Y' , [2.5,0,1], .5, .5,'mm');
680   hfssAssignFiniteCond(fid, 'Pad35', 0, 'um', {'Pad35'});
681  hfssRectangle(fid, 'Pad36', 'Y' , [2.5,0,2], 1.5, .5,'mm');
682   hfssAssignFiniteCond(fid, 'Pad36', 0, 'um', {'Pad36'});
683  hfssRectangle(fid, 'Pad37', 'Y' , [3,0,2], 1.5, .5,'mm');
684   hfssAssignFiniteCond(fid, 'Pad37', 0, 'um', {'Pad37'});
685  hfssRectangle(fid, 'Pad38', 'Y' , [3.5,0,3], .5, .5,'mm');
686   hfssAssignFiniteCond(fid, 'Pad38', 0, 'um', {'Pad38'});
687  hfssRectangle(fid, 'Pad39', 'Y' , [3.5,0,1.5], .5, .5,'mm');
688   hfssAssignFiniteCond(fid, 'Pad39', 0, 'um', {'Pad39'});
689  hfssRectangle(fid, 'Pad40', 'Y' , [3.5,0,2.5], .5, .5,'mm');
690   hfssAssignFiniteCond(fid, 'Pad40', 0, 'um', {'Pad40'});
691  hfssRectangle(fid, 'Pad41', 'Y' , [4,0,.5], 1,.5,'mm');
692   hfssAssignFiniteCond(fid, 'Pad41', 0, 'um', {'Pad41'});
693  hfssRectangle(fid, 'Pad42', 'Y' , [4,0,2], .5, .5,'mm');
694   hfssAssignFiniteCond(fid, 'Pad42', 0, 'um', {'Pad42'});
695  hfssRectangle(fid, 'Pad43', 'Y' , [4.5,0,0], .5, .5,'mm');
696   hfssAssignFiniteCond(fid, 'Pad43', 0, 'um', {'Pad43'});
```

```
697  hfssRectangle(fid, 'Pad44', 'Y' , [4.5,0,1], .5, .5,'mm');
698   hfssAssignFiniteCond(fid, 'Pad44', 0, 'um', {'Pad44'});
699
700 N=1;
701  for i=1:m
702         NN=0;
703         for j=1:n
704             if Meta(j,i)==1;
705                 NN=1+ NN;
706             end
707         if NN>0
708             if Meta(j,i)==0
709                 N=N+1;
710                 xp=(i)*Pw;
711                 yp=(j)*Pw;
712                 hfssRectangle(fid, sprintf('RecB%d',N), 'Y' , ...
                        [-xp+SRR_LX/2, -.025, yp-(1+NN)*Pw], Pw*NN, Pw,'mm');
713                 hfssAssignFiniteCond(fid, sprintf('RecBPEC%d',N), 0, ...
                        'um', {sprintf('RecB%d',N)})
714                 NN=0;
715             end
716              if j==n
717                  if Meta(j,i)==1;
718                 N=N+1;
719                 xp=(i)*Pw;
720                 yp=(j)*Pw;
721                 hfssRectangle(fid, sprintf('RecB%d',N), 'Y', ...
                        [-xp+SRR_LX/2, -.025, yp-NN*Pw], Pw*NN, Pw,'mm');
722                 hfssAssignFiniteCond(fid, sprintf('RecBPEC%d',N), 0, ...
                        'um', {sprintf('RecB%d',N)})
723                 NN=0;
724                  end
725              end
```

```
726          end
727         end
728  end
729     % Add a Solution Setup.
730     hfssInsertSolution(fid, 'Setup', fC/1e9, 0.02,15);
731     % Save the project to a temporary file and solve it.
732     hfssSaveProject(fid, tmpPrjFile, true);
733     hfssSolveSetup(fid, 'Setup');
734     hfssInsertFarField(fid, 'Infinite Sphere1',0,0,0,0,0,0,'deg')
735     % Export the Network data as an m-file.
736     hfssExportNetworkData(fid, tmpDataFile, 'Setup', 'LastAdaptive');
737      FFc=fC*(1e-9);
738      hfssCreateReportDualComp(fid,FarFieldpath, FFc, 'GHz');
739     hfssCreateReport(fid, FFc, 'GHz');
740
741     % Close the HFSS Script File.
742     fclose(fid);
743     % Execute the Script by starting HFSS.
744     disp('Solving using HFSS ..');
745     hfssExecuteScript(hfssExePath, tmpScriptFile);
746
747
748
749
750
751
752     % Load the data by running the exported matlab file.
753
754  run(tmpDataFile);
755     [heffi2, RadEff] = hdrload('farFieldEff.m');
756     radF=RadEff(:,1);
757     RE=RadEff(:,2);
758     Rfc(ip) = RE;
```

```
759
760      Sfc(ip)=20*log10(abs(S(np,:,:)));
761      fitness(ip)= Rfc(ip)*Sfc(ip);
762
763      % min(S1r) and rad efficiency
764
765  if iga == 1
766
767    Name = ...
768      sprintf('C:\\AFRL_MAT\\Efficiency4GHz\\ ...
769      Gen%d\\Gen%d_%d.hfss',iga,iga,ip);
770       movefile('GALoopGA.hfss',Name)
771
772
773       if ip == popsize
774           Sfc1 = Sfc;
775           Rfc1 = Rfc;
776           ind1 = ind;
777           keep1 = keep;
778           figure
779           scatter(Rfc1,Sfc1)
780           axis([ 0 1 -40 0])
781           set(gca,'FontSize',17);
782           xlabel('Efficiency')
783           ylabel('|S11| (dB)')
784           title('First Generation 4 GHZ')
785
786          savefile = 'Sfc1.mat';
787          save(savefile, 'Sfc1');
788          savefile = 'Rfc1.mat';
789          save(savefile, 'Rfc1');
790          savefile = 'ind1.mat';
791          save(savefile, 'ind1')
```

```
792          savefile = 'keep1.mat';
793          save(savefile,'keep1')
794       end
795      h = h+1
796  end
797
798      if iga ==2
799     Name = ...
800      sprintf('C:\\AFRL_MAT\\Efficiency4GHz\\ ...
801      Gen%d\\Name%d_%d.hfss',iga,iga,ip);
802       movefile('GALoopGA.hfss',Name)
803
804       if ip == popsize
805           Sfc2 = Sfc;
806           Rfc2 = Rfc;
807            ind2 = ind;
808           keep2 = keep;
809           figure
810           scatter(Rfc2,Sfc2)
811           axis([ 0 1 -40 0])
812           set(gca,'FontSize',17);
813           xlabel('Efficiency')
814           ylabel('|S11| (dB)')
815           title('Second Generation 4 GHZ')
816
817          savefile = 'Sfc2.mat';
818          save(savefile, 'Sfc2');
819          savefile = 'Rfc2.mat';
820          save(savefile, 'Rfc2');
821          savefile = 'ind2.mat';
822          save(savefile, 'ind2')
823          savefile = 'keep2.mat';
824          save(savefile,'keep2')
```

```
825       end
826       h = h+1
827      end
828
829      if iga ==3
830     Name = ...
831      sprintf('C:\\AFRL_MAT\\Efficiency4GHz\\ ...
832      Gen%d\\Name%d_%d.hfss',iga,iga,ip);
833       movefile('GALoopGA.hfss',Name)
834
835
836       if ip == popsize
837           Sfc3 = Sfc;
838           Rfc3 = Rfc;
839            ind3 = ind;
840           keep3 = keep;
841           figure
842           scatter(Rfc3,Sfc3)
843           axis([ 0 1 -40 0])
844           set(gca,'FontSize',17);
845           xlabel('Efficiency')
846           ylabel('|S11| (dB)')
847           title('Third Generation 4 GHZ')
848
849          savefile = 'Sfc3.mat';
850          save(savefile, 'Sfc3');
851          savefile = 'Rfc3.mat';
852          save(savefile, 'Rfc3');
853          savefile = 'ind3.mat';
854          save(savefile, 'ind3')
855          savefile = 'keep3.mat';
856          save(savefile,'keep3')
857       end
```

```
858      h = h+1
859      end
860
861
862  CurrentChrom=CurrentChrom+1
863   end %of the evaluation of the current population Muprob= Muprob—Muprob/10
864  % % % %-------------------------------------------------------------
865
866  %Do statistics for new generation
867
868  [fitness,ind]=sort(fitness) ;   %Sort fitness such that the lowest is ...
        at ind 1
869  Pop=Pop(ind,:);   % sorts population with lowest fitness placed at ind 1
870  Sfc = Sfc(:,ind);
871  Rfc = Rfc(:,ind);
872  minc(iga+1)=min(fitness);% minc contains min of population
873  meanc(iga+1)=mean(fitness);
874
875
876
877
878   iga=iga+1
879
880
881
882
883    end
884  % remove all the added paths.
885  rmpath('C:\MatlabHfss\Files\')
```

BIBLIOGRAPHY

BIBLIOGRAPHY

[1] Elliott, Robert S. Antenna Theory and Design. Hoboken, N.J: John Wiley Sons, 2003. Print.

[2] Balanis, Constantine A. Antenna theory: analysis and design. John Wiley Sons, 2012.

[3] Gianvittorio, John P., and Yahya Rahmat-Samii. "Fractal antennas: A novel antenna miniaturization technique, and applications." Antennas and Propagation magazine, IEEE 44.1 (2002): 20-36.

[4] Anguera, Jaume, et al. "Small and highdirectivity bowtie patch antenna based on the Sierpinski fractal." Microwave and Optical Technology Letters 31.3 (2001): 239-241.

[5] Anguera, Jaume, et al. "Miniature wideband stacked microstrip patch antenna based on the sierpinski fractal geometry." Antennas and Propagation Society International Symposium, 2000. IEEE. Vol. 3. IEEE, 2000.

[6] Anguera, Jaume, et al. "Small and highdirectivity bowtie patch antenna based on the Sierpinski fractal." Microwave and Optical Technology Letters 31.3 (2001): 239-241.

[7] C. A. Balanis, Modern Antenna handbook, John Wiley Sons, Hoboken, NJ, 2008.

[8] D. M. Pozar, Microstrip Antennas, John Wiley Sons, Hoboken, NJ, 1995.

[9] Oh, Jungsuek, and Kamal SarabandI. "Low profile, miniaturized, inductively coupled capacitively loaded monopole antenna." Antennas and Propagation, IEEE Transactions on 60.3 (2012): 1206-1213.

[10] Ghosh, Bratin, SK Moinul Haque, and Debasis Mitra. "Miniaturization of slot antennas using slit and strip loading." Antennas and Propagation, IEEE Transactions on 59.10 (2011): 3922-3927.

[11] R. Waterhouse, Small microstrip patch antenna, Electron. Lett., vol. 31, no. 8, pp. 604-605, 1995.

[12] S. Dey, and R. Mittra, Compact microstrip patch antenna, Microwave Opt. Technol. Lett., vol. 13, pp. 12-14, 1996.

[13] C. L. Tang, and K. L. Wong, Small circular microstrip antenna with dual frequency operation, Electron. Lett. vol. 33, pp. 1112-1113, 1997.

[14] K. L. Wong, and W. S. Chen, Compact microstrip antenna with dual frequency operation, Electron. Lett., vol. 33, pp. 646-647, 1997

[15] K. L. Wong, and W. S. Chen, Compact triangular microstrip antenna, Elec- tron. Lett., vol. 33, pp. 433-434, 1997.

[16] S. C. pan, and K. L. Wong, Dual frequency triangular microstrip antenna with a shorting pin, IEEE Trans. Antennas Propag. vol. 45, pp 1889-1891, 1997.

[17] Ghosh, Bratin, SK Moinul Haque, and Debasis Mitra. "Miniaturization of slot antennas using slit and strip loading." Antennas and Propagation, IEEE Transactions on 59.10 (2011): 3922-3927.

[18] Wheeler, Harold A. "Fundamental limitations of small antennas." Proceedings of the IRE 35.12 (1947): 1479-1484.

[19] Skrivervik, A. K., et al. "PCS antenna design: The challenge of miniaturization." Antennas and Propagation Magazine, IEEE 43.4 (2001): 12-27.

[20] McGowan, K. A. Semiconductors: From Book to Breadboard. Cengage Learning.

[21] Haskins, P. M., and J. S. Dahele. "Varactor-diode loaded passive polarisation-agile patch antenna." Electronics letters 30.13 (1994): 1074-1075.

[22] Hum, Sean V., Michael Okoniewski, and Robert J. Davies. "Realizing an electronically tunable reflectarray using varactor diode-tuned elements." Microwave and Wireless Components Letters, IEEE 15.6 (2005): 422-424.

[23] Behdad, Nader, and Kamal Sarabandi. "A varactor-tuned dual-band slot antenna." Antennas and Propagation, IEEE Transactions on 54.2 (2006): 401-408.

[24] Lim, Jong-Hyuk, et al. "A reconfigurable PIFA using a switchable PIN-diode and a fine-tuning varactor for USPCS/WCDMA/m-WiMAX/WLAN." Antennas and Propagation, IEEE Transactions on 58.7 (2010): 2404-2411.

[25] Oh, Se-Keun, Hyung-Sik Yoon, and Seong-Ook Park. "A PIFA-type varactor-tunable slim antenna with a PIL patch feed for multiband applications." Antennas and Wireless Propagation Letters, IEEE 6 (2007): 103-105.

[26] B. R. Holland, R. Ramadoss, S. Pandey, and P. Agrawal, Tunable coplanar patch antenna using varactor, Electron. Lett., Vol. 42, No. 6, pp. 319 - 321, 2006

[27] Greetis, Lynn, et al. "A self-structuring patch antenna: Simulation and prototype." Antennas and Propagation Magazine, IEEE 52.1 (2010): 114-123.

[28] Koga, Yohei, Takashi Yamagajo, and Masahiko Shimizu. "Frequency tunable antenna design technique with MEMS switches for mobile phone." Microwave Conference Proceedings (APMC), 2011 Asia-Pacific. IEEE, 2011.

[29] Jackson Jr, R., and Ramesh Ramadoss. "A MEMS-based electrostatically tunable circular microstrip patch antenna." Journal of Micromechanics and Microengineering 17.1 (2007): 1..

[30] Erdil, Emre, et al. "Frequency tunable microstrip patch antenna using RF MEMS technology." Antennas and Propagation, IEEE Transactions on 55.4 (2007): 1193-1196.

[31] Z. J. Jin, J. H. Lim, and T. Y. Yun, Frequency reconfigurable multi-pleinput multiple-output antenna with high isolation, Microw., Antennas Propag., vol. 6, no. 10, pp. 10951101, 2012.

[32] So, JuHee, et al. "Reversibly deformable and mechanically tunable fluidic antennas." Advanced Functional Materials 19.22 (2009): 3632-3637.

[33] Amin, Muhammad, Robert Cahill, and Vincent F. Fusco. "Mechanically tunable multi-band compact quadrifilar helix antenna with dual mode operation." Antennas and Propagation, IEEE Transactions on 56.6 (2008): 1528-1532.

[34] Al-Dahleh, R., L. Shafai, and C. Shafai. "A frequency-tunable mechanically actuated microstrip patch antenna." Antennas and Propagation Society International Symposium, 2003. IEEE. Vol. 4. IEEE, 2003.

[35] Bose, Jagadis Chunder. "On the rotation of plane of polarisation of electric waves by a twisted structure." Proceedings of the Royal Society of London 63.389-400 (1898): 146-152.

[36] Eleftheriades, George V., and Keith G. Balmain. Negative-refraction metamaterials: fundamental principles and applications. John Wiley Sons, 2005.

[37] Maier, Stefan Alexander. Plasmonics: Fundamentals and Applications. Springer, 2007.

[38] Engheta, Nader, and Richard W. Ziolkowski, eds. Metamaterials: physics and engineering explorations. John Wiley Sons, 2006.

[39] Vesslago, V. G. "The electrodynamics of substances with simultaneously negative values of and '." Sov. Phys. Usp 10 (1968): 509-514.

[40] Caloz, C., C-C. Chang, and T. Itoh. "Full-wave verification of the fundamental properties of left-handed materials in waveguide configurations." Journal of Applied Physics 90.11 (2001): 5483-5486.

[41] Ziolkowski, Richard W., and Ehud Heyman. "Wave propagation in media having negative permittivity and permeability." Physical review E 64.5 (2001): 056625.

[42] Smith, David R., and Norman Kroll. "Negative refractive index in left-handed materials." Physical Review Letters 85.14 (2000): 2933.

[43] Ziolkowski, Richard. "Pulsed and CW Gaussian beam interactions with double negative metamaterial slabs." Optics Express 11.7 (2003): 662-681.

[44] Ziolkowski, Richard W. "Pulsed Gaussian beam interactions with double negative metamaterial slabs: errata." Opt. Express 11 (2003): 1596-1597.

[45] Ziolkowski, Richard W. "Gaussian Beam Interactions with DoubleNegative (DNG) Metamaterials." Negative-Refraction Metamaterials: Fundamental Principles and Applications (2005): 171-211.

[46] Caloz, Christophe, Atsushi Sanada, and Tatsuo Itoh. "A novel composite right-/left-handed coupled-line directional coupler with arbitrary coupling level and broad bandwidth." Microwave Theory and Techniques, IEEE Transactions on 52.3 (2004): 980-992.

[47] Caloz, Christophe, and Tatsuo Itoh. "A novel mixed conventional microstrip and composite right/left-handed backward-wave directional coupler with broadband and tight coupling characteristics." Microwave and Wireless Components Letters, IEEE 14.1 (2004): 31-33.

[48] Grbic, Anthony, and George V. Eleftheriades. "A backward-wave antenna based on negative refractive index LC networks." Antennas and Propagation Society International Symposium, 2002. IEEE. Vol. 4. IEEE, 2002.

[49] Otto, S., et al. "Composite right/left-handed -resonator ring antenna for dual-frequency operation." Antennas and Propagation Society International Symposium, 2005 IEEE. Vol. 1. IEEE, 2005.

[50] Fan Yang; Rahmat-Samii, Y., "Reflection phase characterizations of the EBG ground plane for low profile wire antenna applications," Antennas and Propagation, IEEE Transactions on , vol.51, no.10, pp.2691,2703, Oct. 2003

[51] Balmain, Keith G., A. A. E. Luttgen, and Peter C. Kremer. "Resonance cone formation, reflection, refraction, and focusing in a planar anisotropic metamaterial." Antennas and Wireless Propagation Letters, IEEE 1.1 (2002): 146-149.

[52] Balmain, Keith G., A. A. E. Luttgen, and Peter C. Kremer. "Power flow for resonance cone phenomena in planar anisotropic metamaterials." Antennas and Propagation, IEEE Transactions on 51.10 (2003): 2612-2618.

[53] Ziolkowski, Richard W., and Allison D. Kipple. "Application of double negative materials to increase the power radiated by electrically small antennas." Antennas and Propagation, IEEE Transactions on 51.10 (2003): 2626-2640.

[54] Ziolkowski, Richard W., and Aycan Erentok. "Metamaterial-based efficient electrically small antennas." Antennas and Propagation, IEEE Transactions on 54.7 (2006): 2113-2130.

[55] Chen, Shih-Yuan, et al. "MNG-metamaterial-based efficient small loop antenna." Antennas and Propagation Society International Symposium, 2009. APSURSI'09. IEEE. IEEE, 2009.

[56] O. S. Kim, and O. Breinbjerg, Miniaturised self-resonant split-ring resonator antenna, IEEE Electron. Lett., vol. 45, no. 4, pp. 196-197, February 2009

[57] Mahmoud, Samir F. "A new miniaturized annular ring patch resonator partially loaded by a metamaterial ring with negative permeability and permittivity." Antennas and Wireless Propagation Letters, IEEE 3.1 (2004): 19-22.

[58] Y. Lee, S. Tse, Y. Hao, and C. G. Parini, A compact microstrip antenna with improved bandwidth using complementary split-ring resonator (CSRR) loading, IEEE International Symposium on Antennas and Propagation and URSI Radio Science Meeting Digest, pp. 5431-5434, 2007.

[59] A. U. Limaye, J. Venkataraman, Size reduction in microstrip antennas using left-handed materials realized by complementary split-ring resonators in ground plane, IEEE International Symposium on Antennas and Propagation and URSI Radio Science Meeting Digest, pp. 1869-1872, 2007.

[60] F. Falcone, T. Lopetegi, J. D. Baena, R. Marqus, F. Martin, and M. Sorolla, Effective negative-stop-band microstrip lines based on complementary split ring resonators, IEEE Microw. Wireless Compon. Lett., vol. 14, no. 6, pp. 280-282, 2004.

[61] Zhu, Shaozhen, et al. "Compact low frequency varactor loaded tunable SRR antenna." (2013): 1-1.

[62] Mirzaei, Hassan, and George V. Eleftheriades. "A compact frequency-reconfigurable metamaterial-inspired antenna." Antennas and Wireless Propagation Letters, IEEE 10 (2011): 1154-1157.

[63] Scarborough, C.P.; Werner, D.H.; Wolfe, D.E., "Miniaturized tunable metamaterial antenna design and modeling in the low UHF band," Antennas and Propagation Society International Symposium (APSURSI), 2013 IEEE , vol., no., pp.1574,1575, 7-13 July 2013.

[64] Lee, D. H., et al. "Low frequency tunable metamaterial small antenna structure." Antennas and Propagation, 2007. EuCAP 2007. The Second European Conference on. IET, 2007.

[65] Buell, Kevin, Hossein Mosallaei, and Kamal Sarabandi. "A substrate for small patch antennas providing tunable miniaturization factors." Microwave Theory and Techniques, IEEE Transactions on 54.1 (2006): 135-146.

[66] He, Peng, et al. "Tunable negative refractive index metamaterial in microstrip line for antenna applications." Antennas and Propagation Society International Symposium, 2008. AP-S 2008. IEEE. IEEE, 2008.

[67] Jouvaud, C., J. de Rosny, and A. Ourir. "Adaptive metamaterial antenna using coupled tunable split-ring resonators." Electronics Letters 49.8 (2013): 518-519.

[68] Ouedraogo, R.O.; Rothwell, E.J.; Diaz, A.; Shih-Yuan Chen; Temme, A.; Fuchi, K., "In Situ Optimization of Metamaterial-Inspired Loop Antennas", Antennas and Wireless Propagation Letters, IEEE , vol.9, no., pp.75,78, 2010

[69] R. O. Ouedraogo and E. J. Rothwell, Metamaterial inspired patch antenna miniaturization technique, IEEE International Symposium on Antennas and Propagation and URSI Radio Science Meeting Digest, pp. 1-4, 2010.

[70] R. O. Ouedraogo, E. J. Rothwell, A. R. Diaz, K. Fuchi, and A. Temme, Miniaturization of patch antennas using a metamaterial-inspired technique, IEEE Antennas Wireless Propag. Lett., vol. 9, pp. 75-78, 2010.

[71] R. O. Ouedraogo, E. J. Rothwell, Prem Chahal, A. R. Diaz, and K. Fuchi Design and Optimization of Metamaterial Inspired On-chip Antennas for Wireless Applications. Presented at 2011 IEEE AP-S/URSI confrence.

[72] Haupt, Randy L., and Sue Ellen Haupt. Practical genetic algorithms. John Wiley Sons, 2004.

[73] Goldberg, David Edward. Genetic algorithms in search, optimization, and machine learning. Vol. 412. Reading Menlo Park: Addison-wesley, 1989.

[74] Johnson, J. Michael, and V. Rahmat-Samii. "Genetic algorithms in engineering electromagnetics." Antennas and Propagation Magazine, IEEE 39.4 (1997): 7-21.

[75] E. Michielssen, J. Sajer, S. Ranjithan, and R. Mittra, Design of Lightweight, Broad-Band Microwave Absorbers Using Genetic Algorithms, IEEE Transactions on Microwave Theory and Techniques, MTT-41,6/7, June/July 1993, pp. 1024-1031.

[76] Michielssen, Eric, J. M. Sajer, and Raj Mittra. "Design of multilayered FSS and waveguide filters using genetic algorithms." Antennas and Propagation Society International Symposium, 1993. AP-S. Digest. IEEE, 1993.

[77] Haupt, Randy L. "Thinned arrays using genetic algorithms." Antennas and Propagation, IEEE Transactions on 42.7 (1994): 993-999.

[78] Johnson, J. Michael, and Yahya Rahmat-Samii. "Genetic algorithm optimization and its application to antenna design." Antennas and Propagation Society International Symposium, 1994. AP-S. Digest. Vol. 1. IEEE, 1994.

[79] Johnson, J. Michael, and Yahya Rahmat-Samii. "Genetic algorithms and method of moments (GA/MOM) for the design of integrated antennas." Antennas and Propagation, IEEE Transactions on 47.10 (1999): 1606-1614.